2019

The Structural Basis for Brain Health

Barbara Khalibinzwa Marebwa
Medical University of South Carolina

The Structural Basis for Brain Health

Barbara Khalibinzwa Marebwa

A dissertation submitted to the Medical University of South Carolina in partial fulfillment of the requirements for the degree of Doctor of Philosophy in the College of Graduate Studies.

Department of Neurology

2019

Approved by:

Chairman, Advisory Committee
Leonardo Bonilha, MD/PhD _____

Roberts Adams, MD _____

DeAnna Adkins, PhD _____

Mark A. Eckert, PhD _____

Julius Fridriksson, PhD _____

Chris Rorden, PhD _____

Table of Contents

Acknowledgement

I am eternally grateful to my mentor Dr. Leonardo Bonilha for his interminable support and guidance during this journey. Thank you for showing me an example of a stellar scientist and kind human being, traits that I will aspire to in my own career. I am also indebted to my committee, Dr. Robert Adams, Dr. DeAnna Adkins, Dr. Mark Eckert, Dr. Julius Fridriksson and the C-Star team, and Dr. Chris Rorden for their time, feedback, and invaluable guidance.

I would also like to thank Dr. Troy Herter, who gave me a chance during my masters into a project that would later form the foundation for my doctoral work. Thank you for your infectious passion for science. I am grateful to friends across continents and family away from home: the MUSC international family, my Rovereto family, Bonilha lab members, the Halley's comet of Biomedical imaging classes, my fellow bullpen survivors, and our program director Dr. Truman Brown, for the superhuman restraint he showed during Bloch equations, his patient guidance, scintillating conversations, fun journal clubs, and that weekly dose of mango juice! Thank you.

To my family, especially my mom Lucy Atieno, a constant source of encouragement, my dad Bede Marebwa for your constant prayers, my brothers and their families: Tony, Cony, Sammy and Neema, and Asele, Dorcas, David and Amandla, thank you for your encouragement, prayers, and faith in me.

All glory and honor to our Lord.

... you will be more disappointed by the things you didn't do than by the ones you did do. So, throw off the bowlines. Sail away from the safe harbor. Catch the trade winds in your sails. Explore. Dream. Discover.

-unknown

1 Introduction

Brain health can theoretically be defined as the capacity to perform cognitive tasks such as communication, decision making, learning and memory, sensation and perception, regulating emotions, and having the ability adapt to the environment. Poor brain health eventually manifests clinically as cognitive impairment or dementia, with underlying causes including a high burden of cardiovascular risk factors, stroke, Alzheimer's disease, neurodegenerative disorders and other causes of vascular cognitive impairment. Cumulative evidence indicates that the accrual of sub-clinical injury and exposure to vascular risk factors throughout life diminishes optimal brain function and increases the risk for neurological disease.

There is currently no clinical measure for brain health especially before overt clinical manifestation, leading to the increasing urgency for tools that can detect covert brain injury, and define optimal brain health.

In Search of Brain Health

Cardiovascular disease (CVD) remains the leading cause of mortality in the United States. Stroke and dementia are the leading causes of adult disability worldwide, and the 5th and 6th leading causes of mortality respectively in the United States[1]. Furthermore, CVD produces a great health and financial burden globally, and accounts for about $351.2 billion in direct and indirect costs in the United States annually, with costs projected to increase sharply for adults 65 and older due to increasing life expectancy[1].

While these diseases have different etiologies and present with different clinical manifestations and prognosis, converging evidence increasingly supports the idea of CVD as a common pathophysiological origin of cerebrovascular disease. Regional variation in CVD, stroke, and Alzheimer Disease mortality has consistently followed a similar pattern (figure1) with greater age-adjusted mortality in the southern states, commonly called the "stroke belt", potentially indicating a complex interplay between cerebrovascular and cardiovascular health. Modifiable Cardiovascular risk factors (CVRF) like diabetes, hypertension, hyperlipidemia, physical inactivity, obesity and smoking, have been continually associated with cognitive decline, cardiovascular, and cerebrovascular disease, stroke, and dementia. Cumulative risk factors act synergistically and further increase the risk for cardio- and cerebrovascular diseases. An increasing majority of the population are living with CVRF that increase the risk for cardio- and cerebrovascular events.

Although CVD is the leading cause of mortality in the US, there is evidence of declining rates of CVD mortality, resulting in a projected increase in life-expectancy, which creates the need for strategies to maintain cognitive health, improve healthy ageing and brain health. Maintenance of cognitive health in ageing predicts quality of life, and

independence. However, despite declining rates of CVD mortality[2], there is an increasing prevalence of CVRF and cardio- and cerebrovascular disease in younger adults[3]. This trend also leads to the need for potential preventative therapies to maintain brain health, and ways to define, and detect suboptimal brain health before overt manifestation of clinical symptoms.

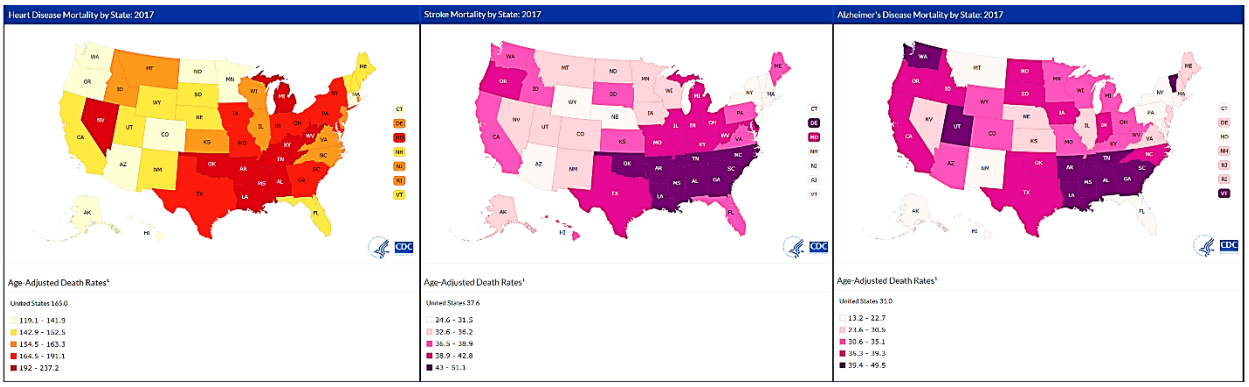

Figure1. Age-adjusted patterns of CVD, Stroke, and Alzheimer Disease mortality among US states in 2017. (https://www.cdc.gov/nchs/pressroom/stats_of_the_states.htm)

There is vast observational evidence from longitudinal studies relating CVRF to development of cognitive impairment. The Maine-Syracuse Longitudinal Study followed 972 community-based individuals (23-98 years) and showed that smoking, obesity, and poor diet were independently associated with poor cognitive performance even after adjusting for age, education and gender[4]. The Coronary Artery Risk Development in Young Adults[5] (CARDIA) study followed 2,932 participants (18-30 years at baseline) for 25 years and showed that participants who maintained cardiovascular health; measured through body mass index, diet score, smoking, physical activity, total cholesterol and blood pressure; in young adulthood had better cognitive function in midlife. The Framingham Heart Study - a 71 year ongoing CV study in Framingham, Massachusetts, has established extensive risk factors for CVD and stroke[6]. In a subset of the cohort, 2175 offspring from

the original Framingham cohort (mean age 60.7 years), individuals with multiple cardiovascular risk factors; measured as the Framingham 10 year stroke risk (calculated from age, systolic blood pressure, antihypertensive medication, diabetes, cigarette smoking status, history of cardiovascular disease, atrial fibrillation (AF), and left ventricular hypertrophy (LVH) as determined by ECG), as well as total serum cholesterol (mm/dL), body mass index, and self-reported mean number of drinks per day; exhibited greater cognitive deficits[7]. Furthermore, factors such as socioeconomic status, diet, psychological, medical and genetic factors may also influence brain integrity thus determining cognitive abilities, and cognitive changes through life. For instance, genetic factors may either predispose and individual to CVRF, or afford an individual a higher cognitive reserve, and with it a higher resistance to damage. The Lothian birth-cohort studies have demonstrated a relationship between WMH in late age to lower childhood IQ[8]. Childhood IQ was determined to be the strongest predictor of late life cognitive ability, indicating at least to some extent, a predefined brain architecture that may have neuroprotective properties, or influence cognitive decline later in life.

These and many more longitudinal studies suggest that CVRF burden has a profound impact on cognition. While the etiopathogenesis of brain damage as a result of CVRF is still under investigation, one promising theory is that CVRF cause micro- and macroangiopathic damage that decrease central nervous system blood supply, causing cellular damage that in the white matter manifest as white matter hyperintensities (WMH) on T2-weighted magnetic resonance imaging, and is associated with cognitive decline. While the pathophysiology of WMH is not yet resolved, evidence suggests that

mechanisms of action involve hypoperfusion, and neuroinflammation, and elucidation of which may lead to better targeted preventative, or otherwise curative therapies.

Pathway to neurodegeneration: Insight from animal models and histopathology

An accumulation of evidence indicates that the genesis of cognitive decline involves the disruption of the cortical angiome, the three-dimensional microvasculature responsible for gaseous exchange in neuronal cells [9].

The human brain, while making up only 2% of the human weight, consumes about 20% of energy even at rest [10, 11]. The energy consumed goes into generating action potentials, neurotransmitter release and recycling, however a large portion of the energy goes into maintaining resting potentials via active transport of ions across the membrane [11]. Neuronal computation is therefore energetically costly, requiring an extensive and reliable vascular architecture to meet these demands, and to dispose of by-products of brain activity and prevent toxic accumulation of waste products. The cortical vasculature transporting oxygenated blood to the brain begins from the circle of Willis, whence the great cerebral arteries including the posterior cerebral artery, the middle cerebral artery, and the anterior cerebral artery arise; forming a planar network of extensively interconnected pial arterioles that cover the entire surface of the cortical mantle and can compensate for blockage in a few branches of the network. Radially penetrating arterioles connect the cortical network to an underlying three-dimensional network of microvessels, which are in-turn drained by penetrating venules that transport the de-oxygenated blood to the cortical surface and into the central sinus[12]. The three-dimensional microvasculature is responsible for a majority of metabolite and gaseous exchange between the brain cells and the vascular network. While the topological organization of this vast network is yet

uncharted, recent promising animal work indicate a non-columnar, lattice network of the cortical angiome[12] that deviates from the neural architecture, with a triad connectivity pattern and inbuilt loops that limits disruption of blood flow, and enables compensation to down- or upstream regions from the blockage.

Cerebral hypoperfusion results in ischemia, accompanied by neuronal dysfunction and cell death, which undoubtedly leads to large- and small vessel pathologies as well as cerebral microinfarcts observed in aged cognitively normal individuals and those with high CVRF burdens, as well as in a myriad of cerebrovascular pathologies such as vascular dementia, AD, vascular parkinsonism, and stroke. Large- and small vessel pathologies may manifest as regions of hyperintensity on T2-weighted MRI scans, but cerebral microinfarcts cannot currently be observed in-vivo using neuroimaging techniques. Although brain microinfarcts can only be observed during autopsy, advances in neuroimaging now enable us to infer micro- and macro-structural changes on brain white matter in vivo.

Early stages of CVRF maybe accompanied by microvascular ischemia and subtle reductions in blood flow that nonetheless already cause diffuse neuronal dysfunction and brain injury and could have far reaching disruption of brain function. Animal models of CVRF, and microvascular injury can help elucidate the pathophysiological consequences of CVRF[13]. The *db/db* mouse model for diabetic dyslipidemia develop obesity, fasting hyperglycemia, and hyperinsulinemia and present with severe cerebrovascular pathology, that includes aneurysms and small strokes that in turn leads to severe cognitive impairment [14]. A mixed model of vascular dementia, with elements of both AD and vascular pathologies; the *db/db* mouse model crossed with the *A*β overexpressing mouse line, to

produce a morbidly obese mouse, with hypertension, type 2 diabetes mellitus with hyperglycemia, that showed profound cognitive deficits in the Morris Water Maze[13]. The authors conclude that diabetes and obesity in the mice leads to aberrant angiogenesis and unstable vasculature that is prone to ischemia and strokes. Models of hypertension develop spontaneous lesions and hemorrhages at around 9-12 months of age [15], with persistent hypoperfusion, weakened microvasculature, hypertension induced vascular remodeling and thickening of vascular walls, increasing susceptibility to microhemorrhage, vascular occlusion, and stroke [16]. Microinfarcts and small strokes observed in these models of CVRF; and usually observed in individuals with cerebrovascular diseases such as atherosclerosis, arteriolosclerosis, and cerebral amyloid angiopathy; have been shown to contribute to vascular cognitive impairment and dementia in humans, with greater microinfarct burden associated with an increased likelihood of antemortem cognitive impairment[17]. These microinfarcts are macroscopically invisible and largely go undetected by conventional neuroimaging. Postmortem studies show a widespread distribution of microinfarcts invisible to the naked eye[17], suggesting that these silent lesions that result in asymptomatic cerebrovascular disease, should be identified before overt clinical symptoms. Animal models of cerebral microinfarcts such as laser- or optically induced microlesions, and targeted photothrombosis reveal diffuse and lasting neural and hemodynamic deficits [18], necessitating the elucidation of mechanisms by which microinfarcts contribute to vascular cognitive impairment. Other studies further demonstrate that distributed microinfarcts also disrupts the brain's glymphatic system[19]; a perivascular network that recirculates CSF through the brain parenchyma and clears interstitial solutes like *A*β and tau during rest; and whose failure is widely thought to be

related to AD pathology. The authors conclude that microinfarcts may trap proteins and other interstitial solutes within the brain parenchyma, thereby enabling *A*β plaque formation. Microinfarcts also affect white matter myelin, cause axonal damage, and reduced protein synthesis, and result in atrophy of neuronal dendrites.

Collectively, this data indicates that CVRF affects the cortical vasculature leading to chronic cerebral hypoperfusion, resulting in cortical microinfarcts and small vessel disease, and contributes to the development of several cerebrovascular diseases vascular dementia, vascular parkinsonism, stroke, and has also been shown to accompany AD pathology [20].

White matter maybe particularly vulnerable to microvascular damage, hypoperfusion and ischemia because of low collateral supply and a reduction in the vascular density as suggested by the cortical angioma. Although one quarter of all stroke occur in the white matter, it is still of importance because even small white matter damage can cause disconnection between critical grey matter regions, causing diffuse, widespread damage beyond the location of the stroke lesion. In particular, long-range white matter fibers; which are energetically more demanding, and therefore less numerous; may have an increased vulnerability to damage, since they span a larger territory and may therefore be supplied by different pockets of the vasculature, and generally have a higher probability for infarction. Optimal brain health is considered as the absence of overt vascular and neurodegenerative injury; observed in stroke, AD and aging; and the absence of white matter hyperintensities and small vessel disease; as observed in CVRF [21]. Recently, optimal brain health also includes the absence of subclinical injury, microinfarcts, and silent strokes that are not readily detected by existing neuroimaging techniques, demonstrating the need for development of quantifiable tools and methods that can detect brain injury even before

overt clinical manifestation; to either prevent further degeneration, or slow down cognitive decline; and to improve on predictive models of functional recovery after brain injury.

Principle organization of complex networks

The human brain is a self-adapting complex system that gives rise to a rich repertoire of functionality such as movement, sensation and perception, memory, emotion, and cognition, from an immutable neuronal architecture. The emergence of complex functionality from such a fixed anatomy remains one of the major mysteries of neuroscience. The emergence of this functionality may lie in the brain's topological architecture; the organization of white matter tracts that link disparate grey matter regions; that is determined not only by evolutionary adaptation and the organism's genetic code but is also heavily influenced by the organism's ontology. This means that diverse functionality, resilience to damage, efficient information processing and ultimately brain health, is characterized by an optimal topological organization of the complex network, and deviations from this optimal topological structure may predict cognitive decline.

Advances in neuroimaging and computational neuroscience now enable us to non-invasively probe the macroscopic organization of the brain and using diffusion-weighted MRI or resting state functional MRI, build a comprehensive map of neural connections in the brain that describe the structural or functional connections respectively between cortical and sub-cortical brain regions. This map can then be abstracted into a connectivity matrix called the connectome, with the nodes representing brain regions and edges, the connections between the regions. Models of optimal structural and functional connectivity that give rise to behavior and cognition can then be tested using graph theory and complex network analysis, which provide a powerful measure of the topological organization, and

interaction between different brain regions. Metrics such global and local efficiency, modularity, small worldness are often used to characterize network properties, and provide measurements that can be compared between different groups and patient populations to provide insight into neurological and developmental conditions. Complex network analysis reveals that the human brain networks display characteristics of efficient wiring and an efficient communication architecture, with segregated, highly connected modules, integrated by a few highly connected hubs [22-24]. Modularity is a property that describes the segregation and integration of complex networks, where modules are made up of highly interconnected brain regions that are sparsely connected to other regions or modules [25]. Segregation allows for functional specialization of highly specialized processes such as word production, while integration allows for transfer of information between functional modules, giving rise to distributed processes such as language, that involves integration of various domains of functional specialization. While brain networks are wired to minimize cost, optimization algorithms have shown that neural systems are not exclusively optimized for minimal global wiring due to the existence long-range projections in neural networks that increase total wiring cost, but facilitate short communication paths and minimize processing steps [26]. The presence of these projections produces a non-random, non-regular, small world organization, with an underlying power law distribution that enables functional specialization, and functional integration of anatomically disparate regions. Brain networks are therefore wired to minimize wiring costs, while maximizing information processing and efficiency (figure 2).

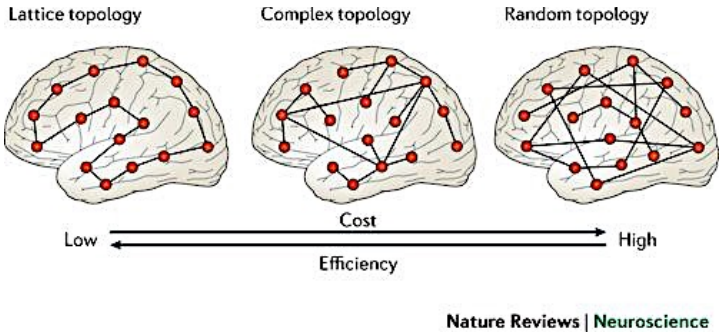

Figure 2. Brain networks have a complex topology that favors global integration by including a few high-cost long-range connections that connect anatomically disparate regions, while minimizing wiring cost[22].

The topological organization changes with aging and development, brain injury, or as a result of genetic abnormality. Deviations from this optimal structure can be captured by network analysis and can either predict disease progression, recovery after injury, treatment efficacy, or detect neuronal correlates of cognitive deficits before overt clinical manifestation.

Brain network analyses reveal diagnostic properties of network disorders that significantly differ from normally developing brain networks. Genetic disorders like Schizophrenia present with an altered structural and functional connectivity, with reduced modularity[27] and small worldness[28] compared to healthy controls, implying reduced local communication, but greater global communication, which would suggest a shift towards randomization of the topology and greater connection cost (figure 2), consistent with abnormal axonal growth and insufficient synaptic pruning[29], that have been suggested as the pathogenesis of schizophrenia. Other clinical disorders such as autism, obsessive compulsive disorder, also show aberrant topological organization that deviated from normal populations. Furthermore, disorders that result from oxidative stress to the brain like Alzheimer's disease, stroke, and CVRF also manifest with network topology abnormalities. If the pathology prevents sufficient supply of oxygen and nutrients to brain cells, and prevents the brain from meeting its metabolic demand, then it is expected that

metabolically expensive nodes (such as hubs), and edges (such as long-range connections), will be particularly vulnerable to functional disruption[22]. Alzheimer's disease is characterized by a disrupted neuronal connectivity with network hubs such as the posterior cingulate, temporal and orbitofrontal cortices, initially impacted by *A*β deposits[30], and micro- and macrostructural white matter abnormalities[31], resulting in the overall disruption of large-scale white matter networks. CVRF result in microinfarcts (that may not be detectable by standard neuroimaging methods), and small vessel damage that results in diffuse injury throughout the brain, undoubtedly affective global network connectivity, that can be detected using network analysis. In participants with CVRF, metabolically demanding long-range fibers are reduced with increasing CVRF co-occurrence compared to a non-CVRF cohort. This reduction in long-range fibers was found to be associated with pre-clinical cognitive decline [32].

Network disruption therefore plays a central role in the pathogenesis of cognitive decline, both in dementia[33], as well as predicting the severity of language deficit in chronic stroke[34]. This data suggests that network science offers compelling and reliable measures of the decline of brain health either as a result of a genetic condition, conditions acquired during development, or later in life. Consequently, this emerging literature demonstrates, a compelling association between brain network organization and disease, providing a target for pharmacological and non-pharmacological interventions from a public health standpoint. In particular, the brain's trade-off between wiring costs and topological efficiency seems to be an important element in the emergence and maintenance of cognition, with a foray towards the lattice or random arrangement resulting in overt clinical symptoms. This optimal topology is made possible by a few costly elements (hubs and

long-range fibers) that are nonetheless vulnerable to pathological attack (e.g. hypoperfusion resulting from CVRF, or *A*β deposits), and abnormal development. Longitudinally, long-range fibers are disproportionately affected compared to short-range fibers in participants with symptomatic small vessel disease[35]. We therefore propose that the loss of metabolically costly long-range white matter fibers, that lead to the disorganization of optimal brain networks thus depriving the brain of its ability to adapt to cognitive demands, is a potential mechanism by which brain health is lost and cognitive decline begins.

Pharmacological and non-pharmacological interventions to maintain brain health

One major advantage of developing models to detect and predict the decline of brain health, especially as a result of modifiable risk factors associated with cerebrovascular health, is the potential to intervene and prevent cognitive decline, or stall its rapid progression. Furthermore, connectome-based therapeutic interventions should be utilized not only in diffuse brain injury such as those resulting from CVRF, but also after focal brain injury such as strokes due to the potential dysfunction of structurally or functionally connected regions that are otherwise anatomically disparate to the lesion location that would otherwise be undetected. Connectome-based treatment strategies can lead to the salvage of functionally connected, or homologous brain regions, or guide connectome change and plasticity, resulting in vicariation and functional recovery.

There are several clinical trials aimed at reducing the progression of cognitive decline especially in elderly population by combating CVRF. The effect of anti-hypertensive medication was demonstrated in the 9-year Honolulu-Asia Aging Study of 2,197 cognitively normal (at baseline) community dwelling hypertensive Japanese men

(mean age 77 years) where β-blocker use was associated with a lower risk of cognitive impairment[36].

The 6-year Systolic Blood Pressure Intervention Trial (SPRINT) study aimed to compare the effect of lowering systolic blood pressure to <120mmHg (using a drug intensive control of SBP) compared to <140mmHg (using the standard control of SBP) in 9250 adults (>50 years) with hypertension and at least one other CVRF. They demonstrated a significant reduction in stroke, myocardial infarction, and cardiovascular death in the intensive SBP control cohort[37]. Furthermore, SPRINT-MIND (454 participants) showed a significant reduction in the increase of white matter lesions in participants undergoing the intensive treatment that lowered BP to <120mmHg.

The recently completed Candesartan vs. Lisinopril Effects on the Brain (CALIBREX) study likewise seeks to determine the effect of Candesartan and Lisinopril on the cognitive function, cerebral perfusion, vascular damage and endothelial function on 143 participants with high blood pressure and mild cognitive impairment (MCI) (https://www.nia.nih.gov/alzheimers/clinical-trials/candesartan-vs-lisinopril-effects-brain-calibrex).

The ongoing Candesartan's Effects on Alzheimer's Disease and Related Biomarkers (CEDAR) will determine the effect of the anti-hypertensive drug Candesartan on vascular stiffness, AD biomarkers (*A*β and tau), and cognitive function in a cohort of 62 participants with MCI (https://www.nia.nih.gov/alzheimers/clinical-trials/candesartans-effects-alzheimers-disease-and-related-biomarkers).

The risk reduction for Alzheimer's Disease (rrAD) clinical trial will test the effect of controlling CVRF such as hypertension and high cholesterol on AD, in a high-risk cohort

of 640 participants (60-85 years). The study will determine if the addition of aerobic exercise to medical management of hypertension and high cholesterol will reduce the risk of cognitive decline over two years (http://www.rradtrial.org/participants/).

There are also non-pharmacological intervention trials that seek to determine the impact of exercise, cognitive training, diet and lifestyle interventions on cognitive decline.

The Lifestyle Enriching Activities for Research in Neuroscience Intervention Trial (LEARNit study) will determine the effects of exercise and healthy living on brain health in 90 adults (60-80 years) (https://clinicaltrials.gov/ct2/show/NCT02726906). Likewise, the Exercise in Adults with Mild Memory Problems (EXERT) will evaluate the effects of physical exercise on cognition, functional status, brain atrophy and blood flow, and cerebrospinal fluid biomarkers of Alzheimer's disease in 300 older adults (65 – 89 years) with a mild memory impairment.

Finally, the MIND diet intervention and cognitive decline (MIND) will test the effect of the MIND diet (Mediterranean-DASH Intervention for Neurodegenerative Delay) on cognitive decline and neurodegeneration on a cohort of 600 cognitively normal, overweight older individuals (65+ years) over a 3-year period.

These clinical trials provide evidence for the importance of CVRF management and prevention to brain health in older adults with clinical manifestations of cognitive decline. Completed studies show significant neuroprotective results of these interventions. Management of these risk factors in early adulthood (CARDIA) or before manifestation of clinical symptoms will undoubtedly increase the chances of maintaining cognitive health well into old-age, therefore shining a light on the importance of diagnostic tools that detect sub-clinical brain damage.

2 Cardiovascular risk factors and brain health

Cardiovascular risk factors are inextricably linked to cognitive decline, dementia and increased risk for stroke. CVRF are potentially modifiable and are therefore well positioned as targets of strategies to prevent cognitive decline, and stroke or reduce stroke severity.

This chapter, based on the following peer-review publication, will determine the impact of increased CVRF burden on structural brain integrity and cognitive function:

Marebwa BK, Adams RJ, Magwood GS, et al. Cardiovascular Risk Factors and Brain Health: Impact on Long-Range Cortical Connections and Cognitive Performance. Journal of the American Heart Association 2018;7:e010054.

Abstract

Background

Cardiovascular risk factor burden in the absence of clinical or radiological "events" is associated with mild cognitive impairment. MRI techniques exploring the integrity of neuronal fiber connectivity within white matter networks supporting cognitive processing could be used to measure the impact of cardiovascular (CV) disease on brain health, and be used beyond bedside neuropsychological tests to detect subclinical changes and select or stratify participants for entry into clinical trials.

Methods and Results

We assessed the relationship between verbal IQ and brain network integrity, and the effect of CV risk factors on network integrity by constructing whole brain structural connectomes from MRI diffusion images (n = 60) with various degrees of CV risk factor burden. We measured axonal integrity by calculating network density and determined the effect of fiber loss on network topology and efficiency, using graph theory. Multivariate analyses were used to evaluate the relationship between CV risk factor burden, physical activity, age, education, white matter integrity, and verbal IQ. Reduced network density, resulting from a disproportionate loss of long-range white matter fibers, was associated with white matter network fragmentation ($r = -0.52$, $p < 10^{-4}$), lower global efficiency ($r = 0.91$, $p < 10^{-20}$), and decreased verbal IQ (adjusted $R^2 = 0.23$, $p < 10^{-4}$).

Conclusions

CV risk factors may mediate negative effects on brain health via loss of energy dependent long-range white matter fibers, which in turn leads to disruption of the topological organization of the white matter networks, lowered efficiency, and reduced cognitive function.

Introduction

"Brain health" can be broadly defined as the physiological state in which sensorimotor and cognitive tasks are performed within a normal level that is comparable across healthy individuals. This definition can also be expanded to imply neurological functional reserve, i.e., the ability to learn and adapt to new knowledge, challenges, or to recover from neurological disease.

Currently, brain health is largely assessed in the context of clinical neuroscience through behavioral measures. Cognitive performance is assessed using standard paper and pencil neuropsychological tests, while sensorimotor abilities are commonly assessed through the neurological exam [38, 39]. Likewise, neurological adaptation is measured through the observation of learning rates or, through recovery after brain injury [40-42].

These behavioral measures provide some insight into the underlying biological phenomena that are fundamentally related to brain health. However, behavioral measures do not yield specific information about the exact underlying neuroanatomical mechanisms that constitute brain health, and as a result, are limited in their ability to predict performance, or reserve, particularly in the context of neurological disease and subclinical changes, where identifying compromised neuroanatomical networks can be important for treatment considerations.

Cardiovascular (CV) risks factors, such as diabetes, hypertension, and hyperlipidemia are detrimental to general health and cognition in particular. They have pervasive and profound effects on end-organ function and peripheral vasculature [43]. CV risk factors result in initial subtle brain structural changes and cognitive decline that may eventually lead to dementia[44, 45]. Likewise, the cumulative effect of microangiopathic changes and perivascular lipohyalinosis is commonly associated with white matter changes in the brain[46]. Although white matter has lower metabolic needs, it's significantly more vulnerable to ischemic damage compared to grey matter. White matter receives less cerebrovascular perfusion [47], and has a declining anaerobic resistance associated with aging[48]. Despite the well-known relationship between white matter susceptibility and ischemic damage, the mechanisms linking small vessel disease, white matter network disruption, brain health and cognitive decline, are not well understood. Likewise, the impact of microangiopathic white matter loss on cognitive performance is not well defined in mild to moderate cases. Therefore, evidence of pre-morbid brain decline coupled with changes in brain structural integrity maybe an early indicator of cognitive decline and dementia.

In this study, we examined the question whether cognitive function is related to CV risk factor burden and loss of network integrity, which can be understood as a biological measure of brain health.

We leveraged methodological advancements in systems and computational neurosciences related to the human brain connectome. The structural connectome is a map of all medium- to large scale white matter connections across the entire brain derived from diffusion tensor Magnetic Resonance Imaging (DTI). The connectome reveals regional pairwise brain

connectivity between all defined brain regions and enables quantification of the topology of complex brain networks, beyond grey or white matter atrophy which may occur with healthy aging. The connectome is an individual map where the topological brain network organization can be compared across individuals in the context of health or disease[49]. By providing a comprehensive overview of neuronal network organization, the brain connectome has been applied successfully to improve the understanding of several broad categories of neurological diseases such as epilepsy, dementia and movement disorders [50-53]. However, it has not been evaluated thus far as a measure of brain health.

Individualized connectomes can be assessed with regards to their integrity and topological network organization, leveraging knowledge from network analyses. Global and regional properties can be assessed with regards to efficiency of transfer of information via network integration and segregation[54]. We evaluated the association between CV risk factors, white matter integrity, and cognitive performance in a group of participants with varying CV risk factor burden. Cognitive performance was evaluated using verbal IQ, calculated from the National Adult Reading Test-Revised (NART-R)[55] that has been standardized against other measures of intelligence (Wechsler adult intelligence scale)[56] and serves as an accurate probe of pre-morbid cognitive performance. Specifically, we evaluated whether CV risk factor burden would be associated with loss of fiber density, especially among short- or long-range white matter connections, whose structural integrity entails a continuum from lower to higher metabolic demand, respectively. We hypothesized that high CV risk factor burden would be associated with loss of energy dependent long axonal projections, leading to lower verbal IQ. The confirmation of our hypothesis would lead to the proposal that

white matter network architecture could provide a singular, quantifiable measure of overall brain health by using imaging connectomics.

Methods

Anonymized data used in this study will be made available to investigators who provide written request to the corresponding author to analyze the data, indicating the study in which the data will be used.

Participants

We recruited 60 participants, (47 females, mean age 55.1 ± 8.6 years) without a history of neurological or psychiatric diseases from the local community through advertisement. All participants were self-reported cognitively normal adults. Thirty-three participants did not have a history of cardiovascular risk factors (healthy control group), while 27 participants had previously been diagnosed with at least one CV risk factor (CVD group): diabetes (14 participants), hyperlipidemia (18 participants), and hypertension (20 participants) (Table1). Seven participants had been diagnosed with all cardiovascular risk factors, (a group henceforth referred to as the "cumulative morbidity" group). These diagnoses were obtained through medical chart review. The Charlson Comorbidity Index[57] (CCI) was calculated for all participants. If participants reported a diagnosis of hypertension and/or hyperlipidemia, and extra point for each diagnosis was added to the overall CCI score. All participants except 4 had at least a high school diploma. The study was approved by the Institutional Review Board at the Medical University of South Carolina, and all participants gave written informed consent.

Behavioral Evaluation

All participants underwent verbal performance assessment using the National Adult Reading Test-Revised (NART-R)[55] as an estimator of pre-morbid cognitive function. Verbal intelligence was calculated in accordance with the NART-R as shown:

Estimated Verbal Scale IQ = 128.7 – 0.89 x NART-R errors.

All participants completed the Community Healthy Activities Model Program for Seniors (CHAMPS)[58], which was used as a measure for physical activity. All behavioral testing was performed within the same week as the neuroimaging assessment.

Image Acquisition

Imaging was performed on a Siemens 3T TIM trio MRI scanner located at the Medical University of South Carolina. We used T1-weighted, and Diffusion images collected from each participant. T1 parameters: MPRAGE sequence with 1 mm isotropic voxels, 256x256 matrix size, and a 9-degree flip angle. We used a 192-slice sequence with TR = 2250 ms, T1 = 925 ms, and TE = 4.15 ms. DTI parameters: twice-refocused echo-planar imaging b = 0, 1000, 2000, 60 diffusion encoding directions, TR = 6100 ms, TE = 101 ms, FOV = 222 x 222 mm^2, matrix = 82 x 82, 2.7 mm slice thickness, and 45 axial slices.

Structural connectome construction

Each participant's individual connectome was built from the neuroimaging data using the following steps: 1) T1 weighted images were segmented into probabilistic grey and white matter maps using SPM12's unified segmentation-normalization; 2) each individual's grey matter map was divided into 1358 regions using the Atlas of Intrinsic Connectivity of Homotopic Areas (AICHA) brain atlas [59]; 3) the grey matter parcellation maps were non-

linearly registered into the diffusion imaging (DTI) space; 4) pairwise probabilistic DTI fiber tracking was computed for all possible pairs of grey matter regions (further details on the DTI tractography parameters below); 5) the weight of each pairwise connectivity link was determined based on the number of probabilistic streamlines connecting the grey matter region pair, corrected by distance travelled by each streamline and by the total volume of the connected regions; and 6) a weighted adjacency matrix M of size 1358 x 1358 was constructed for each participant with $M_{i,j}$ representing the weighted link between region of interest (ROI) *i* and ROI *j*.

Tractography was estimated using FSL's FMRIB's Diffusion Toolbox (FDT) probabilistic method[60] with FDT's BEDPOST being used to assess default distributions of diffusion parameters at each voxel, and probabilistic tractography was performed using FDT's probtrackX (parameters: 5000 individual pathways drawn through the probability distributions on principal fiber direction, curvature threshold set at 0.2, 200 maximum steps, step length 0.5mm, and distance correction). The waypoint mask was set as the white-matter probabilistic map. The weighted connectivity between the regions *i* and *j* was defined as the number of probabilistic streamlines arriving at *j* region when *i* was seeded, averaged with the number of probabilistic streamlines arriving at *i* region when *j* was seeded. The connection weight was corrected based on the distance travelled by the streamlines connecting *i* and *j* (probtrackX's "distance correction"). The number of streamlines connecting each pair of regions was further divided by the sum of the volumes of these regions. In summary, each individual connectome was represented by a 1358 x 1358 matrix, where the nodes corresponded to the AICHA anatomical regions and the edges to the structural connectivity between the nodes.

Network analysis

Connectome density

We assessed the overall connectivity of the networks by calculating the connectome density for each subject, which is defined as the ratio of all connections that exist in the network to all possible connections. Specifically, we assessed the total number of connections in the connectome and divided this by the number of possible connections. As such, a density of 100% indicates a highly connected network, where all potential connections exist. We then compared the connectome density of participants with vs. without CV risk factors.

To determine which fibers were disproportionately lost, we calculated the percentage of short-, mid- and long- range white matter fibers. First, we calculated the Euclidean distance between each pair of node centroids in each connectome and designated all fibers with lengths below the 1st quartile (lowest 25%) "short distance" fibers, and all fibers with lengths above the 3rd quartile (75% and above) "long distance" fibers. Mid-range fibers had lengths above the 1st quartile and below the 3rd quartile (25-75%). We determined the proportion of all existing connections in each connectome that were either short, mid, or long-distance fibers. To determine the effect of CV risk factors on short-, mid- and long-range white matter connectivity, we assessed differences in the percentage of short, mid and long-distance fibers between participants with vs. without CV risk factors.

Connectome Measures

We extracted graph theoretical measures of network organization and efficiency using the Brain Connectivity Toolbox[61].

Each connectome was partitioned into communities or modules by optimizing Newman's modularity algorithm[25]. Modularity (Q) is a value that quantifies the strength of the network's modular organization by identifying groups of nodes that have stronger intra-community coherence than inter-community coherence. Figure 1 provides a neuroanatomical overview of the parcellation scheme (A-D), how modules are calculated (E-H); where ROIs of the same color belong to the same module, and an example module and connectivity profile (G-H) of the pre-motor module.

We also calculated global network efficiency, which quantifies the ease of information flow in the network and is the computed as the inverse of the shortest path length between two nodes[62].

Statistical analyses

We performed general linear regression analyses to determine the effect of fiber loss on verbal IQ, with verbal IQ as the dependent variable, and whole brain fiber density as the predictor variable. We also constructed a second model to adjust for key covariates with whole brain fiber density, age, CCI, education, and physical activity (CHAMPS) predicting verbal IQ. We did not account for gender because the cohort was predominantly made up of women (80%).

For each subject's connectome, we extracted the global efficiency, modularity score, and the optimal community structure that indicates to which communities each ROI belongs. Due to stochasticity of network partitioning, which may lead to assignment of

ROIs to different communities with every run, we performed 100 runs of modularity assessment function for each individual and used the mean as the modularity score. To determine differences in network topology we performed a two-tailed t-test that compared the modularity scores of participants with vs. without CV risk factors. We also explored the community structure of three exemplar participants; one healthy control, a participant with only 1 CV risk factor, and one with all 3 CV risk factors. Finally, to determine the effect of fiber loss on network topology and efficiency, we performed Pearson correlation analyses between whole brain fiber density, and whole brain modularity and global efficiency. All statistical analyses were performed using MATLAB. The statistical significance was set at $p \leq 0.05$ (two-sided), and the p-values were Bonferroni corrected at $p \leq 0.05$.

Results

Participant demographics

Table 1 provides the descriptive statistics of the participants included in this study.

Relationship between connectome density and verbal IQ

Our model revealed that connectome density alone accounted for about 23% of the variance in predicting verbal IQ: $F(1,60) = 18.7$, $p < 10^{-4}$, adjusted $R^2 = 0.23$. When age, years of education, CV risk factor burden, and level of physical activity were added, connectome density ($p = 0.004$), years of education ($p < 10^{-6}$) and CCI ($p = 0.05$) were significant predictors and accounted for about 60% the variance in predicting verbal IQ: $F(5,60) = 18.2$, $p< 10^{-9}$, adjusted $R^2 = 0.59$. Physical activity ($p = 0.31$), and age ($p = 0.29$) were not significant predictors in the model.

Pearson correlations revealed that connectome density was significantly correlated with verbal IQ scores ($r = -0.49$, $p < 10^{-4}$ - figure 2a, 1st panel), such that subjects with densely connected networks performed better in the behavioral task, while subjects who had lost some fiber connections performed worse. The relationship was still significant even when controlling for other significant predictors of verbal IQ; for example, years of education ($r = 0.45$, $p < 10^{-3}$), and CCI ($r = 0.42$, $p < 10^{-3}$). The models were still significant when correcting for multiple comparisons ($p = 0.025$).

Effect of CV risk factors on connectome density and long-range white matter connectivity.

There was decreased connectome density in participants with CV risk factors, and a significant difference between participants with no CV risk factor, and the cumulative morbidity group (figure 2c, 1st panel - left hemisphere, $t(38) = 2.0470$, $p = 0.048$; right hemisphere, $t(38) = 2.1154$, $p = 0.041$).

Across all subjects, 54.4%, 40.1%, and 4.9% of all fibers were classified as short, medium, or long-range fibers respectively. Subjects without CV risk factors had 54.3% short fibers; participants with at least one CV risk factor had 54.7% short fibers while participants with cumulative morbidities had 58.3% short fibers. There was a significant difference in the number of short fibers between healthy controls and participants with cumulative morbidities ($p = 0.017$).

Subjects without CV risk factors had 40.3% medium fibers compared to 39.9% among participants with at least one CV risk factor and 37.6% among participants with cumulative morbidities. There was a significant difference in the number of medium fibers between healthy controls and participants with cumulative morbidity, $p = 0.015$.

Subjects without CV risk factors had 5.0% long fibers while participants with at least one CV risk factor and participants with cumulative morbidities had 4.9% and 3.4% long fibers, respectively. There was a significant difference in the number of long fibers between healthy controls and participants with cumulative morbidity, $p = 0.028$.

These results indicate an overall loss of mid- and long-range connections due to multiple CV risk factors. The results were significant when correcting for multiple comparisons ($p = 0.02$).

Effect of fiber loss on network topology and efficiency

There was a significant correlation between connectome density and modularity ($r = -0.52$, $p < 10^{-4}$), and connectome density and global efficiency ($r = 0.91$, $p < 10^{-20}$) – figure 2a, panels 2 and 3. Furthermore, examination of community structures revealed a fragmentation pattern in both hemispheres of participants with CV risk factors. Figure 2b shows three example participants: 1 participant without CV risk factors, 1 participant with only 1 CV risk factor, and 1 participant with all 3 CV risk factors. There is a gradual decrease in the number of connections, or an increasing sparsity of the networks, and an increase in the number of modules (a fragmentation of the network) from the control on the left, to the participant with cumulative morbidities on the right. Likewise, there was an increase in the left and right hemisphere modularity scores with increasing CV risk factor burden (left hemisphere, $t(38) = -3.6039$, $p < 10^{-3}$; right hemisphere, $t(38) = -3.2001$, $p = 0.0028$) (figure 2c – 2nd panel). The results were significant when correcting for multiple comparisons ($p = 0.01$).

Discussion

We examined the relationship between CV risk factors, the integrity of axonal fibers, and verbal IQ using structural connectomes from a cohort of participants with various degrees of CV risk factors. Our results supported our hypothesis that high CV risk factor burden would be associated with loss of energy dependent long axonal projections, leading to lower verbal IQ. This suggests that CV risk factor burden is associated with loss of longer-range white matter fibers, disruption of network architecture and efficiency, and lower cognitive performance. Network density alone predicted 23% of cognitive performance and including sociodemographic and health variables increased the prediction accuracy to 60%. We found that participants with CV risk factors showed network disruption and a reduction in network density. We further demonstrated a relationship between CV risk factors, brain integrity and functional outcomes, indicating that white matter integrity is one potential approach to measure brain health since it is associated with both CV risk factor status and cognitive performance.

White matter is more vulnerable to injury due to hypoperfusion compared with grey matter [63], with lower collateral blood supply in the deep white matter. For this reason, CV risk factors, particularly hypertension and diabetes mellitus, lead to microangiopathic white matter injuries that are conspicuously observed on routine MRIs in individuals with CV risk factors or in the elderly. These are commonly referred to as cerebral small vessel disease (SVD) [64] and are directly associated with amyloid angiopathy, atherosclerosis, and arteriolosclerosis [65]. Cerebral small vessel disease can be detected on routine MRIs by white matter hyperintensities (WMH) and their progressive accumulation has been shown to be associated with the development of low white matter and low brain volume, dementia, mood disturbances and gait problems [66]. The Radboud University Nijmegen Diffusion

Tensor and Magnetic Resonance Cohort (RUN DMC) study prospectively assessed 503 individuals with SVD and observed that a high WMH volume was associated with a hazard ratio of 1.8 for the development of parkinsonism, most commonly vascular parkinsonism [67]. In the same cohort (503 subjects from the RUN DMC study), the investigators observed a 5.5-year cumulative risk of 11.1% of developing dementia, with white matter volume, WMH, and hippocampal volume explaining most of the variance [68]. The same group also observed that SVD affecting fronto-subortical regions was more common in individuals with depressive symptoms [69].

Interestingly, the associations described above are well-defined in cases of high or cumulative SVD burden, but in most cases, WMH are incidental findings on MRI and their clinical significance is vastly unknown [66]. They likely represent the early manifestation of an insidious process whose consequences remain subclinical until a threshold of structural compromise is reached. The ability to accurately detect these changes in an early stage could lead to strategies to inform decisions about their significance, progression and treatment. Diffusion MRI is a promising technique for this goal since ongoing technological developments have increased its sensitivity to small changes in tissue and white matter microstructure [70]. However, the findings from early studies were not able to definitely conclude whether they added benefit over the simple volume of WMH. For example, in the dementia study cited above, the authors concluded that Tract-Based Spatial Statistics (TBSS), which is a form of quantification of scalar diffusion parameters along the core of white matter pathways, did not reveal additional benefit in predicting dementia [68]. Similarly, the depression study did not observe an additional benefit of radial diffusivity after additional adjustment for WMH and lacunar infarcts [69]. Nonetheless, several more

recent studies have started to disclose the important role of diffusion MRI in identifying subtle white matter changes in the context of SVD. As part of the PRESERVE DTI study, Croall and colleagues observed that after normalization for brain volume, WMH, lesion load, number of lacunes, and scalar diffusion measures such as fractional anisotropy and mean diffusivity were significantly associated with multiple cognitive domains, such as verbal fluency, mental flexibility and cognition [71]. Moonen and colleagues, as part of the DANTE Study Leiden, observed that lower fractional anisotropy in white matter was associated with executive functioning after adjustment for normalized brain volume, but diffusion measures were not associated with mood scores[72]. Ciulii and colleagues observed that a predictor model built on white matter mean diffusivity could forecast executive function (Trail Making Test performance) in patients with mild cognitive impairment and SVD with an accuracy of 77.5%-80.0% [73].

It is important to emphasize that the more recent studies mentioned above were performed using scalar measures (i.e., voxel wise metrics) of diffusion MRI, such as fractional anisotropy and mean diffusivity, whereas modeling of white matter networks and circuitry topology using diffusion tractography is the subsequent step to determine the complexity of brain networks. In a pilot study, Xie and colleagues demonstrated that depressive symptoms in patients with SVD were associated with impairment of global network efficiency, and lower nodal efficiency in several brain regions [74]. More similarly to our approach, Tuladhar and colleagues demonstrated that SVD patients had less dense networks, with lower network strength and efficiency, and with reduced connectivity between hub (rich club) regions [75]. This study did not test the relationship between white matter topology and cognitive symptoms but proposed their likely association.

Our study builds on the literature discussed above, combined with a risk factor determinant, and functional consequence to assess their tri-partite association: CV risk factors <-> white matter integrity <-> functional performance.

We observed that CV risk factors were associated with reduced density. Connectome density gauges how well the network is connected and informs on the wiring or physical cost of connecting the network. Biological networks are sparsely connected, where only a fraction of possible connections occur. For instance, cortical fiber tract connectivity in mammalian brains is between 10 and 30%[24]. Density is dependent on the overall number of white matter projections and we observed that CV risk factors were associated with a reduction in connectome density, i.e., white matter fiber loss in general, with a disproportionate loss of longer connections. The human brain, even at rest, consumes about 20% of energy while making up only 2% of the human weight. The energy consumed goes into generating action potentials, neurotransmitter release and recycling, however a large portion of the energy goes into maintaining resting potentials via active transport of ions across the membrane (about 28% for neurons) [11]. The cost of forming and maintaining these connections increases with increasing surface area, volume, length and activity such that longer fibers are costlier, occupy more space, and generally require more energy. This suggests that to conserve energy and space, most connections in the brain should be short range (as supported by our analysis, 54.4% short range fibers, 40.1% mid-range fibers and 4.9% long range fibers). However, minimizing energy costs must also be balanced against maintaining an efficient topological organization that allows for efficient information processing and transfer. Therefore, the inherent segregation or increased connectivity within modules (that utilizes short distance connections) must be accompanied by

integration or communication between the modules, (that utilizes long distance connections), to allow for a globally efficient topology. We observed a significant loss of long-distance fibers in participants with CV risk factors, which led to a disruption of their topological organization and lowering of their overall network efficiency.

We posit that decreased connectome density, and the loss of long-distance fiber connections in particular led to the observed fragmentation pattern and lowered efficiency of the white matter networks, which was in turn associated with lower verbal IQ. The association between density and verbal IQ remained significant even when accounting for potential confounders such as years of education and age.

The topological organization of brain networks is thought to provide an insight into efficient cognitive processing of the brain, where high intra-modular connectivity favors local processing and functional specialization, and connectivity between modules favors global integration [76]. However, deviations from this optimal structure either with increased or decreased clustering may be the underlying cause or consequence of many cognitive and psychiatric disorders. Of note is that we cannot determine causality as this was a single cross-sectional study, however, we observed that loss of long-range fiber connections resulting from CV risk factors was associated with deviations from this optimal topological architecture that signifies a healthy brain.

Figures

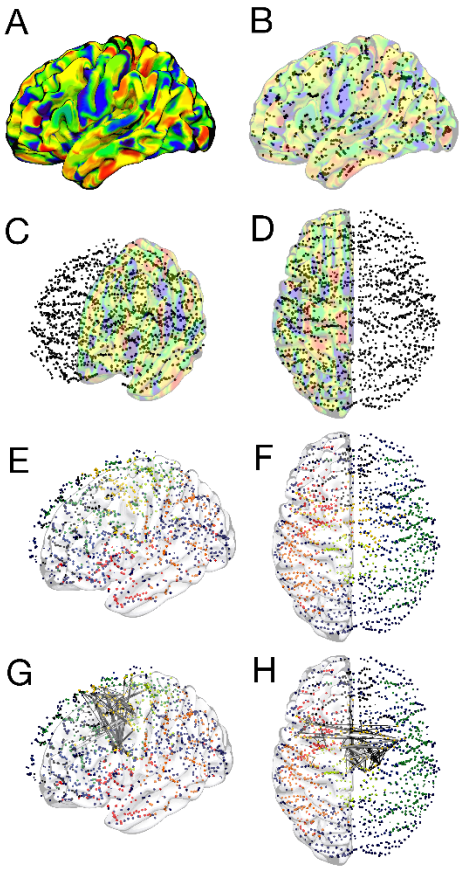

Figure 1. The grey matter regions are divided into 679 regions of interest (ROIs) in each hemisphere, corresponding to neuroanatomical boundaries defined by a parcellation atlas (A, where ROIs are indicated by different colors). To facilitate visualization of networks, each ROI can be represented by a sphere in the ROI's center of mass (B, C, and D). Modularity is calculated by assessing the ROIs that are more closely integrated by their white matter networks, and relatively segregated from the other surrounding modules.

Using the example of one subject, In E,F, G and H, the ROIs that belong to the same module are represented using the same color (i.e., all ROIs in yellow belong to the same module, which is different than the module containing ROIs in green, and so on). G and H demonstrate the edges corresponding to the white matter networks integrating one module (with ROIs in yellow), largely representing pre-motor circuitry.

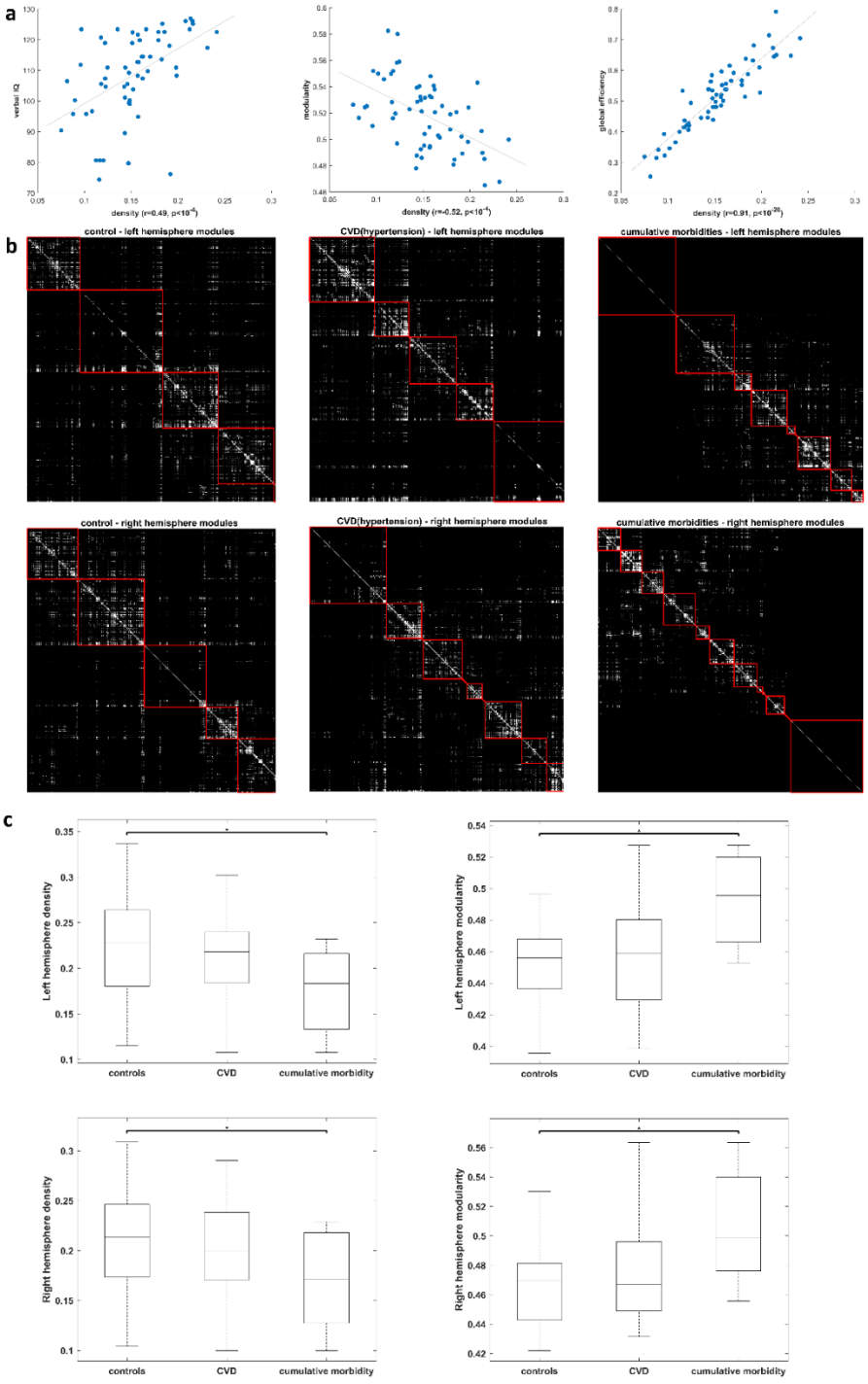

Figure 2a. Panel 1 - correlation between density and verbal IQ ($r = 0.49$, $p < 10^{-4}$). Panel 2 -correlation between density and modularity ($r = -0.52$, $p < 10^{-4}$). Panel 3 - correlation between density and global efficiency ($r = 0.91$, $p < 10^{-20}$),
2b. Exemplar data – number of modules detected in the left and right hemispheres of one healthy control, 1 participant with CV risk factors (hypertension), and 1 participant who had all CV risk factors. Note the breakdown and increased number of modules (or fragmentation of the community structure) with increasing number of CV risk factors. Also note decreasing density with increasing CV risk factors, with the complete loss of connections in the participant with cumulative morbidities.
2c. Panel 1- effect of CV risk factors on density. Decreasing left and right hemisphere density with increasing number of CV risk factors. Significant difference in density between controls and cumulative morbidity ($p = 0.048$), ($p = 0.041$) respectively. Panel 2 - effect of CV risk factors on modularity. Increasing left and right hemisphere modularity with increasing number of CV risk factors. Significant difference in modularity between controls and cumulative morbidity ($p < 10^{-3}$), ($p = 0.0028$) respectively.

Fibroblast growth factor 23 and brain health

3

Elevated levels of FGF23 confers adverse health outcomes and is associated with CVD, cerebrovascular calcification, risk of stroke and mortality. The public health relevance of relevance of this problem is timely since one of the mechanisms leading to elevated FGF23 is the consumption of phosphate, typically present in elevated concentrations in processed foods that are high in phosphate-based preservatives which are cheaper, copious in food deserts and consumed by people with fewer resources. This dietary disparity may be directly associated with the disparities in health outcomes in neurology, mediated through FGF23.This knowledge could be used to change policies related to food products and dietary recommendations, and lead to targeted interventions concerning personal dietary habits that may lower decline of brain health, prevent strokes or improve recovery after stroke.

This chapter, based on the following peer-review publication[77], demonstrates the link between elevated FGF23 and brain health:

Marebwa BK, Adams RJ, Magwood GS, et al. Fibroblast growth factor23 is associated with axonal integrity and neural network architecture in the human frontal lobes. PloS one 2018;13:e0203460.

Abstract

Elevated levels of FGF23 in individuals with chronic kidney disease (CKD) are associated with adverse health outcomes, such as increased mortality, large vessel disease, and reduced white matter volume, cardiovascular and cerebrovascular events. Apart from the well-known link between cardiovascular (CV) risk factors, especially diabetes and hypertension, and cerebrovascular damage, elevated FGF23 is also postulated to be associated with cerebrovascular damage independently of CKD. Elevated FGF23 predisposes to vascular calcification and is associated with vascular stiffness and endothelial dysfunction in the general population with normal renal function. These factors may lead to microangiopathic changes in the brain, cumulative ischemia, and eventually to the loss of white matter fibers. The relationship between FGF23 and brain integrity in individuals without CKD has hitherto not been investigated. In this study, we aimed to determine the association between FGF23, and white matter integrity in a cohort of 50 participants with varying degrees of CV risk burden, using high resolution structural human brain connectomes constructed from MRI diffusion images. We observed that increased FGF23 was associated with axonal loss in the frontal lobe, leading to a fragmentation of white matter network organization. This study provides the first description of the relationship between elevated levels of FGF23, white matter integrity, and brain health. We suggest a synergistic interaction of CV risk factors and FGF23 as a potentially novel determinant of brain health.

Introduction

Fibroblast growth factor-23 (FGF23) is an osteocyte derived phosphaturic hormone that regulates calcium-phosphate and vitamin D metabolism by activating the FGF receptor-α-klotho complex in the kidney[78]. FGF23 induces phosphaturia by decreasing renal reabsorption of phosphate in the proximal tubule, and inhibiting calcitriol (hormonally active metabolite of vitamin D) synthesis[78, 79]. Calcitriol functions to increase calcium and phosphate levels in the blood by increasing kidney and gastrointestinal absorption and increasing calcium and phosphate release from bone into the blood through bone resorption. Calcitriol inhibition by FGF23 induces calcium deficiency resulting in even more production of calcium from the bone. Excess circulating calcium eventually leads to arterial and vascular calcification[80]. Chronic Kidney Disease (CKD) is possibly the most common cause of elevated FGF23, which has been implicated in increased cardiovascular mortality of CKD patients. Elevated FGF23 is also associated with cardiovascular disease, left ventricular hypertrophy [81, 82], and is a putative indicator of Cardiovascular (CV) risk factors [83]. Apart from CKD, high phosphorous diet stimulates FGF23 production, leading to elevated levels of FGF23 [84]. Even among individuals without CKD, elevated levels of FGF23 have been postulated to increase the risk of stroke [85]. Nonetheless, the effects of elevated FGF23 on brain health in non-stroke individuals have not fully been determined. Compared with brain gray matter, white matter is significantly more susceptible to small vessel ischemic injury because it receives less perfusion when adjusting for metabolic demands, due to lower collateral blood supply to deep white matter [63]. Moreover, the maintenance of structural integrity of medium to long range axonal projections is metabolically demanding. For these reasons, we postulated that FGF23 would lead to white

matter compromise particularly within the brain areas with long cortico-cortical, or cortico-subcortical axonal projections, such as the frontal lobes.

We therefore aimed to identify the effects of FGF23 independent of kidney disease by studying a prospective cohort with normal kidney function, but with CV risk factors that included diabetes, hypertension, and hyperlipidemia. We employed the novel neuroimaging method of the high-resolution human brain connectome to fully map white matter networks across the entire brain. We aimed to determine the relationship between FGF23 and neuronal network integrity, with the goal of elucidating the mechanistic aspects related to the impact of FGF23 on brain health. We postulated a synergistic interaction of CV risk factors and FGF23 as a determinant of brain health.

Methods

Participants

We recruited 51 older participants, (40 females, mean age 55.3 ± 8.6 years) without a history of neurological or psychiatric diseases from the local community through advertisement. All participants were self-reported cognitively normal adults. There were 23 African American and 28 white participants. Twenty-eight participants did not have a history of cardiovascular risk factors, while 23 participants had previously been diagnosed with at least one CV risk factor (CV group): diabetes (11 participants), hyperlipidemia (15 participants), and hypertension (16 participants). Six participants had been diagnosed with all CV risk factors. These diagnoses were obtained through medical chart review. The Charlson Comorbidity Index[57] (CCI) was calculated for all participants, including a diagnosis of hypertension and hyperlipidemia at a score of one each to the overall score.

BMI and smoking history were not available for all participants and therefore not included in the analyses. Participants were stratified into two groups: CV risk factor and normal controls based on a previous diagnosis of a cardiovascular disease. One participant had chronic kidney disease and was therefore excluded from further analysis. All participants included in the analysis had normal renal function. The study was approved by the Institutional Review Boards at the Medical University of South Carolina. Written informed consent was obtained from all participants, as approved by our institutions' IRB.

FGF23 Acquisition

Circulating FGF23 was measured using the Human FGF23 ELISA kit from Millipore (EZHFGF23-32K). Samples were collected in EDTA containing tubes and centrifuged at 2-3K to obtain the plasma. Samples were prepared as described by the manufacturer and the concentrations of FGF23 were determined from the standards provided. FGF23 is presented as pg/ml of plasma.

Image Acquisition

Imaging was performed on a Siemens 3T TIM trio MRI scanner located at the Medical University of South Carolina. We used volumetric T1-weighted and Diffusion images collected from each participant. T1 parameters: MPRAGE sequence with 1 mm isotropic voxels, 256x256 matrix size, and a 9-degree flip angle. We used a 192-slice sequence with TR = 2250 ms, T1 = 925 ms, and TE = 4.11 ms. DTI parameters: twice-refocused echo-planar imaging b = 0, 1000, 30 diffusion encoding directions, TR = 8500 ms, TE = 98 ms, FOV = 222 x 222 mm2, matrix = 74 x 74, 3 mm slice thickness, and 40 axial slices.

Structural connectome construction

Each participant's individual high-resolution structural connectome was built from structural T1 and diffusion tensor imaging (DTI) neuroimaging data using the following steps: 1.T1 weighted images were spatially registered into standard space and segmented into probabilistic grey and white matter maps using SPM12's unified segmentation-normalization; 2.Each individual's grey matter map was divided into 1358 approximately evenly sized regions using the Atlas of Intrinsic Connectivity of Homotopic Areas (AICHA) brain atlas [59]; 3.The grey matter parcellation maps were then non-linearly registered into the diffusion imaging (DTI) space, and pairwise probabilistic DTI fiber tracking was computed for all possible pairs of grey matter regions 4. The weight of each pairwise connectivity link was determined based on the number of probabilistic streamlines connecting the grey matter region pair, corrected by distance travelled by each streamline and by the total volume of the connected regions. Finally, a weighted adjacency matrix M of size 1358 x 1358 was constructed for each participant with $M_{i,j}$ representing the weighted link between region of interest (ROI) *i* and ROI *j*. Tractography was estimated through the software FSL FMRIB's Diffusion Toolbox (FDT), including eddy current correction, motion correction[86], and probabilistic method [60] with BEDPOST being used to assess default distributions of diffusion parameters at each voxel, and probabilistic tractography was performed using FDT's probtrackX (parameters: 5000 individual pathways drawn through the probability distributions on principal fiber direction, curvature threshold set at 0.2, 200 maximum steps, step length 0.5mm, and distance correction). The weighted connectivity between the regions *i* and *j* was defined as the number of probabilistic

streamlines arriving at *j* region when *i* was seeded, averaged with the number of probabilistic streamlines arriving at *i* region when *j* was seeded.

Figure 1 provides a workflow of the connectome construction process and network analysis.

Modular organization detection

The integrity of neuronal network architecture can be assessed through the quantification of the modular parcellation of the network (modularity). Modularity provides a measurement of the balance between segregation and integration of the network in its entirety, or within regional sub-networks. This balance is known to be a fundamental principle in biological network organization, including neuronal networks [22]. Our analysis was based on the modular organization of each brain region for every participant. For each participant the whole brain connectome was divided into the left and right frontal, temporal, parietal, and occipital lobe sub-networks. The lobe sub-networks were assessed regarding their modularity using Newman's modularity algorithm [25] implemented in the Brain Connectivity Toolbox [61], (e.g. [Ci,Q] = modularity_und(W), where W is the weighted undirected connectivity matrix; gamma was maintained at the default: gamma = 1).

Statistical analyses

For each group (CV risk factor and healthy controls), we performed general linear regression analysis to examine the relationship between brain integrity and FGF23, adjusting for key covariates –sex, race, and CCI. Linear regressions were modelled for each

group separately to minimize noise inherent in the healthy control group, and to avoid type II error. Brain integrity measured via modularity was set as the dependent variable, and FGF23, sex, race and CCI as the predictor variables. We used this model to determine the association between FGF23, and the integrity of each brain region (modularity scores for the frontal, temporal, parietal and occipital regions) for both left and right hemispheres. Linear correlations were evaluated using a two-tailed Pearson correlation coefficient. We evaluated the association between FGF23 and modularity of the left and right frontal hemispheres. Correlation was performed independently on the CV risk factor group and the control group.

We further assessed the overall connectivity of the frontal lobe by calculating the density; a measure of axonal integrity; as the number of all connections present. We then determined the relationship between FGF23 and fiber density of the left and right hemisphere frontal regions.

Of the 22 participants with CV risk factors, 17 had serum creatinine scores from the latest available comprehensive metabolic panel obtained from the hospital. We re-calculated the Pearson correlation for these participants, with partial correlations accounting for the creatinine score. Natural log transformed FGF23 scores were used in all analyses. All statistical analyses were performed using MATLAB. The statistical significance was set at $p \leq 0.05$.

Results

To account for possible confounding by age, sex and race, we determined the association between these factors and FGF23. Pearson analysis revealed no correlation between age and FGF23 ($r = 0.13$, $p = 0.17$), and student's t-test revealed no differences in FGF23 levels

between female and male participants two-sample t(48) = 0.91, p = 0.37, or between African American and Caucasian participants two-sample t(48) = 0.53, p = 0.6. There was also no significant difference in FGF23 levels between the control and CV risk factor groups, two-sample t(48) = 0.69, p = 0.49.

Relationship between modularity and FGF23

Our model revealed that FGF23 was associated with left hemisphere frontal lobe modularity in the CV risk factor group: $F(4,22) = 4.2$, $p = 0.015$, adjusted $R^2 = 0.38$. FGF23 was not associated with brain integrity among individuals without CV risk factors. In that group, brain integrity was associated with sex, race and CCI (table 1). A model of only FGF23 (predictor variable) and left hemisphere frontal lobe modularity (dependent variable) revealed that FGF23 levels alone accounted for about 29% of brain integrity in the left hemisphere frontal lobe of participants with CV risk factors: $F(1,22) = 9.46$, $p = 0.006$, adjusted $R^2 = 0.29$, while the same was not observed in the control group: $F(1,22) = 0.6$, $p = 0.45$, adjusted $R^2 = 0.015$.

Linear correlations revealed that left hemisphere frontal lobe modularity was significantly correlated with FGF23 (figure 2a left panel) in participants with CV risk factors, such that higher modularity was associated with higher FGF23 levels ($r = 0.57$, $p = 0.006$). This association was also significant when controlling for creatinine levels ($n = 17$) (partial correlation controlling for creatinine: $r = 0.48$, $p = 0.03$). In the control group, the left hemisphere frontal lobe modularity was not associated with FGF23 levels (figure 2a right panel, $r = 0.05$, $p = 0.4$).

Table 1a: Multiple linear regression models for modularity in participants with cardiovascular risk factors.

Outcome	**Model**	**Variables**			
		FGF23	Gender	Race	CCI

			Female vs male	White vs black	
LH frontal					
Adj.R^2=0.38	B (SE)	0.03 (0.01)	-0.06 (0.03)	-0.01 (0.03)	0.02 (0.01)
F=4.20	β	0.52*	-0.43*	-0.10	0.31
RH frontal					
Adj.R^2=0.21	B (SE)	0.02 (0.02)	-0.05 (0.04)	0.01 (0.04)	0.04 (0.02)
F=2.40	β	0.17	-0.26	0.05	0.55*
LH parietal					
Adj.R^2=0.12	B (SE)	-0.02 (0.02)	-0.01 (0.04)	0.09 (0.04)	-0.01 (0.02)
F=1.72	β	-0.25	-0.07	0.57*	-0.10
RH parietal					
Adj.R^2=0.03	B (SE)	-0.01 (0.02)	-0.05 (0.03)	0.03 (0.03)	0.01 (0.01)
F=1.19	β	-0.18	-0.36	0.23	0.14
LH temporal					
Adj.R^2=-0.12	B (SE)	-0.00 (0.01)	-0.02 (0.02)	-0.01 (0.02)	0.01 (0.01)
F=0.44	β	-0.07	-0.22	-0.10	0.30
RH temporal					
Adj.R^2=0.12	B (SE)	0.01 (0.01)	-0.05 (0.03)	0.01 (0.03)	0.01 (0.03)
F=1.70	β	0.11	-0.44	0.04	0.34
LH occipital					
Adj.R^2=0.22	B (SE)	-0.01 (0.01)	-0.02 (0.03)	0.07 (0.03)	0.01 (0.01)
F=2.49	β	-0.21	-0.18	0.55*	0.10
RH occipital					
Adj.R^2=-0.10	B (SE)	0.01 (0.01)	-0.01 (0.03)	0.02 (0.03)	0.01 (0.01)
F=0.51	β	0.12	-0.07	0.20	0.12

*p < .05. **p < .01.

B=parameter estimate, SE=standard error, β= standardized estimate, CCI = Charlson Comorbidity Index, LH=left hemisphere, RH=right hemisphere

Table 1b: Multiple linear regression models for modularity in healthy controls.

Outcome	**Model**	**Variables**			
		FGF23	Gender Female vs male	Race White vs black	CCI
LH frontal					
Adj.R^2=0.38	B (SE)	0.03 (0.01)	-0.06 (0.03)	-0.01 (0.03)	0.02 (0.01)
F=4.20	β	0.52	-0.43	-0.10	0.31
RH frontal					
Adj.R^2=0.32	B (SE)	0.02 (0.01)	0.08 (0.04)	0.10 (0.03)	0.02 (0.01)
F=4.12	β	0.17	0.29	0.62**	0.20
LH parietal					
Adj.R^2=0.23	B (SE)	-0.01 (0.02)	0.10 (0.06)	0.11 (0.04)	0.03 (0.02)
F=2.97	β	-0.04	0.31	0.52**	0.27
RH parietal					
Adj.R^2=0.15	B (SE)	0.01 (0.02)	0.12 (0.07)	0.11 (0.04)	0.03 (0.02)
F=2.21	β	0.06	0.32	0.47	0.22
LH temporal					
Adj.R^2=0.49	B (SE)	0.02 (0.01)	0.02 (0.03)	0.08 (0.02)	0.04 (0.01)
F=7.48	β	0.20	0.08	0.57**	0.50**
RH temporal					
Adj.R^2=0.06	B (SE)	0.01 (0.01)	0.01 (0.04)	0.05 (0.02)	0.01 (0.01)
F=1.45	β	0.18	0.07	0.40	0.18
LH occipital					
Adj.R^2=0.31	B (SE)	-0.01 (0.01)	0.06 (0.03)	0.03 (0.02)	0.03 (0.01)
F=4.08	β	-0.20	0.37*	0.24	0.49**
RH occipital					
Adj.R^2=0.23	B (SE)	0.01 (0.01)	-0.02 (0.03)	0.05 (0.02)	0.02 (0.01)
F=3.07	β	0.16	-0.12	0.47*	0.24

*p < .05. **p < .01.

B=parameter estimate, SE=standard error, β=standardized estimate, CCI = Charlson Comorbidity Index, LH=left hemisphere, RH=right hemisphere

Relationship between density and FGF23

Frontal Lobe

There was a significant correlation between the left frontal lobe density and FGF23 (figure 2b left panel) in participants with CV risk factors such that participants with elevated FGF23 had fewer fiber connections in their left frontal lobe ($r = -0.42$, $p = 0.05$). We further calculated correlation on 17 participants with creatinine scores (partial correlation controlling for creatinine: $r = -0.40$, $p = 0.07$). An association was not observed in the left frontal hemisphere of participants without CV risk factors ($r = -0.04$, $p = 0.58$, figure 2b right panel).

Discussion

In this study, we aimed to determine the relationship between CV risk factors, FGF23 levels, integrity of axonal fibers, and white matter network topological organization. We employed high resolution structural connectomes constructed from diffusion imaging to measure individual network integration and segregation via modularity. We hypothesized that elevated FGF23 levels would be associated with the reduction of white matter fiber connections, and loss of organization (fragmentation) of white matter networks. We demonstrated a relationship between FGF23 and left frontal lobe network integrity, and showed that in participants with CV risk factors, FGF23 levels accounted for up to 29% of left hemisphere frontal lobe network integrity, meaning that participants with elevated FGF23 levels and CV risk factor burden had higher modularity scores, indicating a disruption of the brain network organization. Sex, race, and CCI explained a further 9% of left frontal lobe integrity. FGF23 was not significantly associated with brain integrity in

participants without CV risk factors, although race, sex and CCI were significantly associated with brain integrity in this group.

Our results complement and help explain previous findings suggesting that elevated FGF23 is associated with stroke and small vessel disease (SVD) independent of CKD. SVD is routinely observed in normal ageing or individuals with CV risk factors and discovered incidentally on routine MRIs by white matter hyperintensities (WMH). The Northern Manhattan study (NOMAS) prospectively assessed 2,525 individuals from a racially diverse population and concluded that elevated FGF23 conferred an overall risk of stroke and intracerebral hemorrhage independent of CKD[85]. In a subset of the same cohort, (n = 1170), they also showed that elevated FGF23 was associated with WMH, demonstrating a link between FGF23 and SVD in the absence of CKD[87]. The Professional Follow-up Study (n = 1261) further showed elevated FGF23 in individuals with established CV risk factors and higher dietary phosphate intake.

Our study builds on this previous literature by employing an approach that quantifies network integrity; and may detect subclinical structural compromise; to assess the tripartite association between CV risk factors, FGF23, and white matter integrity. We employed a fine-grained atlas to improve our statistical power, and for a more detailed connectome; we did not assess the effect of using functionally relevant atlases, although whole brain tractography did yield functionally relevant modules (figure 1 panel C)

We observed reduced network density, and a disorganization of the left frontal hemisphere network topology related to elevated FGF23, exclusively in participants with CV risk factors. Importantly, we showed that FGF23 is an independently associated with brain integrity in participants diagnosed with CV risk factors. Since FGF23 is a modifiable risk

factor, understanding this association may be an important step in reducing stroke incidences, stroke severity, and improving outcome after stroke. Brain integrity of normal ageing individuals was still explained by age and comorbidity (captured by CCI), sex, and race, although with the current limited sample size, we cannot conclusively draw any conclusions on the significance of sex and race.

The frontal hemisphere supports several cognitive processes including problem solving, memory, language, judgement, social behavior and impulse control. Therefore, the association between FGF23 and compromised structural integrity of the frontal lobe further provides an interesting first step towards understanding the impact of FGF23 on cognition. The fiber loss localized to the left hemisphere, indicating that the relationship between FGF23 and network fragmentation is restricted to the dominant hemisphere (all participants except 1in the CV group were right handed). This observation may indicate a more pronounced susceptibility to injury in the dominant hemisphere.

The limitations of this study are: 1) we did not assess the association between white matter network integrity and behavioral function since a comprehensive assessment of neuropsychological performance was not available in this cohort. We believe that this would be an important future direction, specifically testing the impact of FGF23 on cognitive control and executive function, which are frontal lobe dependent measures. 2) This is an initial pilot study with a relatively small sample size. Furthermore, the multiple linear regression models were not controlled for multiple comparisons, even though we did account for multiple confounders. 3) BMI and smoking history are important CV risk factors that were not included in the analyses. 4) Our cohort is made up of 80% women and is therefore not a not representative sample of the general population.

Based on the findings of this study, we believe that there are important possible future directions to continue to elucidate the impact of FGF23 on brain health, namely 1) the assessment of the cognitive impact of FGF23, and whether FGF23 leads to subclinical yet quantifiable cognitive compromise, particularly in frontal lobe functions; 2) the evaluation of the continuum between the impact of FGF23 on brain health across the spectrum ranging from normal kidney function to end-state CKD; 3) the assessment of the synergistic effects of FGF23 with other CV, electrolyte and kidney function biomarkers; and 4) the concurrent evaluation of connectome with other measures of brain integrity, including T2 weighted microangiopathic lesion burden.

In summary, we demonstrated the association between elevated serum FGF23, fiber loss and network disintegration in the frontal region of the left hemisphere. This relationship between FGF23 and brain integrity was noted in individuals without CKD, but with CV risk factors. We postulate a synergistic interaction of CV risk factors and FGF23 as a potentially novel determinant of brain health.

Figures

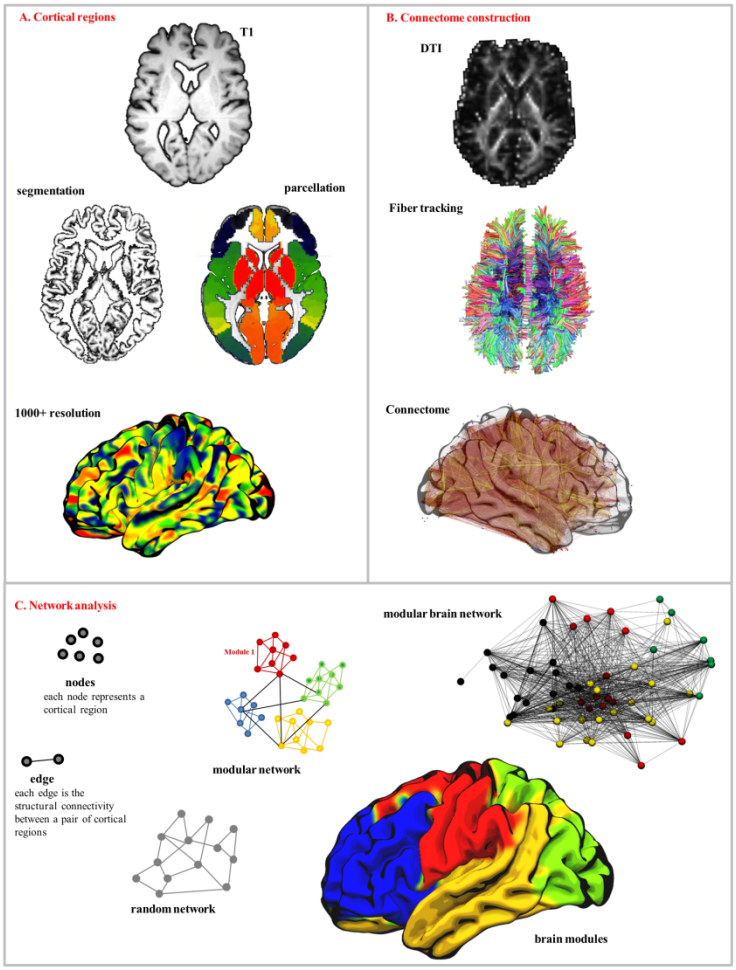

Fig 1. Connectome generation and network analysis. In A, the T1 image is normalized, and segmented (into CSF, gray and white matter). The gray matter is parcellated into 1358 regions of interest (ROI). The T1 is warped into diffusion space where fiber tracking occurs, finding the connections between each pair of ROIs, generating a connectome, or network of connectivity between all brain regions. C is an example of whole brain modular partition into modules using Newman's modularity algorithm, which groups ROIs that are more closely associated by their white matter networks and relatively segregated from surrounding groups (each module is represented by the same color).

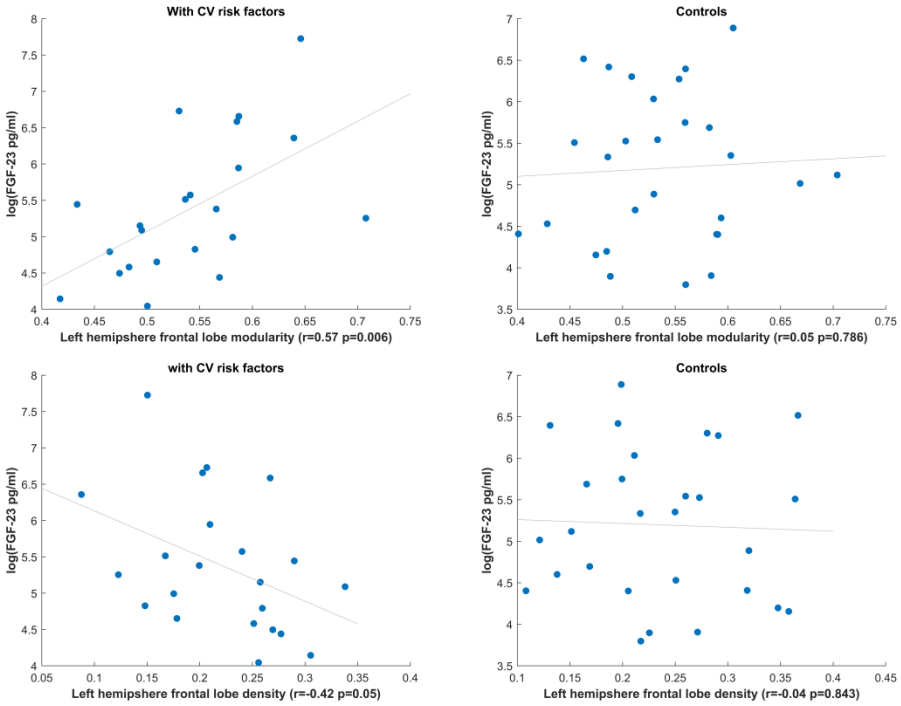

Fig 2a. Left panel – correlation between left hemisphere frontal lobe modularity and FGF23 in the CV risk factor group. Right panel – correlation between left hemisphere frontal lobe modularity and FGF23 in the control group.

Fig 2b. Left panel – correlation between left hemisphere frontal lobe density and FGF23 in the CV risk factor group. Right panel – correlation between left hemisphere frontal lobe density and FGF23 in the control group.

4 The impact of brain health on functional recovery in acute stroke

Prediction of functional recovery in the acute period after stroke is necessary especially for the development of more effective rehabilitation strategies. In this chapter, we examine the effect of brain health, determined by the presence of long-range fibers, on overall functional recovery after stroke.

This chapter is based on the following manuscript:

Marebwa BK, Adams RJ, Magwood GS, et al. Functional impairment in sub-acute strokes is related to damage in long-range white matter connections.

Abstract

Background Functional impairment after stroke is only partly explained by the size and the location of the lesion, age, and pre-stroke function. Brain plasticity and resilience to injury depends not only on the integrity of specific brain regions, but also on the organization of the connections between them. A balance between long- and short-range white matter connections is a marker of optimal topological network organization. We hypothesized fewer long-range fibers in individuals with worse functional outcomes, since long-range white matter fibers may be more vulnerable to ischemic injury from the stroke or from cumulative small vessel disease before the stroke.

Methods We assessed probabilistic white matter connections in 30 stroke survivors and determined the relationship between remote (non-affected hemisphere) integrity of long-

range white matter connections and functional impairment sub-acutely after stroke. Multivariate analyses were used to determine the relationship between long-range fibers and functional impairment measured through the Stroke Self-Efficacy Questionnaire (SSEQ), and the Stroke Impact Scale (SIS).

Results Lower values of long-range connections were associated with higher SIS scores (SIS-physical $R^2 = 0.35$, $p = 0.02$; SIS-mood $R^2 = 0.46$, $p = 0.003$; SIS-communication $R^2 = 0.25$, $p = 0.1$); SIS-memory $R^2 = 0.22$, $p = 0.15$, and lower SSEQ scores ($R^2 = 0.56$, $p = 0.0003$) controlling for the lesion, cardiovascular risk factors, and time since stroke.

Conclusion Our findings support the mechanistic hypothesis that the imbalance between long- and short-range white matter connections is a pathophysiological variable associated with worse subacute outcomes after a stroke.

Introduction

Stroke is the 5th cause of death and the leading preventable cause of long-term adult disability in the United States [88]. However, not all individuals who survive a stroke persist with debilitating sequelae. Unfortunately, our current models cannot fully explain the degree of functional impairment in the acute and subacute periods. They are only partly predicted by the size and the location of the stroke lesion, or by individual factors such as age, pre-stroke function and education. For this reason, there is pressing need for a better understanding of the pathophysiological mechanisms associated with stroke-related impairments.

One promising theory regarding stroke recovery suggests that impairment depends as much on the health of the individual who suffered the stroke ("the host") as on the type, size and location of the stroke. More specifically, resilience to injury is a concept that relates to the

integrity or health status of the remaining brain after a stroke has ensued, since the remaining brain is responsible for overcoming the functional limitations caused by the regional damage from the stroke[34, 89-91] .

Broadly stated, the structural integrity of the remaining brain can be compared to brain health. Its measurement could aid in refinement of the models to explain functional deficits after the stroke, taking into account other important variables such as stroke characteristics and age.

In this study, we aimed to assess the relationship between residual brain integrity after the stroke and subacute functional impairment. We employed a neuroimaging approach, which permits a comprehensive assessment of the structural integrity of white matter networks across the entire brain, the brain connectome. We leveraged post-processing methods recently defined to accurately measure the structural connectome from post-stroke brains, aiming to test the specific hypothesis that long-range white matter structural integrity is directly associated with functional impairment.

We focused on white matter for a few important pathophysiological reasons: cardiovascular risk factors (CVRF) such as diabetes, hyperlipidemia, hypercholesterolemia, hypertension and smoking are commonly observed among stroke patients and are known to result in atherosclerosis, small vessel disease and microangiopathic changes [92]. White matter, compared to grey matter, is more vulnerable to ischemic damage due to hypoperfusion[47], and lower collateral supply in the deep white matter [63]. Many studies have demonstrated cumulative white matter disease in individuals with CVRF [92], and our group has previously shown that loss of white matter due to CVRF is associated with lower cognitive performance and verbal IQ.

Not only is white matter more vulnerable to injury, but we also postulate that long-range white matter connections may be particularly vulnerable to injury in cerebrovascular disease. Compared with short-range connections, long-range connections are less numerous as a result of higher metabolic demands but are nonetheless essential for network integration and efficiency. Fewer long-range white matter connections could impair functional integration and neuroplasticity. A lower balance between long- and short-range fibers as a result of fewer long-range fibers is therefore a proposed mechanism by which brain health is lost.

In this study, part of the ongoing Wide Spectrum Investigation of Stroke Outcome Disparities on Multiple Levels [93] (WISSDOM), we aimed to test this proposed mechanism in a cohort of sub-acute stroke participants by determining the association between long-range white matter connections and functional impairment evaluated by the Stroke Self-Efficacy Questionnaire [94] (SSEQ), and the Stroke Impact Scale [95](SIS).

Methods

Participants

We recruited 30 participants, (17 males, mean age 57.9 ± 9.2) as part of an ongoing disparity study aimed at determining the effect of a nurse guided intervention on stroke recovery (CINGS ClinicalTrials.gov Identifier: NCT02982278). Participants with mild or moderate ischemic stroke were recruited in the sub-acute stages (14-164 days). Twenty-six participants (87%) had previously been diagnosed with at least one CVRF: diabetes (15 participants), hyperlipidemia, and hypercholesterolemia (22 participants), hypertension (24 participants), and 6 smokers. Four participants had not been previously diagnosed with any CVRF and were non-smokers. The total Charlson Comorbidity index [57] (CCI) was

calculated for all participants. We also collected the year each participant had been diagnosed with the 1st CVRF and used this as a proxy for the minimum number of years they had lived with the risk factor. Over half the participants (51.9%) diagnosed with CVRF had lived with one or more CVRF for at least 10 years. Participant demographic, clinical and behavioral characteristics are presented in table 1. For comparison of identified white matter fibers to a non-stroke cohort, we included 58 age matched self-reported cognitively normal individuals (45 females, 54.9 ± 8.3 years) without a history of neurological or psychiatric illness, but with a similar cardiovascular risk profile to the stroke participants. Twenty-seven participants (47%) of the non-stroke cohort had previously been diagnosed with at least one CVRF: diabetes (14 participants), hyperlipidemia (18 participants), and hypertension (20 participants). Thirty-one participants did not have a history of CVRF.

The study was approved by the Institutional Review Board at the Medical University of South Carolina, and all participants gave written, informed consent.

Behavioral Evaluation

All participants underwent functional performance assessment using the SIS to assess stroke specific functional outcomes that capture 8 individually scored domains: purpose, memory, mood, communication, typical daily activities, ability to be mobile at home or in the community, ability to use the most affected hand, and physical problems. Each section had a transformed score computed as:

*score = (actual raw score – lowest possible raw score)/(possible raw score range) * 100.*

Transformed scores of the latter four domains (activities, ability, hand function and physical problems) were combined to form the physical domain. Participants also

completed the SSEQ that assesses an individual's confidence in functional performance after stroke. Behavioral assessment was performed either on the same day, or within the same week of neuroimaging assessment.

Table 1: Demographic, clinical and behavioral data of study participants (N=30).

Race, N (%)	17(56.7) African American, 13(43.3) White
Sex, N (%)	13 (43.3) females, 17 (56.7) males
Age at test (years); mean (SD), range	58.3 (9.1), 35-75
Time post-stroke$^{\pm}$ (days); mean (SD), range	55.3 (40.2), 14-164
Time with CVRF (years); mean (SD), range	12.7 (14.2), 0-40
Affected hemisphere	15 left, 14 right, 1 brainstem
Lesion volume$^{\pm}$ (in ml); mean (SD), range	19.8 (30.8), 0.07-110.3
BMI; mean (SD), range	31.1 (8.9), 21.3-55.8
Pulse pressure; mean (SD), range	54.8 (22.9), 20-118
SSEQ; mean (SD), range	104 (20.4), 63-130
SIS physical; mean (SD), range	27.5 (23.0), 0-94.1
SIS purpose; mean (SD), range	27.1 (26.0), 0-100
SIS memory; mean (SD), range	23.9 (20.8), 0-64.3
SIS mood; mean (SD), range	25.6 (21.3), 0-69.4
SIS communication; mean (SD), range	18.0 (20.5), 0-82.1

BMI=body mass index, SSEQ=stroke self-efficacy questionnaire, SIS=stroke impact scale.
$^{\pm}$clinical variables included in the regression models.

Image Acquisition

Imaging was performed on a Siemens 3T Prisma scanner with a 20-element head/neck (16/4) coil at the Medical University of South Carolina. We used whole-brain T1-weighted, T2-weighted, and Diffusion EPI images collected from each participant. T1 parameters: MPRAGE sequence with 1 mm isotropic voxels, a 256 x 256 matrix size, a 9-degree flip angle, and a 192-slice sequence with TR = 2250 ms, TI = 925 ms, TE = 4.11 ms with parallel imaging (GRAPPA = 2, 80 reference lines). T2-weighted images were acquired using a sampling perfection with application optimized contrasts using a different flip angle evolution (3D-SPACE) sequence, TR = 3200 ms, TE = 567 ms, variable flip angle, 256 × 256 matrix scan with 176 slices (1 mm thick), using parallel imaging (GRAPPA = 80

reference lines). Diffusion parameters: mono-polar EPI scan that uses 43 volumes sampling 36 directions with b = 1000 s/mm^2 (with 7 volumes b = 0), TR = 5250 ms, TE = 80 ms, 140 × 140 matrix, 90-degree flip angle, 210 × 210 mm field of view, with parallel imaging GRAPPA = 2, 80 contiguous 1.5 mm slices. This sequence was acquired twice, with phase encoding polarity reversed for the second series. Control data T1-weighted and Diffusion images and connectome generation had been described in our previous publication[32].

Image processing

Lesion volume

The sub-acute stroke lesions were manually drawn on T2-weighted scans using MRIcron (https://www.nitrc.org/projects/mricron) software by a researcher blinded to the functional scores at the time of lesion drawing.

To spatially normalize the lesion maps to standard space, the T2 scan was co-registered with the individual's T1 scan and the transforms used to resliced the lesion into native T1 space. The resliced lesion maps were smoothed with a 3mm full-width half maximum Gaussian kernel to remove jagged edges associated with manual drawing. Finally, an enantiomorphic normalization [96] approach using SPM12's unified segmentation-normalization [97] was applied to normalize the T1-weighted images into standard space. Lesion volume was determined as the sum of lesioned voxels (figure 1a).

Structural connectome construction

Each participant's connectome was built from neuroimaging data as previously described by our group [98], as follows: 1) T1 weighted images were segmented into probabilistic grey

and white matter maps using SPM12's unified segmentation-normalization; 2) each individual's grey matter map was divided into 384 regions using the Atlas of Intrinsic Connectivity of Homotopic Areas (AICHA)[59]; 3) the grey matter parcellation maps were non-linearly registered into the diffusion tensor imaging (DTI) space; 4) pairwise probabilistic DTI fiber tracking was computed for all possible pairs of grey matter regions; 5) the weight of each pairwise connectivity link was determined based on the number of probabilistic streamlines connecting the grey matter region pair, corrected by distance travelled by each streamline (using probtrackX's "distance correction") and by the total volume of the connected regions (to compensate for the unequal size of grey matter regions of interest (ROI s); 6) a weighted adjacency matrix M of size 384 x 384 was constructed for each participant with $M_{i,j}$ representing the weighted link between ROI *i* and ROI *j*. Diffusion images were undistorted using TOPUP[99] and Eddy[86]. Tractography was estimated using FSL's FMRIB's Diffusion Toolbox (FDT) probabilistic method[60] with FDT's accelerated BEDPOST[100] used to assess default distributions of diffusion parameters at each voxel. Probabilistic tractography was performed using FDT's probtrackX (parameters: 5000 individual pathways drawn through the probability distributions on principal fiber direction, curvature threshold set at 0.2, 200 maximum steps, step length 0.5mm, and distance correction). The waypoint mask was set as the white-matter probabilistic map excluding the stroke lesion. In summary, each individual connectome was represented by a 384 x 384 matrix, where the nodes corresponded to the AICHA anatomical ROIs and the edges to the structural connectivity between the nodes.

Network analysis

To access the quantity of fibers in each individual connectome, we calculated the number of all identified connections and separated them into short-, mid- and long-range connections. This was done by calculating the Euclidean distance between each pair of node centroids and designating all identified fibers with lengths below the 1st quartile "short range" fibers, and all fibers with lengths above the 3rd quartile "long range" fibers. Mid-range fibers were between the 1st and 3rd quartiles. Long-range fibers were used as the primary connectome predictor (figure 1b). To ensure our primary predictor was not influenced by the lesion, we restricted our analysis to the contralesional hemisphere, except for the participant with a brainstem stroke, where we included whole brain long-range fibers. We further compared the number of identified short, mid, and long-range fibers to an age-matched non-stroke cohort with and without CVRF. Due to differing acquisition sequences, comparisons were only made between short, mid and long-range fibers normalized to the number of all identified fibers for each subject (figure 1c).

Statistical analysis

We performed bivariate analysis to determine correlations between the SSEQ, the five domains of the SIS, and long-range fibers.

We further constructed 6 linear regression models with the SSEQ, SIS-physical, SIS-purpose, SIS-memory, SIS-mood, and SIS-communication individually as the dependent variables for each model, and long-range fibers as the predictor variable. For each model, we adjusted for key covariates including time post stroke, cardiovascular risk factors, lesion volume and location. Specifically, the pre- and post-central gyri, Broca and Wernicke areas, optic radiation and the cortico-spinal tracts lesion volumes were included

in the models. All statistical analyses were performed using MATLAB, and the statistical significance was set at $p \leq 0.05$.

Data Availability Statement

Anonymized data used in this study will be made available to investigators who provide written request to the corresponding author to analyze the data, indicating the study in which the data will be used.

Results

Participants with stroke had significantly more short-range fibers (0.74 ± 0.03) than non-stroke controls (0.65 ± 0.04) ($p < 10^{-11}$) and the CVRF group (0.65 ± 0.03) ($p < 10^{-15}$), but fewer mid-range fibers (0.24 ± 0.02) than non-stroke controls (0.29 ± 0.03) ($p < 10^{-8}$), and the CVRF group (0.30 ± 0.02) (10^{-10}). Participants with stroke also had significantly fewer long-range fibers (0.023 ± 0.008) compared to the non-stroke controls (0.043 ± 0.014), and the CVRF group (0.042 ± 0.01) (both $p < 10^{-11}$) (figure 1c).

Relationship between SSEQ, SIS, and long-range connections - Bivariate analysis

Long-range fibers were significantly correlated with SSEQ ($r = 0.49$, $p = 0.007$), and the physical ($r = -0.46$ $p = 0.01$), memory ($r = -0.44$, $p = 0.02$), mood (r -0.51, $p = 0.005$) and communication ($r = -0.47$, $p = 0.01$) domains of the SIS. This implies that participants with a lower number of long-range fibers had higher SIS scores, and lower SSEQ, i.e., were more severely impaired, and assessed themselves to be more functionally impaired. Purpose was not significantly correlated with long range-fibers ($r = -0.12$, $p = 0.53$) (table 2).

Relationship between SSEQ, SIS, and long-range connections - Multivariate analysis

Our model accounted for about 49% of variance in participant self-reported functional self-efficacy, SSEQ: $F(4,30) = 7.8$, $p = 0.0003$, $R^2 = 0.56$, adjusted $R^2 = 0.49$. Time post stroke and long-range fibers were significant predictors in this model ($p = 0.0005$ and $p = 0.01$ respectively).

The physical, mood, memory and communication models were significant while the purpose model did not reach statistical significance. In the physical domain, our model accounted for about 25% of the variance in physical impairment: $F(4,30) = 3.4$, $p = 0.02$, $R^2 = 0.35$, adjusted $R^2 = 0.25$. In this model, the contralesional long range fibers were the only significant predictor ($p = 0.012$). In the mood domain, our model accounted for about 37% of the variance: $F(4,30) = 5.21$, $p = 0.003$, $R^2 = 0.46$, adjusted $R^2 = 0.37$. In this model, contralesional long-range fibers ($p = 0.01$) were a significant predictor. In the communication domain, our model account for about 13% of variance, $F(4,30) = 2.06$, $p = 0.1$, $R^2 = 0.13$, adjusted $R^2 = 0.25$. The contralesional long-range fibers was also the only significant predictor in this model ($p = 0.018$). In the memory domain, our model accounted for 10% of the variance, $F(4,30) = 1.84$, $p = 0.15$, $R^2 = 0.22$, adjusted $R^2 = 0.10$. Contralesional long-range fibers were the only significant predictor ($p = 0.02$).

Table 2: Partial Pearson correlations controlling for lesion size between Stroke Impact Scale scores and contralesional long-range fibers (N=30).

	Long-range fibers
	r/p-value
SSEQ	0.49/0.007

SIS physical	-0.46/0.01
SIS purpose	-0.12/0.53
SIS memory	-0.44/0.02
SIS mood	-0.51/0.005
SIS communication	-0.47/0.01

Table 3: Linear regression analyses

Dependent variable: Stroke Self-Efficacy Questionnaire				
	β coefficients	Standard error	t	p
Model (r^2=0.49, p=0.0003)				
Time post stroke*	-0.28	0.07	-3.99	0.0005
Charlson index	2.55	2.85	0.89	0.38
Lesion volume	0.53	6.8	0.08	0.94
Long-range fibers*	0.01	0.004	2.66	0.01

Dependent variable: SIS physical domain				
	β coefficients	Standard error	t	p
Model (r^2=0.25, p=0.02)				
Time post stroke	0.1	0.10	1.0	0.31
Charlson index	8.36	3.89	2.15	0.04
Lesion volume	15.09	9.26	1.63	0.12
Long-range fibers*	-0.02	0.006	-3.02	0.006

Dependent variable: SIS purpose				
	β coefficients	Standard error	t	p
Model (r^2=-0.09, p=0.8)				
Time post stroke	0.13	0.13	0.98	0.34
Charlson index	2.3	5.3	0.43	0.67
Lesion volume	5.67	12.62	0.45	0.66
Long-range fibers	-0.004	0.008	-0.53	0.60

Dependent variable: SIS memory				
	β coefficients	Standard error	t	p
Model (r^2=0.10, p=0.15)				
Time post stroke	0.06	0.10	0.65	0.52
Charlson index	2.08	3.84	0.54	0.59
Lesion volume	11.05	9.15	1.21	0.24

Long-range fibers*	-0.01	0.006	-2.4	0.02

Dependent variable: SIS mood				
	β coefficients	Standard error	t	p
Model (r^2=0.37, p=0.003)				
Time post stroke	0.16	0.08	1.89	0.07
Charlson index	-3.10	3.31	-0.94	0.36
Lesion volume	11.59	7.87	1.47	0.15
Long-range fibers*	-0.01	0.005	-2.64	0.01

Dependent variable: SIS communication				
	β coefficients	Standard error	t	p
Model (r^2=0.13, p=0.1)				
Time post stroke	0.08	0.09	0.84	0.41
Charlson index	0.94	3.73	0.25	0.8
Lesion volume	2.29	8.88	0.26	0.8
Long-range fibers*	-0.01	0.006	-2.54	0.018

Discussion

We aimed to determine the impact of residual brain health and integrity on functional outcome, quantified by the SSEQ, and the SIS, using structural brain connectomes constructed from a cohort of patients in the sub-acute stage of stroke. Our results supported our hypothesis that brain integrity, quantified by long-range fiber connections, is a significant predictor of functional deficit in both the self-reported measure of functional self-efficacy, and in 6 of the 8 domains of the SIS. Participants with a lower proportion of long-range fibers scored higher on all domains of the SIS and had lower self-efficacy scores. Our cohort consisted mainly of participants who had lived with at least one CVRF for several years. Converging evidence suggest that CVRF burden and the length of affliction maybe a major contributing factor in the decline of brain integrity. This is because

CVRF and established cardiovascular disease are known to be strongly related to the presence and progression of small vessel disease (SVD) and white matter injury [101]. Greater burden of SVD is in turn associated with cognitive [102] and movement impairment [103], depression , higher incidences of stroke, and worse outcome after stroke. While the pathophysiology of SVD remains undefined, studies correlating histopathology and postmortem MRI propose mechanisms that include hypoperfusion as a result of altered cerebrovascular autoregulation, hypoxia, blood-brain barrier leakage, inflammation, degeneration, amyloid angiopathy [104] and endothelial dysfunction [105]. Indeed, this subsequent damage to the white matter leads to structural compromise that may determine the severity of functional impairment, and also hamper the potential for neuro-plasticity and functional recovery after stroke beyond the size and location of the lesion. As demonstrated in our cohort, associations between the proportion of long-range fibers and functional impairment after stroke was observed even after controlling for time post-stroke, CVRF, lesion size and location, implying that long-range fibers have an important, and independent contribution to functional recovery after stroke. Physical activity, memory, mood, and communication are domains that require extensive involvement of specialized functional modules and widespread networks, implying the need for functional segregation (short-range connections), and subsequent integration (long-range connections) for efficient transfer of information. The loss of these long-range white matter fibers, possibly as a result of CVRF disrupts the topological integrity of the brain network, causing diffuse but covert injury that can occur sub-clinically, before overt manifestation of clinical symptoms, stroke, and or cognitive decline.

From our results, we therefore posit that the loss of long-range fiber connections is a mechanism that captures a pattern of brain integrity decline that begins long before overt clinical damage, and subsequently determines severity of functional impairment and potential for recovery after stroke.

Figures

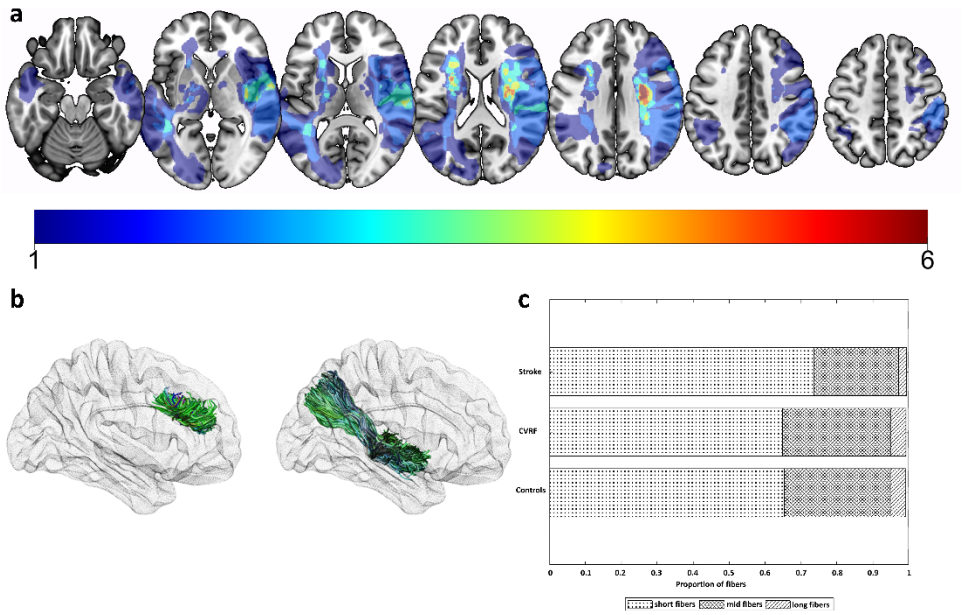

Figure1. a) Lesion overlay across all participants (N=30). Colors represent the number of patients with a lesion in that area, with the hotter colors indicating more overlap. Note the heterogeneity of the lesion locations. b) Example of short-range (anterior-cingulate to superior-frontal and) long-range (superior-temporal to superior-parietal) fibers c) Identified whole brain fibers. The stroke cohort had significantly more short-range fibers compared to the control and cardiovascular risk factor (CVRF) groups, and significantly fewer mid- and long-range fibers compared to the control group.

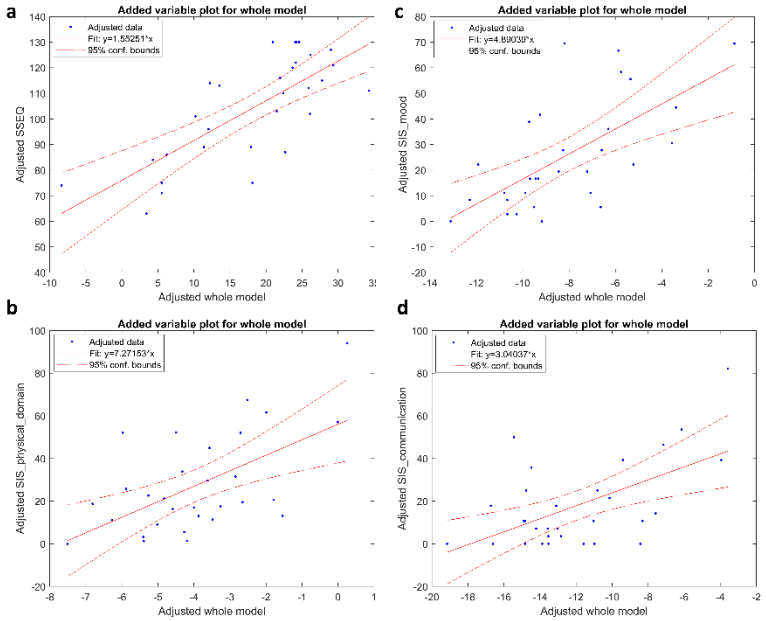

Figure2. Significant linear regression models.

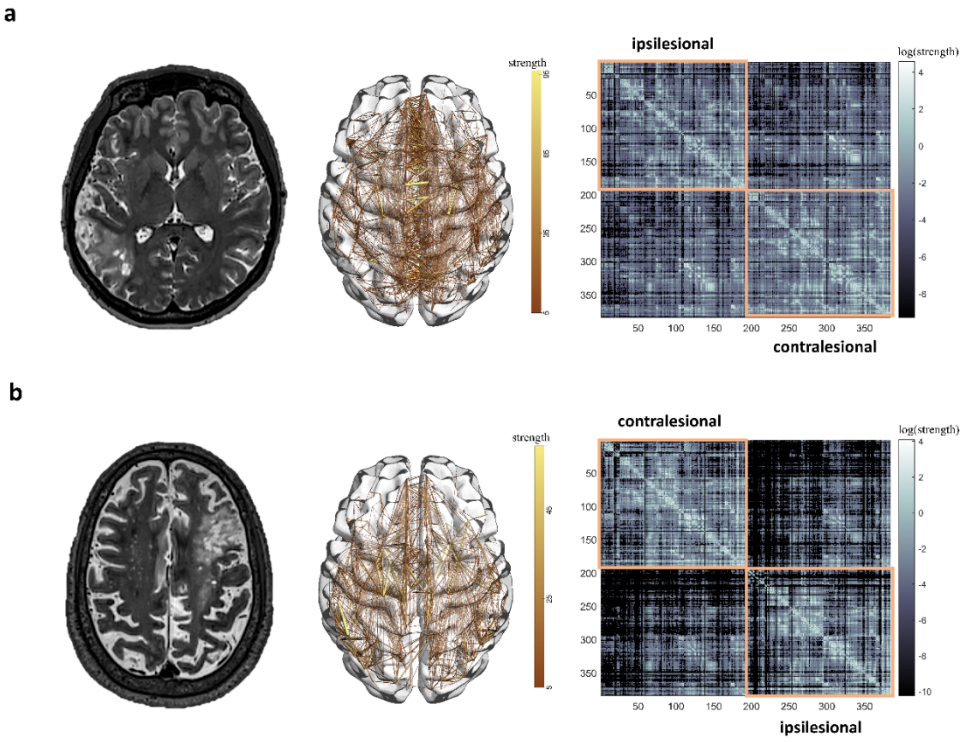

Figure3. Example subjects showing lesions and reconstructed whole brain connectomes: a) Subject 1 has a SIS index of 97.92, lesion volume of 43.51 ml with about 3.2% of long-range fibers, while subject 2 has a smaller lesion volume (29.8 ml) but with fewer identified long range fibers (2.4%), and a SIS index of 159.47. Also note the occurrence of leukoaraiosis on subject 2's contralesional hemisphere compared to subject 1.

5 Stroke as a network disorder: impact of stroke on brain network topology

Although stroke primarily affects the brain through a focal lesion, distant regions from the lesion location are nonetheless affected and may significantly contribute to functional impairment.

This chapter, based on the following peer reviewed publication, examines the effect of stroke on the residual network topology and its impact on language recovery in chronic stroke:

Marebwa BK, Fridriksson J, Yourganov G, Feenaughty L, Rorden C, Bonilha L. Chronic post-stroke aphasia severity is determined by fragmentation of residual white matter networks. Sci Rep 2017;7:8188.

Abstract

Many stroke survivors with aphasia in the acute period experience spontaneous recovery within the first six months after the stroke. However, approximately 30-40% sustain permanent aphasia and the factors determining incomplete recovery are unclear. Suboptimal recovery may be influenced by disruption of areas seemingly spared by the stroke due to loss of white matter connectivity and network integrity. We reconstructed individual anatomical whole-brain connectomes from 90 left hemisphere stroke survivors using diffusion MR images. We measured the modularity of the residual white matter network organization, the probability of brain regions clustering together, and the degree

of fragmentation of left hemisphere networks. Greater post-stroke left hemisphere network fragmentation and higher modularity index were associated with more severe chronic aphasia, controlling for the size of the stroke lesion. Even when the left hemisphere was relatively spared, subjects with disorganized community structure had significantly worse aphasia, particularly when key temporal lobe regions were isolated into segregated modules. These results suggest that white matter integrity and disorganization of neuronal networks could be important determinants of chronic aphasia severity. Connectome white matter organization measured through modularity and other topological features could be used as a personalized variable for clinical staging and aphasia treatment planning.

Introduction

Human communication relies on complex interactions of higher-order processes, such as general knowledge, memory, semantic association, syntax, and phonological processing. Taken together, key cortical regions need not only to be preserved, but also connected and integrated into a neural network in order to permit language processing.

Stroke is the leading cause of long-term language impairments (aphasia) in adults[106]. However, many stroke survivors with aphasia in the acute phase experience spontaneous recovery within the first six months after the stroke. Nonetheless, approximately 30-40% do not recover fully and experience aphasia for the rest of their lives [107]. Even though ischemic stroke may lead to necrotic damage affecting specific brain areas, the functional impairment after stroke can be exacerbated by dysfunction of seemingly spared areas[108].

The neurobiological bases for loss of function in remote and spared areas are not completely understood. However, extensive work on disconnection syndromes, including from our group[109] [110,] [111], have demonstrated that white matter loss and cortical

disconnection can extend beyond the stroke lesion[108]. Importantly, the degree of white matter disconnection of Broca's area is an independent predictor of naming impairments after a stroke, controlling for the degree of cortical ischemic damage[112, 113]. Furthermore, residual anatomical connectivity of spared areas plays a significant role in therapy-related improvement in object naming in subjects with aphasia[114].

Nonetheless, it is still unclear whether post-stroke white matter damage can be used as personalized predictor of chronic aphasia severity.

Our group has recently described how the comprehensive map of white matter connectivity (the connectome) can be measured in stroke survivors by combining innovations in image registration probabilistic tractography, diffusion tensor imaging and statistical assessment of residual networks[98, 115]. While understanding the effect of single elements such as node strength or degree, can explain some of the behavioral impairments after stroke, further understanding the complex topological organization of these elements may provide a valuable panoramic perspective that may not be captured otherwise.

Examining the community organization via modularity is one such approach to assess the mesoscale organization in the network. Therefore, in this study, we applied connectome methods to test the hypothesis that post-stroke residual white matter connectivity in chronic stroke survivors is associated with long-lasting aphasia severity. We employed graph theory methods to assess the community structure of white matter networks and we hypothesized that the fragmentation of the connectivity structure of the networks in the dominant hemisphere, even when cortical regions are relatively spared, would be associated with more severe aphasia.

Methods

Participants

We recruited 90 participants, (mean age 58.8 ± 12.1 years, 34 women) with a single left hemisphere ischemic or hemorrhagic stroke at least 6 months before the study (mean 42.8 ± 50 months post stroke). Participants were included in the study if they did not have a history of any other neurological illness apart from the stroke, could follow simple instructions, and were MRI compatible. All participants were right handed. The cohort of participants included in this study was also reported in previous study by our group[98]. The study was approved by the Institutional Review Boards at the Medical University of South Carolina and at the University of South Carolina. Written informed consent was obtained from all participants or their legal guardians, as approved by our institutions' IRB. All methods were performed in accordance with guidelines and regulations from our institutions' IRB.

Behavioral Evaluation

All the participants underwent language assessment using the Western Aphasia Battery (WAB-R)[116]. The variable of interest to the current study was the WAB Aphasia Quotient (WAB-AQ), which yields a global measure of aphasia severity on a scale of 0-100, with lower scores indicating worse aphasia. WAB-AQ reflects overall severity of language impairment in aphasia and is derived from various subtest scores including spontaneous speech fluency, auditory comprehension, speech repetition, and naming. Each subtest score was obtained by combining the data from its corresponding categories and calculated in accordance with the WAB-R manual. Aphasia types were classified according to the WAB. The following aphasia types were observed in our participant sample: anomic

(26 participants); Broca's (30 participants); conduction (9 participants); global (8 participants); Wernicke's (5 participants); no aphasia (12 participants) with WAB-AQ > 93.7; a cut-off typically applied in clinical grounds but may otherwise exclude individuals with milder deficits.

Image Acquisition

MRI scanning was performed within two days of behavioral testing. Images were acquired on a Siemens Trio 3T scanner equipped with a 12-element head coil located at the University of South Carolina. In this study, we used whole brain T1-weighted, T2-weighted and Diffusion EPI images collected from each patient.

1) T1-weighted image utilizing an MP-RAGE sequence with 1 mm isotropic voxels, a 256×256 matrix size, and a 9-degree flip angle. For the first 25 individuals we used a 160-slice sequence with TR=2250 ms, TI=900 ms, TE=4.52 ms. For the latter 65 individuals we used a 192-slice sequence with TR=2250 ms, TI=925ms, TE=4.15 with parallel imaging (GRAPPA=2, 80 reference lines). Each of these scans required approximately 7 minutes to acquire.

2) T2-weighted image using a sampling perfection with application optimized contrasts using a different flip angle evolution (3D-SPACE) sequence. This 1 mm isotropic 3D TSE scan uses a TR=2800 ms, a TE of 402 ms, variable flip angle, 256×256 matrix scan with 192 slices, using parallel imaging (GRAPPA x2, 120 reference lines).

3) Diffusion EPI scan which varied in terms of b-value (s/mm^2), spatial resolution and other parameters across participants. Fifty-two participants had a sequence with 65 isotropic (2.0mm) volumes (x1 B=0, x64 B=1000), TR = 7700ms,

TE = 90ms, 112×112 matrix, with parallel imaging GRAPPA=2, 60 contiguous slices. Thirty-eight individuals had a monopolar sequence with 82 isotropic (2.3mm) volumes (x10 B=0, x72 B=1000), TR = 4987ms, TE = 79.2ms, 90×90 matrix, with parallel imaging GRAPPA=2, 44 contiguous slices. This sequence was acquired in two series (41 volumes in each series) with opposite phase encoding allowing us to spatially undistort the images with TOPUP [99].

Lesion Mapping

Lesions were manually drawn on each individuals T2 scan by a neurologist (LB). The T2 scan was co-registered with the individual's T1 scan with the transforms applied to the lesion map. The T1 scans were warped to standard space using enantiomorphic segmentation-normalization [96], with these transforms applied to the lesion maps. These normalized lesion maps were used to compute the proportion injury to each of the 189 regions in the JHU as a ratio of lesioned voxels to the total number of voxels in that region.

Brain parcellation

Normalized brains were segmented into 189 regions using the Johns Hopkins University (JHU) brain atlas [117]. We aligned the anatomical brain atlas containing the JHU parcellation with each individual's T1-weighted images. The T1-weighted images were segmented into probabilistic grey and white matter maps, and the grey matter map was divided into regions according to the atlas. We then computed the percentage of damage for each grey matter region as a ratio of lesioned voxels to the total number of voxels in that region.

Anatomical connectome construction

Each participant's individual connectome was built using the following steps: 1) T1 weighted images were segmented into probabilistic grey and white matter maps using SPM12's unified segmentation-normalization, 2) the probabilistic grey matter map was divided into the JHU anatomical regions using the parcellation scheme described in 2.3.2., 3) the white matter and gray matter parcellation maps were registered into the diffusion imaging (DTI) space, 4) pairwise probabilistic DTI fiber tracking was computed for grey matter regions, 5) the weight of each pairwise connectivity link was determined based on the number of streamlines connecting the grey matter region pair, corrected by distance travelled by each streamline and by the total volume of the connected regions, and 6) a weighted adjacency matrix **M** of size 189 x 189 was constructed for each participant. $\mathbf{M_{i,j}}$ representing the weighted link between ROI **i** and ROI **j**.

The T2-weighted image (co-registered into the T1-weighted image) was normalized into the B0 non-diffusion image (from the diffusion MRI sequence); this spatial transform was applied to register the probabilistic white and gray matter maps (the latter divided into JHU regions of interest) as well as the stroke lesion into the diffusion MRI space, where all subsequent calculations were performed.

Tractography was estimated through FDT's probabilistic method [60] with FDT's BEDPOST being used to assess default distributions of diffusion parameters at each voxel, and probabilistic tractography was performed using FDT's probtrackX (parameters: 5000 individual pathways drawn through the probability distributions on principle fiber direction, curvature threshold set at 0.2, 200 maximum steps, step length 0.5mm, and

distance correction). The waypoint mask was set as the white-matter probabilistic map excluding the stroke lesion, ensuring that the subsequent weighted connectivity matrix is composed of only the surviving connections. The weighted connectivity between the regions *i* and *j* was defined as the number of probabilistic streamlines arriving at *j* region when *i* was seeded, averaged with the number of probabilistic streamlines arriving at *i* region when *j* was seeded. The connection weight was corrected based on the distance travelled by the streamlines connecting *i* and *j* (probtrackX's "distance correction"). The number of streamlines connecting each pair of regions was further divided by the sum of the volumes of these regions**,** giving the number of connections per unit surface. The distance correction is essential to eliminate linear bias towards longer fibers, and the volume correction avoids oversampling of larger ROIs compared to ROIs with smaller areas [118]. We did not perform a network density correction because as previously demonstrated by our group[119], in a weighted or non-binarized network, network density does not affect network properties as all possible connections are taken into account and scaled based on their weight.

Each individual connectome was represented by a 189 x 189 matrix, where the nodes corresponded to the JHU anatomical regions, and the edges the anatomical connectivity between the nodes. For this study, our analyses were restricted to 57 x 57 matrices that included only grey matter regions (i.e., ventricles and white matter regions were excluded).

Succinctly, the following procedures were performed: the lesion was manually drawn on a T2 weighted image by a rater who was blinded to the WAB-AQ, the T2 and the T1 weighted image were co-registered and the T1 weighted image was spatially registered (non-linearly normalized) into standard space using an enantiomorphic segmentation-

normalization procedure. Then the transformation matrix (T1 to standard space) was used to transform the JHU atlas into native T1 space, and a non-linear normalization procedure was used to register the T1 to the B0 image, and this transformation matrix was used to transform the JHU atlas from T1 to diffusion space. The same procedure was used to transform the lesion (in T1 space) to diffusion space, and finally fiber tracking was performed using the JHU ROIs while excluding the lesion mask.

Community Detection

Each connectome created above was partitioned into communities or modules by optimizing Newman's modularity algorithm[25], implemented in the Brain Connectivity Toolbox[61] (e.g. [Ci,Q] = modularity_und(W), where W is the weighted undirected connectivity matrix; gamma was maintained at the default gamma = 1). Modularity (Q) is a value that quantifies the strength of the network's modular organization by identifying groups of nodes that have a stronger intra-community coherence than inter-community coherence, and is defined as

$$Q = \sum_{i=1}^{m}(e_{ii} - a_i^2) \quad (1)$$

where **m** is the total number of modules, $\boldsymbol{e_{ii}}$ is the fraction of edges in the network that connect nodes that occur within the same module ***i*,** and $\boldsymbol{a_i}$ is the fraction of edges connecting a node in module **i** to any other random node, such that if the modules were assigned randomly, then $\mathbf{e_{ij}} = \mathbf{a_i a_j}$. Modularity values are positive if the number of edges within modules exceeds the number of edges expected by a chance distribution of edges between nodes regardless of modules [25].

Statistical analysis

For each subject, in the left and right hemisphere, we extracted the modularity score, and the optimal community structure, which indicates to which communities each ROI belongs**.** Since two different sequences were used to acquire the DTI data, we first ran an unpaired two-tailed t-test and determined there was no significant difference in the modularity scores acquired from the two groups left hemisphere ($p = 0.3340$), right hemisphere ($p = 0.1455$). Due to stochasticity of network partitioning which may lead to assignment of ROIs to different communities with every run, we performed 100 optimizations of the modularity quality function for each connectivity matrix and created a community affiliation matrix **A**, from the optimal community structure vector. $\mathbf{A_{ij}}$ represented the probability that region $\mathbf{A_i}$ and $\mathbf{A_j}$ are consistently grouped in the same community over 100 iterations. We then calculated the mean of all entries in the upper triangular community affiliation matrix, to obtain the left and right hemisphere community affiliation index (C).

For each subject, we quantified how intact the community structure of the left hemisphere was, compared to the right hemisphere via a ratio of the right to left community affiliation index, which we called the *fragmentation index* (FI) defined as

$$FI = \frac{RH_C - LH_C}{RH_C + LH_C} \quad (2),$$

where RH_C is the right hemisphere community affiliation index, and LH_C is the left hemisphere community affiliation index.

We then performed a one-tailed Pearson correlation analysis**,** since we had an a priori

expectation of effect in one direction - higher modularity to correspond to lower behavioral scores, to evaluate relationship between modularity, community affiliation index, and fragmentation index with WAB-AQ scores. We also calculated partial correlations controlling for whole brain grey and white matter damage, and for damage in a subnetwork of language specific regions as defined by Fedorenko and colleagues[120]. We further calculated the sum of weighted links to each node; the node strength. The mean node strength of left hemisphere nodes was then correlated with WAB-AQ.

To determine which pairs of nodes should be in the same module for better WAB-AQ score, we calculated for every entry in the left hemisphere community affiliation matrix $\mathbf{A_{ij}}$, an unpaired one-tailed t-test that compared the WAB-AQ scores for participants that had a community affiliation index of 1 against those that had an index <1. The t-test was run only if both groups had at least 5 participants. To control for damage, the analysis was further restricted to pairs of regions that were at least 50% preserved for each individual. The p-values were Bonferroni corrected at $p \leq 0.05$.

In order to assess the relationship between modularity and regional gray matter hubs, the number of preserved hubs in the left hemisphere was assessed. Network hubs were defined in accordance with rich club networks [121] as previously applied to lesion brains and aphasia by our group[122] **,** by identifying nodes with high degree that were also more densely connected to other high degree nodes than would be expected by chance .

We performed multiple linear regression analyses to evaluate the relationship between WAB-AQ and cortical damage, modularity, and the number of hubs. In the first model, WAB-AQ was defined as the dependent variable, with damage as the independent variable.

The second model had WAB-AQ as the dependent variable, and damage and number of hubs as independent variables. The third model had WAB-AQ as the dependent variable, and damage and modularity as independent variables. Adjusted R^2 indicated the explanatory power of the model with statistical significance set at $p < 0.05$.

Contributions of the domain general and language specific networks

To determine which community structures were associated with aphasia severity, we performed a subsequent analyses evaluating a sub-network composed of 9 language specific and 8 domain general regions of the networks as defined by Fedorenko and colleagues [120]. Language specific regions included the posterior segment of the middle frontal gyrus (MFG), the inferior frontal gyrus opercularis, inferior frontal gyrus triangularis, angular gyrus (AG), superior temporal gyrus (STG), pole of the superior temporal gyrus, middle temporal gyrus (MTG), posterior superior temporal gyrus (PSTG), and the posterior middle temporal gyrus (PMTG) which corresponds to PSMG in the JHU atlas. We also included the posterior inferior temporal gyrus (PITG) which corresponds to PSIG in the JHU atlas. Domain general regions included the posterior segment of the superior frontal gyrus (SFG), the dorsal prefrontal cortex of the middle frontal gyrus (MFG-DPFC), inferior frontal gyrus orbitalis, precentral gyrus (PrCG), superior parietal gyrus (SPG), supramarginal gyrus (SMG), posterior cingulate gyrus (PCC) and the insular. For every node in the language specific and domain general networks we calculated the frequency with which the node occurred in the same module with other regions in the brain for each subject, in other words, when they were not fragmented. We then correlated this value with WAB-AQ scores to determine the correlation between the composition of the

modules and aphasia severity.

In order to assess the strength of the connections within the communities, we further selected the traditional language regions: Broca's area (inferior frontal gyrus opercularis and inferior frontal gyrus triangularis), and Wernicke's area (superior temporal gyrus), and for each subject, extracted modules that contained these regions. We then calculated the average intra-modular degree for the modules containing these regions, and the participation coefficient for the three ROIs, which were then correlated with WAB-AQ, controlling for gray matter damage to the ROIs contained in each module.

Statistical analyses were performed in MATLAB Release 2015b

Results

Relationship between Aphasia Severity and Modularity (Q)

The mean aphasia quotient (WAB-AQ) was 62.6 ± 28.9. As indicated in the left panel of Figure 1, left hemisphere modularity (Q) was significantly correlated with WAB-AQ scores such that greater modularity was associated with worse aphasia severity ($r = -0.42$, $p < 0.00001$) - partial correlation controlling for ROI-specific proportion of damage in the left hemisphere ($r = -0.21$, $p = 0.0246$), partial correlation controlling for language specific network damage in the left hemisphere ($r = -0.21$, $p = 0.0225$), partial correlation controlling for white matter damage in the left hemisphere ($r = -0.28$, $p = 0.0044$). Right hemisphere modularity (Q) was not significantly correlated with WAB-AQ (see right panel of Figure 1). Figure 2 shows the correlation between left hemisphere modularity and WAB subscores: auditory comprehension, fluency, object naming, and repetition. There was no significant correlation between the whole brain modularity score and WAB-AQ ($r = 0.1445$, $p = 0.1742$), or any of the WAB subscores.

Relationship between Aphasia Severity and mean node strength

The left hemisphere mean node strength was significantly correlated to WAB-AQ ($r = 0.3625$, $p < 0.0001$), but did not survive partial correlation controlling for the grey and white matter damage**.** Supplementary figure 3 and 4 shows the relationship between WAB-AQ (and WAB subscores) and node strength

Relationship between Aphasia severity and Community Affiliation Index (C)

The left hemisphere community affiliation index was significantly correlated with WAB-AQ ($r = 0.44$, $p < 0.00001$), Figure 3 left panel). The direction of the effect indicates that subjects whose connectomes exhibited more consistent left-hemispheric node-community assignments across optimizations of the clustering algorithm had higher WAB-AQ. Aphasia severity and community affiliation index was not significantly correlated when controlling grey or white matter damage. There right hemisphere community affiliation index was not significantly correlated with WAB-AQ (Figure 3 right panel)

Relationship between Aphasia severity and Fragmentation Index (FI)

There was a significant negative correlation between the fragmentation index and WAB-AQ ($r = -0.43$, $p < 0.0001$, Figure 4), indicating that subjects with more fragmented left hemispheres had more severe aphasia**.**

Aphasia severity and fragmentation index was not significantly correlated when controlling grey matter damage but was significantly correlated when controlling for white matter damage ($r = -0.22$, $p = 0.0175$). To illustrate the network fragmentation, figures 5 and 6

show two example participants with very different lesion volumes (subject 1: 359.4 cm^3 percent white matter damage: 0.168; subject 2: 76.1 cm^3 , percent white matter damage). The impact of the lesion into the white matter fragmentation is remarkable. Subject 1's left hemisphere was partitioned into 14 modules. The fronto-parietal and middle-temporal networks are highly fragmented, with relative disconnection between the frontal and subcortical regions, which are grouped into different modules (Figure 5a). The right panel of figure 5a. shows the left hemisphere community affiliation matrix of subject 1, which is visibly sparser compared to the right hemisphere, indicating an unstable clustering with very few nodes consistently grouped in the same modules over 100 runs. Figure 5b is the same subject's right hemisphere, which was partitioned into 4 groups, and displays significantly less fragmentation, and a more stable clustering. Figure 6a and b represents subject 2 left and right hemisphere respectively, whose modularity pattern did not reveal dramatic fragmentation. Subject 1 had a WAB-AQ score of 48.1 while subject 2 scored 88.1. Figures 7 and 8 show two example participants, subject 3 has mean percent matter damage, lesion volumes and locations comparable to subject 2 (subject 3: 99.24 cm^3 , percent white matter damage: 0.096). Subject 3's left hemisphere is however fragmented into 9 modules compared to subject 2's 4 modules. This fragmentation occurs mainly in the inferior frontal temporal regions, with the same subject's right hemisphere remaining relatively intact (4 modules – figure 7b). Subject 3 had a WAB-AQ score of 58.2 Subject 4 had behavioral and fragmentation patterns similar to subject 1 even with a significantly smaller lesion volume (subject 4: 206.36 cm^3, percent white matter damage: 0.035). Subject 4 revealed a similar pattern of fragmentation in the left hemisphere, with a

relatively intact right hemisphere (figure 8a and b respectively) and had a WAB score of 41.8.

Figure 9 shows the lesion locations of all 4 example subjects.

Supplementary Table 1 shows pairs of regions that when in the same module, are associated with a higher WAB-AQ score. Overall, they indicate that nodes in the temporal, inferior frontal, middle temporal and insular regions need to be more tightly associated in the context of the overall community structure for preservation of language.

Relationship between Aphasia severity and cortical damage, modularity, and hubs.

There was a significant relationship between WAB-AQ and total brain damage ($F = 49.1$, $p < 0.00001$, adjusted $R^2 = 0.351$). When number of hubs was added as a predictor, the model composed of damage and number of hubs had equivalent explanatory power, and number of hubs was not a significant predictor of deficit ($F = 25.7$, $p < 0.00001$, adjusted $R^2 = 0.357$; damage ($p = < 0.00001$), hubs ($p < 0.18$)). With modularity added as a predictor, the model composed of damage and modularity had a higher explanatory power, with modularity being a significant predictor of deficit in addition to cortical damage ($F = 27.4$, $p < 0.00001$, adjusted $R^2 = 37.2$; damage ($p < 0.00001$), modularity ($p = 0.049$)).

Relationship between Aphasia severity and inter- and intra-module connectivity.

There was a significant relationship between aphasia severity and the reduced size of the modules containing regions of the language specific regions in the temporal lobe. The superior temporal gyrus ($p = 0.0053$), the pole of the superior temporal gyrus (0.0054), the

middle temporal gyrus ($p = 0.0042$), the posterior middle temporal gyrus ($p = 0.0448$), and the posterior inferior temporal gyrus ($p = 0.0123$) we all significantly correlated with WAB-AQ as shown on figure 10. (Not corrected for multiple comparison).

Nodes from the domain general network did not significantly correlate with aphasia severity.

Pars triangularis:

There was a significant relationship between intra-modular degree and WAB-AQ ($r = 0.265$, $p = 0.0058$), and between the node's participation coefficient and WAB-AQ ($r = 0.4848$, $p < 10^{-5}$). Participation coefficient survived partial correlation with module specific damage ($r = 0.271$, $p = 0.0051$). Intra modular degree did not survive partial correlation.

There was no significant correlation between module size and WAB-AQ.

Pars opercularis:

There was a significant relationship between intra-modular degree and WAB-AQ ($r = 0.3520$, $p < 0.0001$), and between the node's participation coefficient and WAB-AQ ($r = 0.4308$, $p < 0.00001$). Participation coefficient survived partial correlation with module specific damage ($r = 0.2865$, $p = 0.0032$). Intra modular degree did not survive partial correlation. Module size was significantly correlated with WAB-AQ ($r = 0.2073$, $p = 0.0250$).

Superior temporal gyrus

There was a significant relationship between intra-modular degree and WAB-AQ ($r = 0.5112$, $p < 10^{-7}$), and between the node's participation coefficient and WAB-AQ ($r = 0.3915$, $p < 0.00001$). Both participation coefficient ($r = 0.2112$, $p = 0.0235$) and intra modular degree ($r = 0.2898$, $p = 0.0029$) survived partial correlation with module specific damage.

Module size was significantly correlated with WAB-AQ ($r = 0.2538$, $p = 0.0079$), and also survived partial correlation ($r = 0.1782$, $p = 0.0474$).

Discussion

The primary purpose of the current study was to determine the degree to which post stroke fragmentation of brain anatomical connectivity affects language ability after stroke. To investigate this hypothesis, we analyzed the anatomical connectome from a large cohort of chronic stroke survivors with left hemisphere focal damage and employed graph theory methods to assess the community structure of global and peri-Sylvian networks. We hypothesized that the fragmentation of the brain community structure and the disintegration of peri-Sylvian networks, even when these regions are relatively spared, would be associated with worse chronic aphasia. Our findings strongly supported our hypothesis: fragmentation to the brain neuronal network community structure, even when the cortical structures were relatively spared, were directly associated with more severe aphasia in the chronic period.

These results have direct implications for a better understanding of the mechanisms associated with post-stroke language recovery, as well as the relationship between neuronal network integrity and complex cognitive functions. Network modularity is one of the hallmarks of complex biological systems. It confers computational advantages, efficient

processing, and robust responses to perturbations [22]. Modularity represents a fine balance between integration and segregation where both extremes can lead to poorly efficient networks. Very high modularity can lead to disintegrated or fragmented networks, while very low modularity can lead to lack of specialization. In our cohort, we observed the stroke lesions are associated with higher mean modularity in the lesioned hemisphere ($\mu = 0.4226$) compared to the intact hemisphere ($\mu = 0.3450$), suggesting that anatomical damage caused by the stroke is not only related to regional destruction, but may affect the entire organization of the remaining neuronal network architecture, resulting in a more segregated organization that hinders communication between modules. The clinical impact of this measured change in modularity was confirmed by the fact that subjects with very high modularity scores had more severe chronic aphasia, even when controlling for degree of cortical lesion.

Post-stroke high modularity scores are likely related to a combination of increased local clustering or modular fragmentation, weaker inter-modular integration, and, as our group previously demonstrated in post-stroke damage, loss of connectivity hubs [122]. These variables lead to less efficient information transfer.

It is important to acknowledge that we used each participant's own right hemisphere as a control, which assumes anatomical integrity of the right hemisphere. This is a limitation for two reasons. First, is assumes that the right hemisphere is relatively preserved after the stroke, when in fact there could be remodeling due to deafferentation or demand for compensation due to loss of function. Second, it does not consider the physiological asymmetries in anatomical connectivity. It would therefore be essential to determine the reliability of the right hemisphere as a self-hemispheric control. Despite this potential

limitation, there is an inherent advantage of using the subject's own non-lesioned hemisphere anatomy as the control, since it considers the relative disruption of network topology when controlling for other issues such as age, pre-stroke microangiopathic white matter loss and global network organization, which affect both hemispheres equally. Furthermore the right hemisphere re-organization has been implicated in aphasia recovery [123] and therefore assessing the degree of re-organization in relation to the lesioned hemisphere maybe more informative than comparison to healthy controls. For this reason, this approach was successful to demonstrate a strong and significant correlation between the left hemisphere community affiliation index and WAB-AQ, indicating that language was preserved if more regions were consistently grouped in the same module and not segregated across modularity optimization runs.

While modularity is a measure of global network organization, the mutual participation of key regions into the same module is of potential interest. Thus, we identified pairs of regions that when in the same module, were associated with a higher WAB-AQ score (supplementary table 1). We did not explore the typical composition of modules beyond two pairs but were still able to observe consistent pairing of the classical language regions, as well as other cortical and insular regions in patients who did not have severe aphasia. The impact of changes of the typical composition of modules (with two or more regions) may be a topic for further focused study. Furthermore, we acknowledge that we did not perform direct out of sample prediction, perhaps a more informative measure of recovery, to determine the predictive power of modularity, we still propose this to be an important first step in the understanding of topological changes post-stroke.

Importantly, our results suggest that connectome community structure may be a very useful, personalized, and unique score to inform about language prognosis after stroke. Currently, our ability to predict aphasia recovery is still suboptimal and tied to lesion size and location even though evidence points to the reorganization of the remaining brain networks beyond the lesion as being crucial for recovery**.** Our results show a significant correlation between disintegration of the community structure and long-term aphasia severity, providing an indication into one of the many determinants of the biological substrates of stroke recovery. There are no other methods that can provide an accurate description of post-stroke prognosis regarding language. This may be the optimal usage of the connectome community structure, which can inform clinicians and patients about the magnitude of brain framework damage. Furthermore, this is an optimal approach for clinical translation of computational neuroscience because the connectome community structure provides a unique and yet abridge window to the basic framework from which complex cognitive functions arise, i.e., the systems organization of neuronal networks.

In conclusion, we confirm that preservation of anatomical white matter network architecture is directly related to long-term aphasia severity. Loss of white matter integrity, even when the cortical regions are preserved, is associated with more severe aphasia. Modularity provides a single index that indicates the integrity of system-level organization of neuronal networks.

Figures

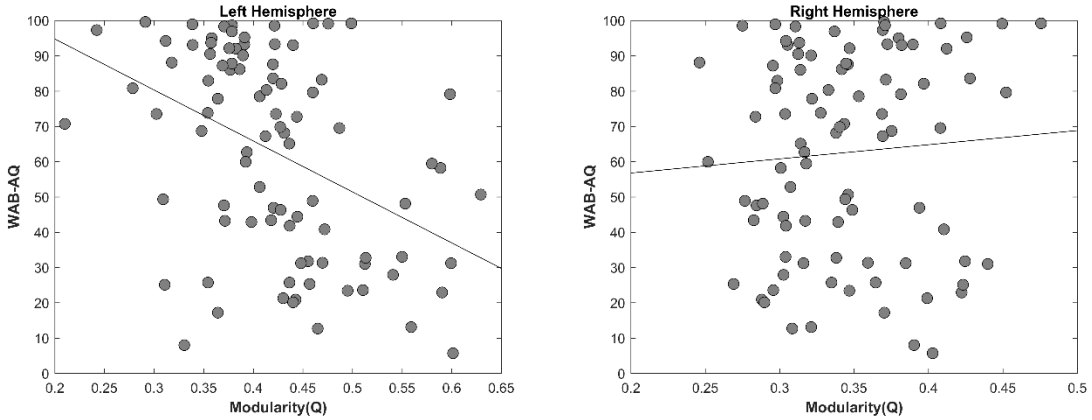

Figure 1. Correlation between modularity and aphasia severity in the left hemisphere (r = -0.4215, p < 0.00001), right hemisphere (r = 0.0698, p = 0.5135).

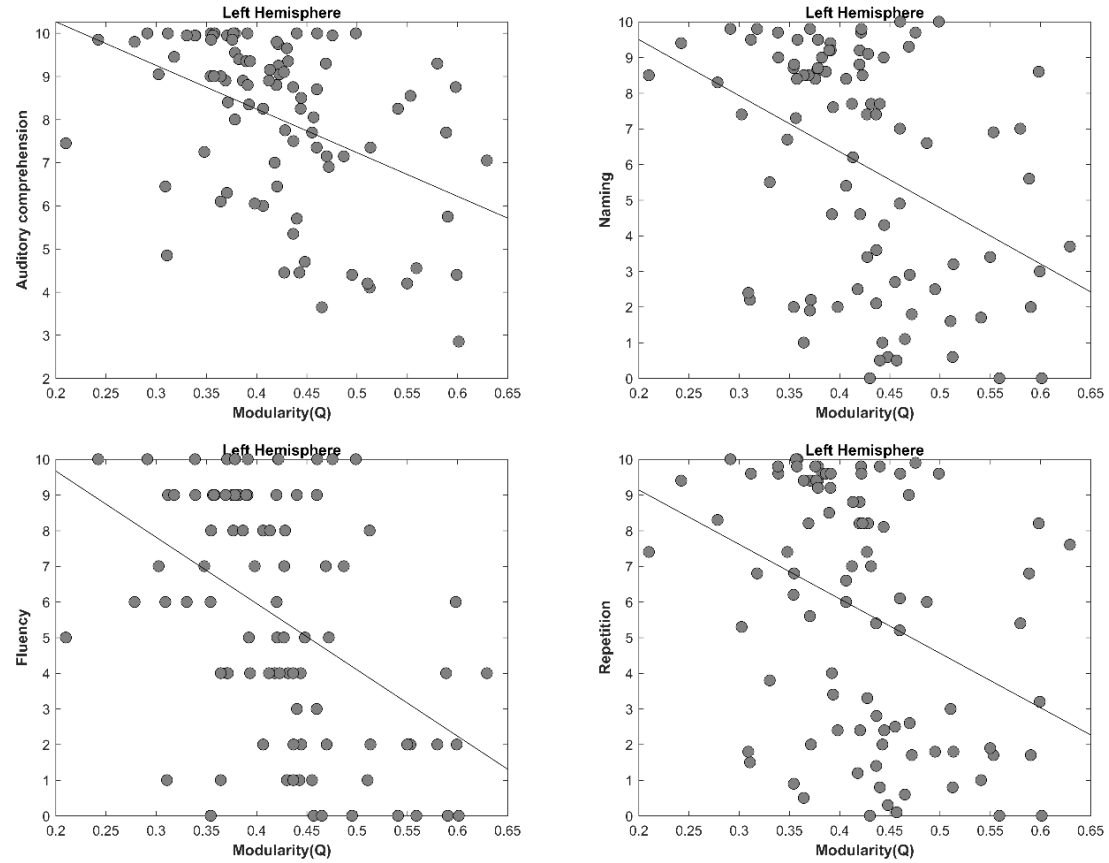

Figure 2. Correlation between left hemisphere modularity and subsets of WAB-AQ: Auditory comprehension (r = -0.4345, p < 0.00001), Fluency (r = -0.4561, p < 0.00001), Naming (r = -0.3948, p < 0.00001), and Repetition (r = -0.3644, p < 0.00001).

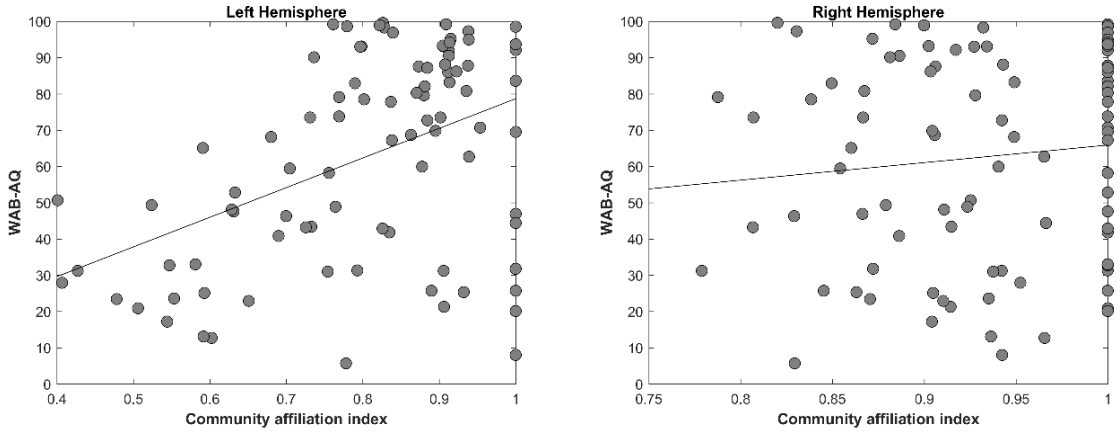

Figure 3. Correlation between community affiliation index (C) and aphasia severity. Left Hemisphere ($r = 0.4438$, $p < 0.00001$), Right Hemisphere ($r = 0.12$, $p = 0.3144$).

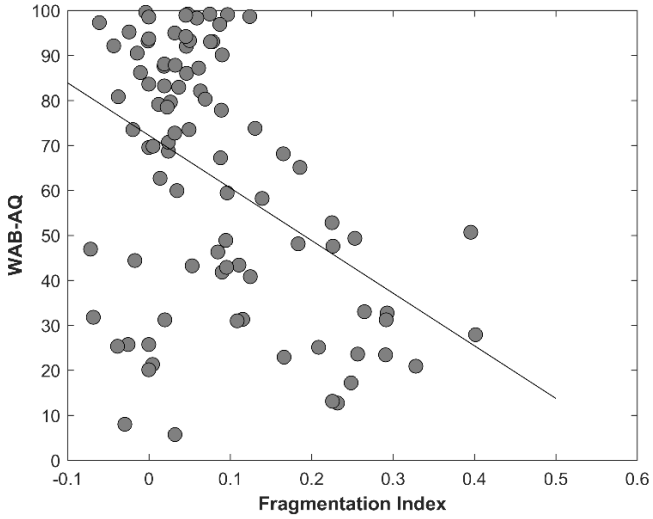

Figure 4. Correlation between Fragmentation index and aphasia severity ($r = -0.4302$, $p < 0.0001$).

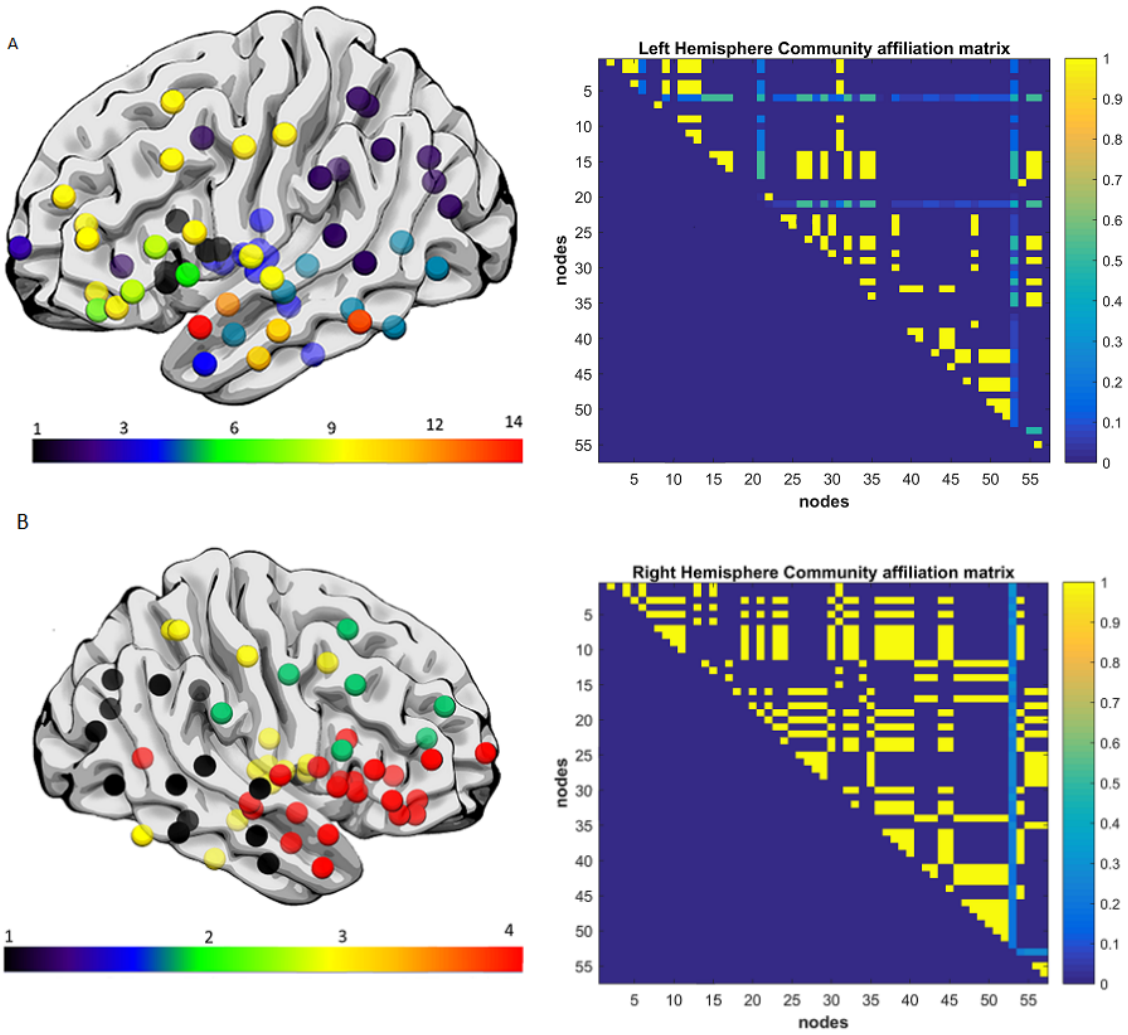

Figure 5a. Exemplar data Subject 1, left hemisphere lateral view, each color represents a single community. Note the fragmentation of the fronto-parietal and middle-temporal networks with relative disconnection between the frontal and subcortical regions, which are grouped into different modules. Subject 1 had a lesion volume of 359.4 cm^3, percent white matter damage of 0.168, and a WAB-AQ score of 48.1. (Supplementary table S2 shows the labels associated with the nodes on the community affiliation matrix). Note the fragmentation, unstable clustering shown and missing nodes in the community affiliation matrix compared to the right hemisphere matrix.

Figure 5b. Exemplar data Subject 1, right hemisphere lateral view, each color represents a single community. There was no apparent fragmentation, and the network was divided into 4 communities. The community affiliation matrix also showed stable clusters over 100 runs

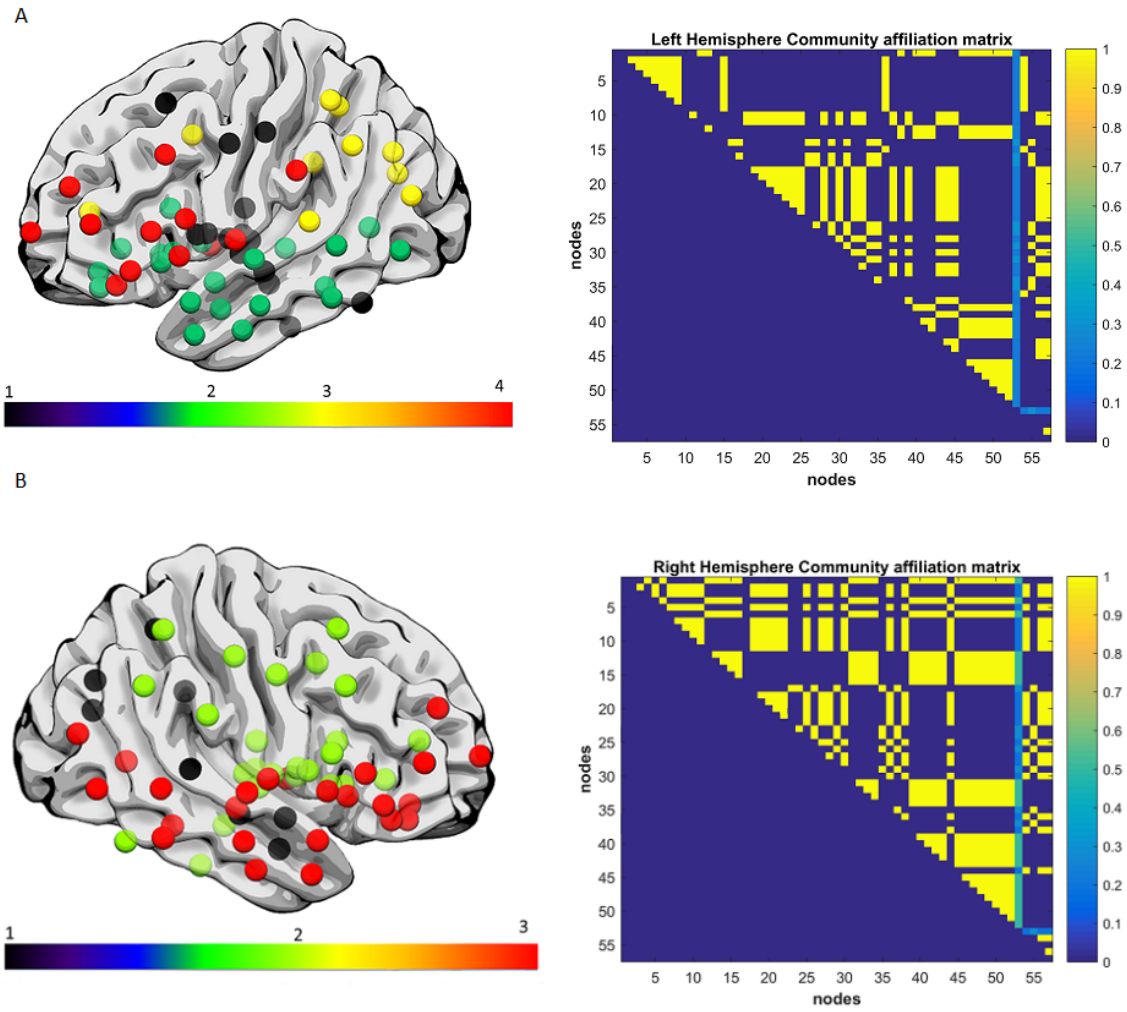

Figure 6a. Exemplar data Subject 2, each color represents a single community left hemisphere lateral view. Both hemispheres did not reveal dramatic fragmentation patterns. Subject 2 had a lesion volume of 76.1 cm^3, percent white matter damage of 0.099, and a WAB-AQ score of 88.1. The community affiliation matrix showed relatively stable clustering over 100 runs.

Figure 6b. Exemplar data Subject 2, right hemisphere lateral view, each color represents a single community, and again there was no apparent fragmentation, and the network was divided into 4 communities. The community affiliation matrix showed stable clustering over 100 runs.

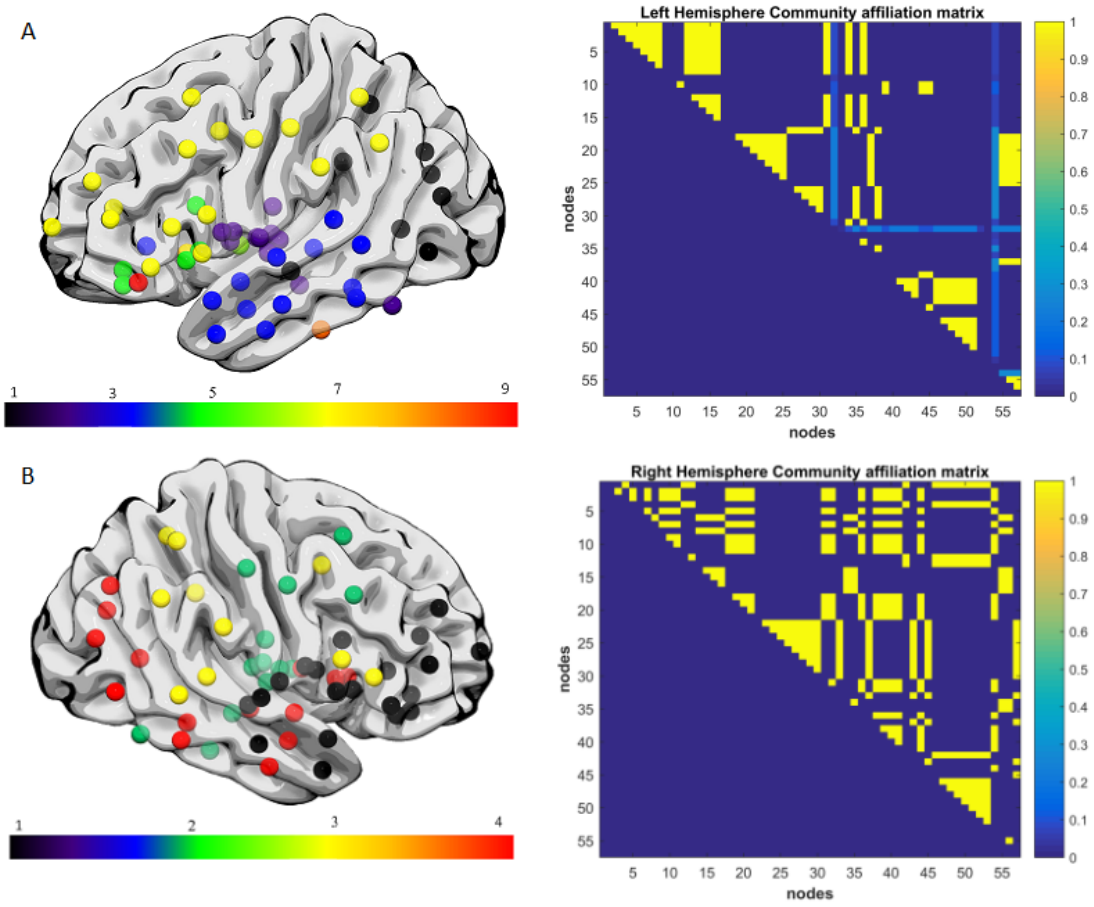

Figure 7a. Exemplar data Subject 3, each color represents a single community left hemisphere lateral view. There was marked fragmentation of the inferior frontal and middle-temporal networks with relative disconnection between the frontal and subcortical regions, with the left hemisphere grouping into 9 modules. Subject 3 had a lesion volume of 99.24 cm^3, percent white matter damage of 0.096, and a WAB-AQ score of 58.2. There was unstable clustering and missing nodes in the community affiliation matrix compared to the right hemisphere matrix.

Figure 7b. Exemplar data Subject 3, right hemisphere lateral view, each color represents a single community. There was no apparent fragmentation, and the network was divided into 4 communities. The community affiliation matrix showed relatively stable clustering over 100 runs.

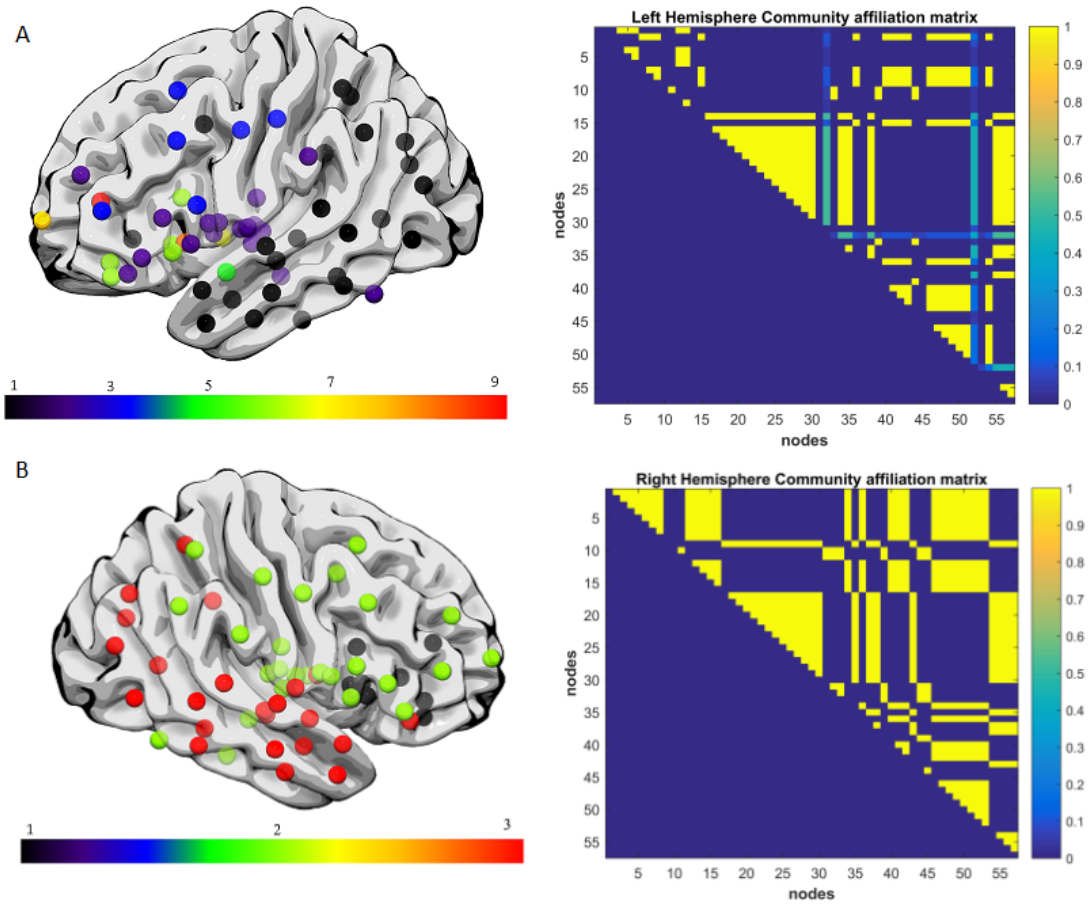

Figure 8a. Exemplar data Subject 4, each color represents a single community left hemisphere lateral view. Note the fragmentation of the fronto-parietal, inferior frontal and middle-temporal networks with the hemisphere grouping into 9 modules. Subject 4 had a lesion volume of 206.36 cm^3, percent white matter damage of 0.035, and a WAB-AQ score of 41.8. Note the missing nodes and unstable clustering in the community affiliation matrix.

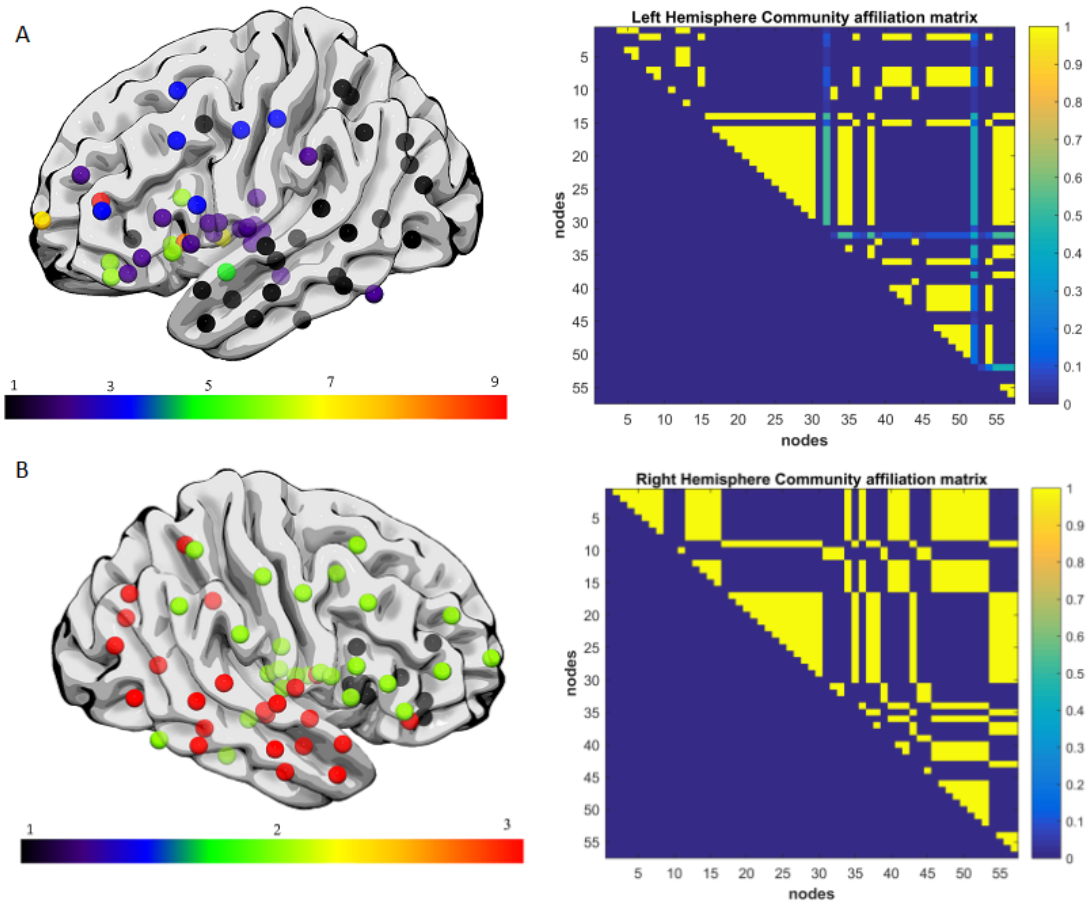

Figure 8b. Exemplar data Subject 4, right hemisphere lateral view, each color represents a single community. There was no apparent fragmentation, and the network was divided into 3 communities. The community affiliation matrix also showed stable clustering over 100 runs.

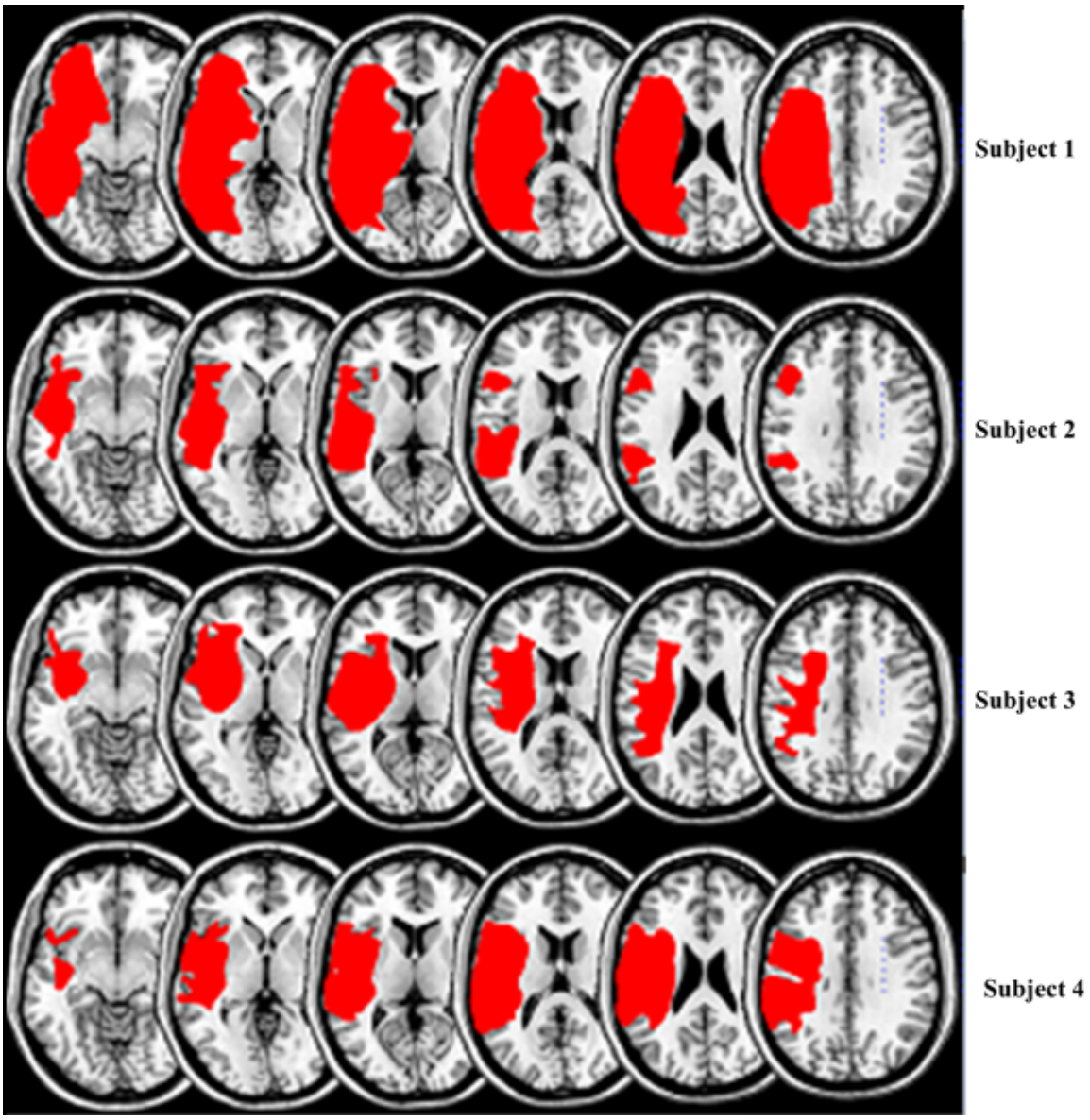

Figure 9. Overlap plot of damage locations in our 4 exemplar subjects. Subject 1: total lesion volume 359.4 cm^3, Subject 2: total lesion volume 76.1 cm^3, Subject 3: total lesion volume 99.24 cm^3, Subject 4: total lesion volume 206.36 cm^3.

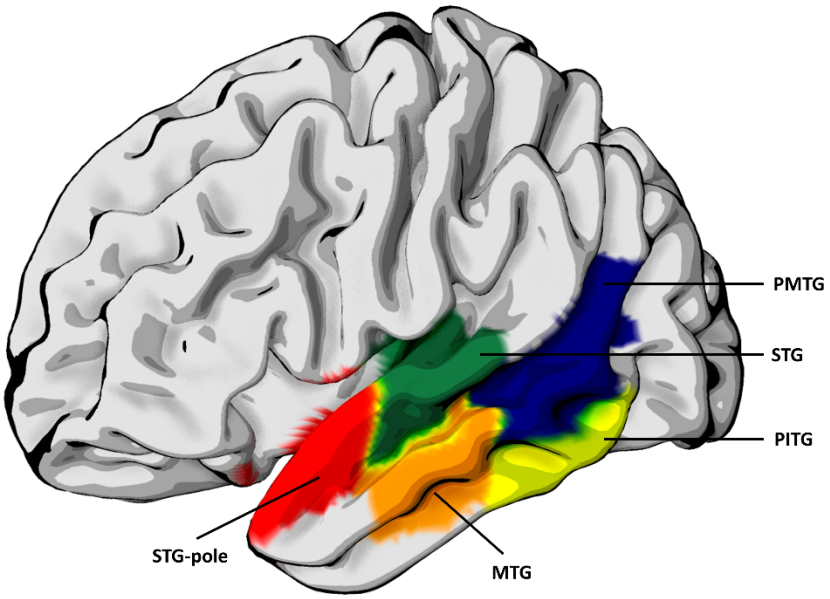

Figure 10. Regions from the language specific and domain general networks whose module sizes were significantly correlated with aphasia severity. STG-superior temporal gyrus (p = 0.0053), STG-pole -the pole of the superior temporal gyrus (0.0054), MTG- middle temporal gyrus (p = 0.0042), PMTG- posterior middle temporal gyrus (p = 0.0448), and PITG- posterior inferior temporal gyrus (p = 0.0123).

The pathophysiology of small vessel disease

6

Small vessel brain disease is common in individuals with CVRF and commonly associated with stroke and dementia. While the underlying pathophysiology of SVD is still under investigation, its impact on brain health is not in doubt.

This chapter, based on the following manuscript, determines the link between SVD and long-range fibers, and their impact on language recovery after stroke:

Wilmskoetter J & **Marebwa BK**, et al. Long-range fiber damage in small vessel brain disease affects aphasia severity.

Abstract

We sought to determine the underlying pathophysiology relating white matter hyperintensities (WMH) to post-stroke outcomes. We hypothesized that: 1) WMH are associated with damage to fibers of any length but to a higher percentage of long-range compared to mid- and short-range intracerebral white matter fibers, and 2) the number of long-range fibers mediates the relationship between WMH and chronic post-stroke aphasia severity. We measured severity of periventricular (PVH) and deep white matter hyperintensities (DWMH), calculated number and percentages of short-, mid- and long-range white matter fibers, and determined aphasia severity of 48 individuals with chronic post-stroke aphasia. Correlation and mediation analyses were performed to assess the relationship between WMH, connectome fiber-length measures and aphasia severity. We

found that more severe PVH and DWMH correlated with a lower proportion of long-range fibers (r=-0.423, p=0.003; and r=-0.315, p=0.029; respectively), counterbalanced by a higher proportion of short-range fibers (r=0.427, p=0.002; and r=0.285, p=0.050; respectively). More severe PVH also correlated with a lower proportion of mid-range fibers (r=-0.334, p=0.020), while DWMH did not correlate with mid-range fibers (r=-0.169, p=0.250). Mediation analyses revealed: 1) a significant total effect of PVH on WAB-AQ (standardized beta=-0.348, p=0.008), 2) a non-significant direct effect of PVH on WAB-AQ (p>0.05), 3) significant indirect effects of more severe PVH on worse aphasia severity mediated in parallel by the lower number of long-range fibers (effect=-6.23, Bootstrapping: SE=2.64, lower limit 95-CI=-11.82, upper limit 95%-CI=-1.56) and higher number of short-range fibers (effect=4.50, Bootstrapping: SE=2.59, lower limit 95-CI=0.16, upper limit 95%-CI=10.29). We conclude that small vessel brain disease seems to affect chronic aphasia severity through a change of the proportions of long- and short-range fibers. This observation provides insight into the pathophysiology of small vessel brain disease, and its relationship with brain health and aphasia severity.

Introduction

White matter hyperintensities or leukoaraiosis (WMH) are an important marker for small vessel brain disease [35]. WMH are usually identified as periventricular and/or deep white matter signal abnormalities on T2-weighted, or fluid-attenuated inversion recovery (FLAIR) MRI imaging. WMH are commonly observed in older individuals [124], affecting up to 95% of individuals age 60 or older [125, 126]. Cardiovascular diseases, such as new or

recurrent strokes and dementia, [127-131], and cerebro- and cardiovascular risk factors, such as hypoperfusion, hypertension, diabetes mellitus, reduced renal function, are strongly associated with WMH [124, 132-134]. WMH are linked to cognitive decline [135] and worse outcomes after strokes [136], such as persistent language impairments (naming and fluency) [137], swallowing impairments [138], physical and cognitive impairments [139], as well general functional deficits [136, 140].

While several studies have indicated the relationship between WMH and compromised stroke outcome, little is known about the underlying pathophysiology that mediates their relationship. Revealing the mechanisms of WMH is crucial to identify patients at risk for compromised outcomes, predict recovery, plan rehabilitation, and develop future prevention and treatment strategies. More specifically, a better understanding of how WMH relate to white matter integrity at a neural network level could provide important information regarding the relationship between small vessel brain disease and neurological function.

Within white matter, it is now increasingly recognized that long-range axonal fibers connecting gray matter regions provide integration between distant areas, which are locally segregated by shorter range fibers [23, 141]. Even though long-range fibers are crucial for the maintenance of network organization and efficiency, they are less numerous and require more energy [142]. Their higher metabolic demand to support their larger structural integrity makes them preferentially susceptible to small vessel cerebrovascular ischemia [35].

Language is a complex cognitive function which requires knowledge association, information binding, and semantical, syntactical, morphological as well as phonological

mapping. Since long-range fibers are necessary for multi-modal integration, and are likely more susceptible to ischemia, we speculated that the damage to long-range fibers may be a mechanistic mediator between WMH and chronic aphasia severity.

The objective of this study was to assess the relationships between WMH, axonal fiber damage, and chronic aphasia severity. We hypothesized that: 1) WMH are associated with damage to a higher percentage of intracerebral long-range white matter fibers compared to medium- and short-range fibers, and 2) the decrease in the proportion of long-range fibers mediates the relationship between WMH and worse chronic post-stroke aphasia severity.

Methods

Participants

Participants were recruited as part of an ongoing, multi-site study identifying factors predictive of treated aphasia recovery in individuals with chronic aphasia. Participants were recruited if they had experienced an ischemic or hemorrhagic stroke to the left hemisphere, were at least 12 months post-stroke, had a diagnosis of aphasia according to the Western Aphasia Battery-Revised (WAB-R) [143], and were between 21-80 years of age. Participants were excluded if they had severely limited verbal severely limited verbal output (i.e., a score $\leq$1 on the spontaneous speech scale), limited auditory comprehension (i.e., a WAB-R comprehension score $\leq$1), bilateral stroke, stroke affecting the right hemisphere, or other neurological illness/injury affecting the brain. In total, 48 participants (32 males, 16 females) were included in this study. Participants were 54.44 months post-stroke (SD=53.64, range=12-245), and mean age at testing was 60.44

(SD=11.96, range=29-76). Forty-four participants (92%) were premorbid right handed and thirty-seven (77%) had an ischemic stroke. Table 1 presents participant characteristics Fig. 1 the lesion overlay of all participants. Data were collected from the University of South Carolina and Medical University of South Carolina. Institutional Review Boards at each University approved all study procedures, and participants provided informed consent to participate.

White matter hyperintensities scoring

We used a rating scale developed by Fazekas and colleagues (the Fazekas scale) [144] to rate the presence and extent of WMH in the right, contralesional hemisphere [131, 137]. WMH were rated in the right hemisphere only to avoid bias from the left hemisphere stroke lesion, since the goal of this study was to assess the effects of small vessel disease, and not the white matter damage that would have occurred as a consequence of the large vessel occlusion that caused the aphasia. Of note, it is generally assumed that the extent of WMH is symmetrical across hemispheres. WMH were rated separately for the periventricular space (periventricular hyperintensities; PVH) and in the deep white matter (deep white matter hyperintensities; DWMH), each rating being measured on a four-point scale, ranging from 0 (absence of WMH) to 3 (confluent WMH). Ratings were made on T2-weighted MRI scans. Per Fazekas and colleagues (1987), WMH in the periventricular area (PVH) were defined as "caps or pencil-thin lining" (PVH score of 1), "smooth halo" (PVH score of 2), and periventricular hyperintensities that extended into surrounding deep white matter (PVH score of 3). DWMH were defined as punctate foci (DWMH score of 1), the beginning of confluent foci (DWMH score of 2), and confluent areas

(DWMH score of 3) [144]. Figure 2 presents examples of PVH and DWMH ratings from selected participants in this study sample.

WMH ratings were based on a consensus between the primary rater (AB) and secondary raters (BS and LJ), who each rated a subset (50% each) of MRIs. Raters were blind to all participant demographics and test scores. The group averages of Fazekas scale scores are presented in Table 1.

Image Acquisition

Imaging was acquired on a Siemens Prisma 3 T scanner equipped with a 20-element head/neck (16/4) coil at the University of South Carolina or Medical University of South Carolina. Images were generally acquired within two days of behavioral testing. This study used whole-brain T1-weighted, T2-weighted, and Diffusion EPI images collected from each participant. Parameters are as follows:

1. T1-weighted image utilizing an MP-RAGE sequence with 1 mm isotropic voxels, a 256 x 256 matrix size, a 9-degree flip angle, and a 192-slice sequence with TR = 2250 ms, TI = 925 ms, TE = 4.11 ms with parallel imaging (GRAPPA = 2, 80 reference lines).
2. T2-weighted image utilizing a sampling perfection with application optimized contrasts using a different flip angle evolution (3D-SPACE) sequence. This 3D TSE scan uses a TR = 3200 ms, a TE of 567 ms, variable flip angle, 256 × 256 matrix scan with 176 slices (1 mm thick), using parallel imaging (GRAPPA = 80 reference lines).

3. Diffusion mono-polar EPI scan that uses 43 volumes sampling 36 directions with b = 1000 s/mm2 (with 7 volumes b = 0), TR = 5250 ms, TE = 80 ms, 140 × 140 matrix, 90-degree flip angle, 210 × 210 mm field of view, with parallel imaging GRAPPA = 2, 80 contiguous 1.5 mm slices. This sequence was acquired twice, with phase encoding polarity reversed for the second series.

Image processing

Lesion Mapping

The chronic post-stroke lesions were drawn by a stroke neurologist (LB) or by a researcher with extensive experience with brain imaging in stroke populations; both were blinded to behavioral scores at time of lesion drawing. Lesions were manually drawn using the software MRIcron.

Using SPM12 and MATLAB scripts developed in-house, the stroke lesion maps were spatially normalized to standard space through the following steps: 1) The T2 scan was co-registered with the individual's T1 scan with the transforms used to resliced the lesion into native T1 space; 2) The resliced lesion maps were smoothed with a 3mm full-width half maximum Gaussian kernel to remove jagged edges associated with manual drawing; 3) an enantiomorphic normalization [96] approach using SPM12's unified segmentation-normalization [97] was applied to normalize the T1-weighted images onto the standard space, using a chimeric T1-weighted image where the area corresponding to the stroke lesion was replaced by the mirrored equivalent region in the intact (right) hemisphere; 4) The lesion mask was then binarized, and only voxels with a probability greater than 50% were maintained in the final normalized lesion mask.

Once the lesion masks were placed in standard space, each image was divided into anatomical grey matter regions based on the Atlas of Intrinsic Connectivity of Homotopic Areas (AICHA) [59] brain atlas to determine the overall lesion size.

Structural connectome

Each participant's individual connectome was built from the neuroimaging data using steps defined in our previous publication [145]. Briefly, 1) T1 weighted images were segmented into probabilistic grey and white matter maps using SPM12's unified segmentation-normalization; 2) each individual's grey matter map was divided into 384 regions using the AICHA brain atlas [59]; 3) the grey matter parcellation maps were non-linearly registered into the diffusion tensor imaging (DTI) space; 4) pairwise probabilistic DTI fiber tracking was computed for all possible pairs of grey matter regions; 5) the weight of each pairwise connectivity link was determined based on the number of probabilistic streamlines connecting the grey matter region pair, corrected by distance travelled by each streamline and by the total volume of the connected regions; and 6) a weighted adjacency matrix M of size 384 x 384 was constructed for each participant with $M_{i,j}$ representing the weighted link between region of interest (ROI) *i* and ROI *j*. Diffusion images were undistorted using TOPUP [99] and Eddy [86]. Tractography was estimated using FSL's FMRIB's Diffusion Toolbox (FDT) probabilistic method [60] with FDT's accelerated BEDPOST [100]being used to assess default distributions of diffusion parameters at each voxel, and probabilistic tractography was performed using FDT's probtrackX (parameters: 5000 individual pathways drawn through the probability distributions on principal fiber direction, curvature threshold set at 0.2, 200 maximum

steps, step length 0.5mm, and distance correction). The waypoint mask was set as the white-matter probabilistic map excluding the stroke lesion. The weighted connectivity between the regions *i* and *j* was defined as the number of probabilistic streamlines arriving at *j* ROI when *i* was seeded, averaged with the number of probabilistic streamlines arriving at *i* ROI when *j* was seeded. The connection weight was corrected based on the distance travelled by the streamlines connecting *i* and *j* (probtrackX's "distance correction"). The number of streamlines connecting each pair of ROIs was further divided by the sum of the volumes of these ROIs to compensate for the unequal size of grey matter ROIs. In summary, each individual connectome was represented by a 384 x 384 matrix, where the nodes corresponded to the AICHA anatomical ROIs and the edges to the structural connectivity between the nodes.

White matter fiber length

In order to determine the number of short-, mid- and long-range white matter connections we calculated the Euclidean distance between each pair of ROI centroids in standard MRI space. The connections were then grouped into whether they connected ROIs whose distance was within the 1st quartile (lowest 25%) as "short distance" fibers, and all fibers within the 4th quartile (75% and above) as "long distance" fibers. Mid-range fibers had lengths within the 2nd and 3rd quartiles (25-75%). We calculated the total number of connections and determined the percentage of all existing connections in each connectome that were either short-, mid-, or long-range fibers.

Lesion volume

To account for the influence of the lesion in the left hemisphere on the WAB-AQ scores, we controlled for lesion volume in statistical analyses. The stroke lesion maps were normalized into standard space and co-registered to the MNI 152 1 mm atlas. Stroke lesion volume (in ml) was equal to the number of lesioned voxels in cubic mm divided by 1000, because each voxel had a size of 1 mm x 1mm x 1mm.

Assessment of aphasia: WAB-AQ

The Western Aphasia Battery-Revised (WAB-R [146]) is a commonly used clinical evaluation of aphasia that evaluates the presence, type, and severity of aphasia on a 0-100 scale (scores <93.8 are indicative of aphasia). The WAB-R broadly assesses the domains of expression and comprehension, yielding summary scores for the following four domains: spontaneous speech, auditory verbal comprehension, repetition and naming and word finding. The Aphasia Quotient (AQ), the weighted composite of these four scores, was used as the dependent (behavioral) variable of interest in this study and is indicative of the overall severity of the individual's aphasia.

Statistical analyses

IBM SPSS Statistics for Windows (version 24, released 2016, IBM Corp., Armonk, N.Y., USA) was utilized for all analyses. P-values ≤ 0.05 were considered statistically significant.

In order to determine the relationship between WMH and fiber length, we performed correlation analyses on PVH, DWMH and the number and percentage of short-, mid-, and long-range fibers. We used one-tailed statistical tests for the number of fibers, because

we hypothesized WMH are associated with a general decrease and not gain in the number of fibers independently of fiber length, but we used two-tailed statistical tests for percentage of fibers, because we hypothesized a proportional change for each fiber length group. Based on visual inspection of the data and the Shapiro-Wilk test for normality, we found that all variables were not normally distributed, thus, we used non-parametric, bivariate Spearman correlations. The strength of correlations was interpreted as weak for $|r|<0.3$, as moderate for $0.3\leq |r| < 0.5$, and as strong for $|r| \geq 0.5$ [147].

To assess whether WMH and fiber length types (short-, middle-, long-range fibers) had an independent or combined effect on the distribution of percentages of fiber length types, we performed a two-way analysis of variance (ANOVA) for unbalanced designs, because there were no equal sized groups across the factors.

Mediation analysis

In order to determine if the relationship between WMH and aphasia severity is related to fiber length, we performed a statistical mediation analysis by employing the PROCESS macro [148], a validated, freely available computational tool. We conducted multivariable regression modelling for the mediation analysis and used stroke lesion volume as a control variable to account for the impact of the stroke lesion in the left hemisphere on communicative abilities.

As shown in Figures 3A and 3B, steps for a parallel mediation analysis with two mediators include the determination of 1) the total effect of the independent variable (X) on the dependent variable, (Y); 2) the direct effect of X on Y when accounting for mediating variables (in our study two mediators: M1 and M2); and 3) the two indirect

effects of X on Y through M1 and of X on Y through M2. Using parallel mediation we can test each mediator's contribution while holding another mediator constant [149].

In this study we assessed the total, direct and indirect effects of WMH (X) on WAB-AQ (Y). Based on our hypothesis that damage to a higher proportion of long-range fibers counterbalanced by damage to a lower percentage of short-range fibers mediate the relationship between WMH and worse chronic post-stroke aphasia severity, we assessed the indirect effect of WMH on WAB-AQ through the number of long-range (M1) and number of short-range fibers (M2). Using model 4 in the PROCESS macro, we modeled two indirect effects of WMH on WAB-AQ mediated by the number of short- and long-range fibers, and we modeled the direct effect of WMH on WAB-AQ. To determine the indirect effects we performed two regression models for each mediator. First, we assessed the impact of WMH on the number of long-/short-range fibers while controlling for the other mediator (Models 1 and 2 in Table 3), and second, we assessed the impact of the number of long-/short-range fibers while controlling for the other mediator and WMH (Model 3). The last regression model (Model 3), was also used to determine the direct effect of WMH on WAB-AQ while controlling for both mediators.

We used bias corrected bootstrapping with 5000 samples and 95% confidence intervals (CI) to evaluate our hypothesis of indirect effects of WMH on WAB-AQ. We rejected our null hypothesis (no indirect effect present) if the CI did not include zero.

We chose the number instead of percentage of fiber types to avoid multicollinearity in the regression models, because the variables percentage of short-, mid-, and long-range fibers were interdependent. We tested all regression models for multicollinearity by calculating the variance of inflation factor (VIF) and considered VIF>6 as evidence for

multicollinearity [150]. All variables in all performed regression models had VIF<6 and thus, we assumed that multicollinearity was absent or within acceptable means.

Results

Relationship between WMH and axonal fiber damage.

As expected, the two subscales PVH and DWMH significantly correlated with each other (r=0.454, p=0.001). The correlation size was moderate, confirming that PVH and DWMH measure inter-related, but distinct, phenomena.

Relationship with fiber length

We assessed the association between WMH (PVH and DWMH) and the absolute (count) and relative (percentage) number of short-, mid- and long-range fibers in the right hemisphere. Regarding the absolute fiber count, Spearman correlations were statistically significant for PVH and DWMH scores and all three fiber length types (Table 2, see supplementary Figures 1 for scatterplots). The higher (more severe) the PVH / DWMH scores, the lower the number of all three fiber length groups. From the lowest, least severe PVH score of "0" to the highest, most severe score of "3", there was a 15% decrease (median) in the absolute number of short-, 35% decrease in mid-, and 47% decrease in long-range fibers. For DWMH there was a 19% decrease in the absolute number of short-, 36% decrease in mid-, and 51% decrease in long-range fibers.

PVH and DWMH scores were significantly correlated with the percentage of short- and long-range fibers (Table 2). Higher (more severe) PVH and DWMH scores were

associated with a significantly lower percentage of long-range, but significantly higher percentage of short-range fibers (reflecting a disproportionate damage to long-range fibers, compared with short-range fibers) (Fig 4). Correlations between PVH scores and axonal fiber damage were weak to moderate in size.

Using a two-way ANOVA, there were no significant interaction effects for PVH and fiber length types, $F(6, 135)=1.95$, $p=0.07$, and for DWMH and fiber length type, $F(6, 135)=1.41$, $p=0.2168$. Assessing the distribution of WMH scores across the fiber length types, the score of "1" showed the largest variability (widest range) of percentages for each fiber type. When we excluded the score "1" from the WMH scores to only include scores of "0", "2" and "3", we found significant interaction effects for both PVH and fiber length types, $F(4, 99)=6.67$, $p=0.0001$, and for DMWHs and fiber length types $F(4, 42)=3.23$, $p=0.0213$, indicating that the effect of fiber length types was dependent on these WMH scores.

In post-hoc analyses, we assessed whether the relationship between WMH and fiber types in the right hemisphere was confounded by the stroke lesion in the left hemisphere, as the lesion may have indirect effects on right hemisphere white matter. We performed multivariable linear regression modeling with the number or percentage of fiber types as the dependent variable, PVH or DWMH as the main independent variable, and lesion volume as the control variable. We confirmed the significant relationships ($p\leq0.05$) between higher (more severe) PVH / DWMH scores and a lower number of mid- and long-range fibers, and higher (more severe) DWMH scores and a lower percentage of long-range fibers. Higher (more severe) PVH scores showed a strong trend towards significance for a decrease in the percentage of long-range fibers ($p=0.054$). These *post-*

hoc analyses indicate an effect of WMH on fiber length groups independently of the stroke lesion, with damage to a higher percentage of long-range compared to short- and mid-range fibers.

Relationship between WMH, axonal fiber damage, and chronic aphasia severity.

We found a significant total effect of PVH on WAB-AQ with higher (more severe) PVH scores linked to lower (more severe) WAB-AQ scores (unstandardized beta=-6.607, standard error=2.386, standardized beta=-0.348, p=0.008) when controlling for stroke lesion volume. There was no effect of DWMH on WAB-AQ ($p>0.05$), thus, we further explored direct and indirect effects for PVH only.

We performed mediation modeling with PVH as the independent variable, WAB-AQ as the dependent variable, percentage of long-range fibers in the whole brain as the first mediator variable, percentage of short-range fibers in the whole brain as the second mediator variable, and lesion volume as the control variable. Contrary to the first objective where we assessed only the right hemisphere, we chose to specify the percentage of long- and short-range fibers in the whole brain instead of the right hemisphere only, because 1) of the importance of the left hemisphere for aphasia severity, and 2) WMH are usually symmetric, thus the extent of WMH should be similar between both hemispheres.

Results from the mediation analysis are presented in Table 3 and Figure 5. The results indicated that there was a (marginally failed) non-significant direct effect of PVH on WAB-AQ (effect=-4.8803, SE=2.4617, lower limit 95-CI=-9.8483, upper limit 95%-CI=0.0877, p=0.0540), but there were significant indirect effects of PVH on WAB-AQ

mediated by the number of long-range fibers (effect=-6.2273, Bootstrapping: SE=2.6426, lower limit 95-CI=-11.8243, upper limit 95%-CI=-1.5599) and the number of short-range fibers (effect=4.5006, Bootstrapping: SE=2.5881, lower limit 95-CI=0.1631, upper limit 95%-CI=10.2897). More severe PVH scores were associated with a lower number of long-range fibers, and in turn a lower number of long-range fibers were associated with more severe WAB-AQ scores. Further, more severe PVH scores were associated with a lower number of short-range fibers, and in turn a lower number of short-range fibers were associated with less severe WAB-AQ scores. Thus, the total effect of PVH on WAB-AQ that we had found initially, was mainly based on indirect effects and not direct effects of PVH on WAB-AQ.

Discussion

Most individuals 60 years or older show evidence of cerebral WMH on neuroimaging [125, 126]. Increasing severity of WMH has been linked to decline and worse recovery of physical, functional and cognitive abilities in stroke survivors [136-140]. The underlying neurophysiological correlates are poorly understood, hampering the strategic development of treatment approaches for stroke survivors that could take the neurophysiological changes resulting from WMH into account. In the study presented here, we sought to investigate the relationship between WMH, structural brain network integrity, and post-stroke aphasia severity.

Relationship between WMH and axonal fiber damage.

In the first part of the study, we assessed the relationship between WMH (PVH and DWMH) and structural brain connectivity measured by axonal damage of white matter fibers with different lengths. Our findings indicate that WMH are associated with damage to a higher percentage of long-range fibers compared to mid- and short-range fibers. Axonal damage as a microstructural correlate of WMH has been described before [104, 151]. Recent explorative research further suggests that long-range fibers are more susceptible to WMH-related damage than short-range fibers [35]. Our study supports and expands on these findings by using sophisticated fiber tracking methods. We found that while the absolute number (count) of all fibers – independent of length – decreased with more severe WMH, the relative number (proportion/percentage) of long-range fibers decreased more than twice as much as short-range fibers.

Possible reasons for the WMH-related proportionally greater damage to long-range fibers are that 1) white matter in general is susceptible to damage when lesioned, because of its lower blood flow compared to grey matter [63], and 2) long-range fibers in specific are susceptible to damage when lesioned likely because of their higher metabolic demands [35, 142].

In general, it is possible that our findings on the relationship between WMH and axonal fiber damage can assist in the development of therapeutic interventions for stroke survivors that target the neurophysiological correlates of WMH. Although not tested here, this information could be used to track if interventions such as close control of blood glucose, blood pressure, cholesterol, diet, exercise, lead to preservation of long-range fibers and improve neurorehabilitation outcomes. Likewise, preservation of long-range fibers could be used as a marker of interventional efficacy.

Relationship between WMH, axonal fiber damage, and chronic aphasia severity.

In the second part of the study, we assessed the impact of WMH and axonal fiber damage on language performance in stroke survivors. We found that PVH were associated with worse WAB-AQ scores, mediated by the proportion of long-range and short-range white matter fibers. Thus, PVH did not directly impact language abilities, but did so indirectly. With more severe PVH, the percentage of long-range fibers was lower, the percentage of short-range fibers higher, and aphasia more severe. Thus, patients, whose residual neural network consisted of a higher proportion of long-range fibers (counterbalanced by a lower proportion of short-range fibers), were more likely to show milder aphasia compared to patients with a lower proportion of long-range fibers (counterbalanced by a

higher proportion of short-range fibers). These findings are in line with our previous research, showing that the severity and treatment response of post-stroke aphasia depend on the preservation of residual neural networks [152, 153]. The study presented here provides novel information by addressing the specific role of long-range and short-range white matter fibers regarding chronic aphasia severity in individuals with small vessel brain disease.

Limitations

We chose to measure WMH with a published ordinal visual rating scale, because of its wide-spread and easy use. However, the scale does not take exact brain locations into account, what could be important information to understand neurophysiological and functional correlates. Further, we conducted a cross-sectional study, however, a longitudinal study is warrented to assess possible changes in white matter hyperintensities and their long-term effects on aphasia severity.

Conclusions

Our findings indicate that 1) WMH are related to damage to long-range white matter fibers and 2) WMH lead to worse chronic aphasia in chronic stroke due to a higher percentage of long-range fibers counterbalanced by a lower percentage of short-range fibers. Thus, small vessel brain disease predisposes stroke survivors to worse language outcomes because of a compromised balance of long-range and short-range white matter fibers. As such, therapeutic interventions for stroke recovery could target the damage to

long-range fibers in order to preserve brain health and foster better recovery in individuals with small vessel brain disease.

Figures

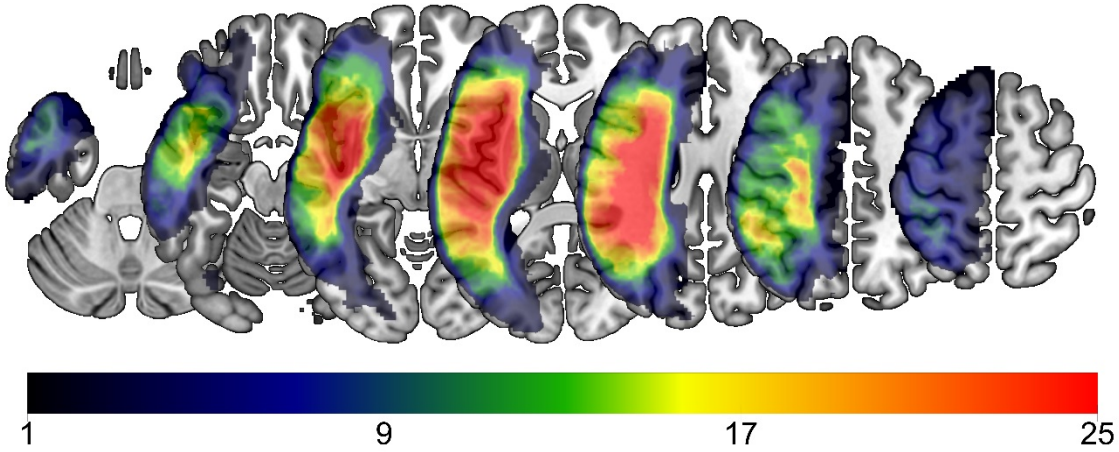

Figure 1: Lesion overlay of all participants (N=48). Colors represent the number of patients with a lesion in that area, with warmer colors indicating greater regions of overlap.

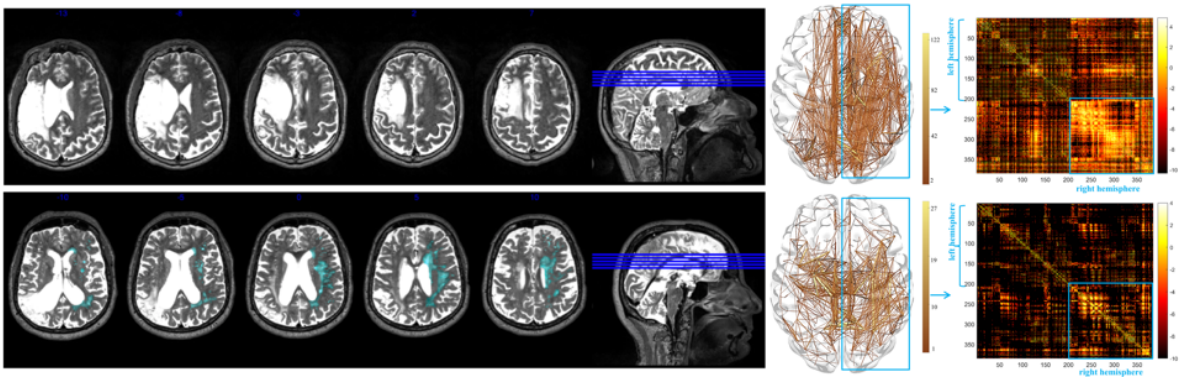

Figure 2: T2-weighted MRI images from two patients of the study sample, exemplifying PVH and DWMH ratings (left side of figure, WMH are highlighted in light blue), as well as the corresponding fiber tracking and structural connectome matrix (right side of figure; x- and y-axes correspond to the AICHA ROI numbers, warmer colors represent higher connectivity between ROIs). Patient 1 (first row) did not present with WMH; patient 2 (second row) presented with the most severe scores (3 for PVH and 3 for DWMH). The connectome matrices show that the more severe WMH scores for patient 2 coincided with less connections, particularly in brain areas with long range projections such as the

frontal lobe, compared to patient 1. (AICHA=atlas of intrinsic connectivity of homotopic areas, DWMH=deep white matter hyperintensities, PVH=periventricular white matter hyperintensities, ROI=region of interest, WMH=white matter hyperintensities).

3A

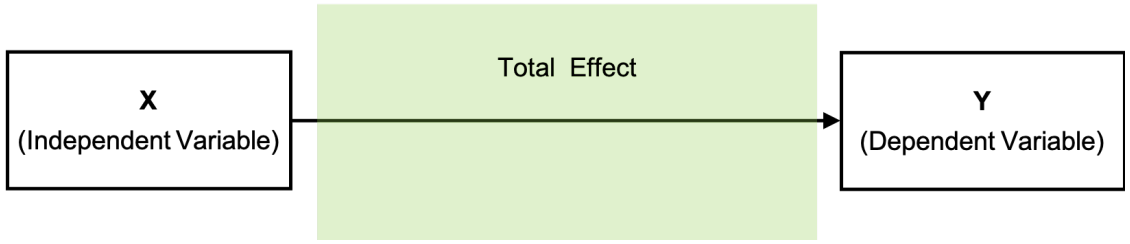

3B

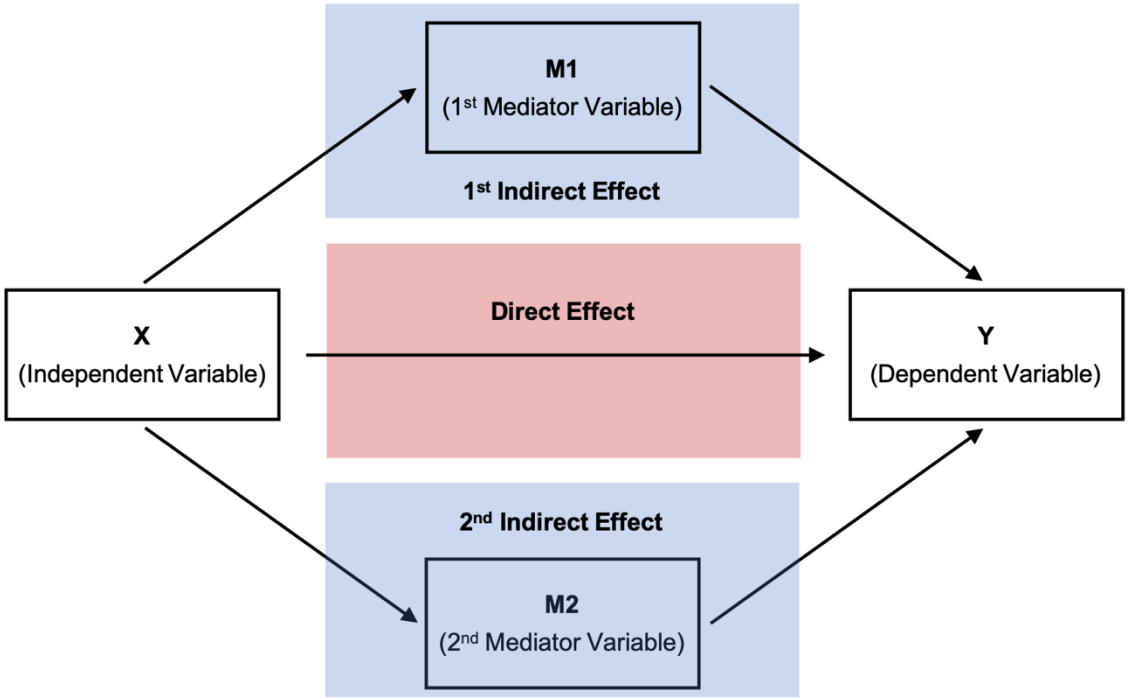

Figure 3: Simplified schematic representation of the serial meditation analysis with two mediators. The total effect (green box) of the independent variable (X) on the dependent variable (Y) (Fig 3A) is the predictive power of X on Y without taking mediators into account. The direct effect (red box) is the predictive power of X on Y while controlling for M1 and M2 (Fig 3B). The indirect effects (blue box) of X on Y are the processes of the impact of X on M (M1, M2) and M on Y (Fig 3B). In the serial mediation model with

two mediators, there are three different indirect effects: 1) X on M1 and M1 on Y; 2) X on M2 and M2 on Y, 3) X on M1, M1 on M2 and M2 on Y. Thus, the total effect is the sum of the indirect (blue box) and direct effects (red box) of X on Y while accounting for mediating variables (M1 and M2) [154].

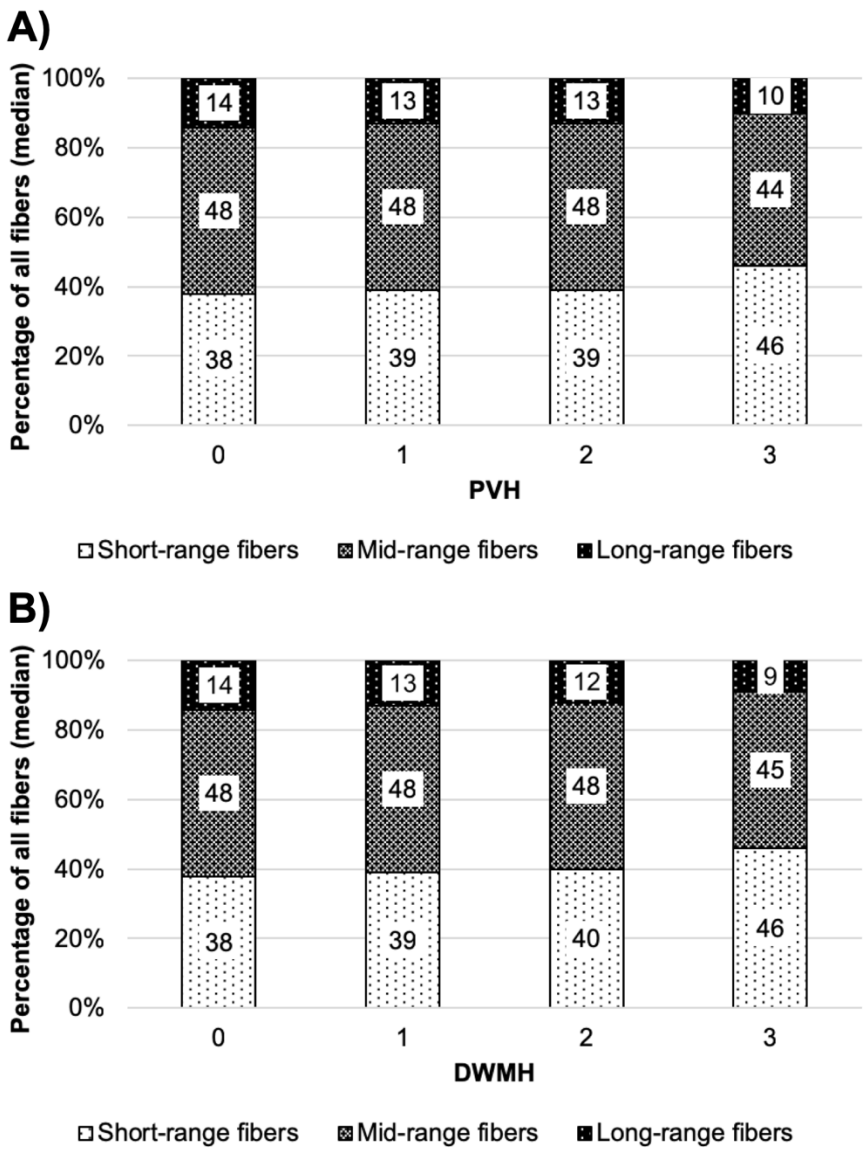

Figure 4: Median percentage of short-, mid- and long-range fibers in the right hemisphere for patients (N=48) with different PVH (periventricular white matter hyperintensities; Fig 4A) and DWMH (deep white matter hyperintensities; Fig 4B) scores.

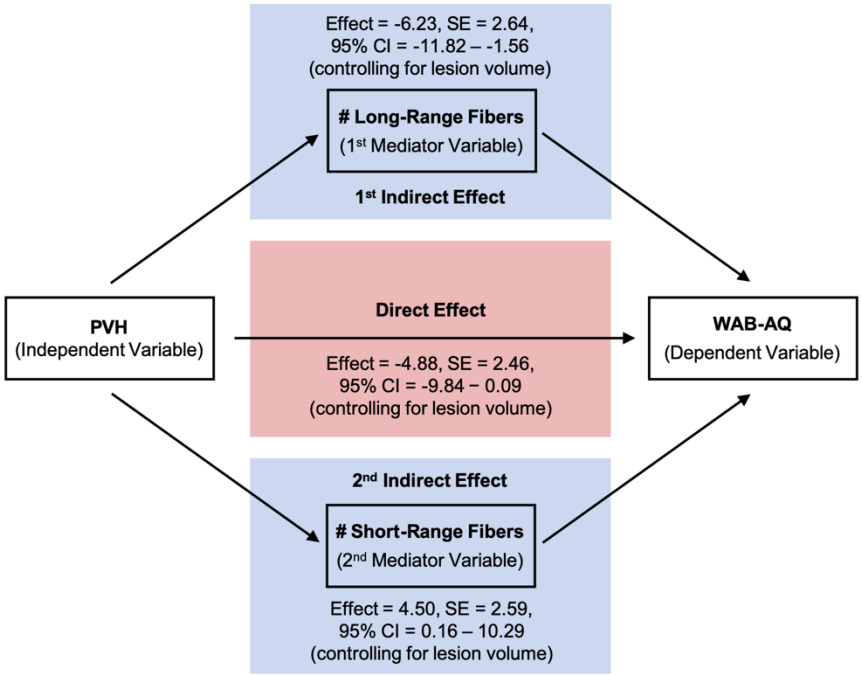

Figure 5: Direct and indirect (mediated) effects of PVH (periventricular white matter hyperintensities) on WAB-AQ (Western Aphasia Battery – Aphasia Quotient) estimated through regression modeling. The direct effect was non-significant. The Indirect effect through the two mediating variables – percentage of long-range and percentage of short-range fibers – was significant (bootstrapping 95% CI (confidence interval) did not include zero). SE=standard error.

Tables

Table 1: Demographic and medical information of study participants (N=48).

Race, N (%)	11 (23) Black/African American, 37 (77) White
Ethnicity, N (%)	48 (100) Not Hispanic or Latino
Sex, N (%)	16 (33) females, 32 (67) males
Education (in years); mean (SD), range	15.49 (2.45), 12-20
Age at test (in years); mean (SD), range	60.44 (11.96), 29-76
Age at stroke (in years); mean (SD), range	55.92 (12.39), 27-75
Time post-stroke (in months); mean (SD), range	54.44 (53.64), 12-245
Stroke type, N (%)	37 (77) ischemic, 9 (19) hemorrhagic, 2 (4) unknown
Number of strokes (before enrollment), N (%)	43 (90) one, 3 (6) two, 1 (2) three, 1 (2) four

Lesion volume (in ml); mean (SD), range	133.93 (98.80), 4.93-467.46
WAB-R aphasia quotient; mean (SD), range	59.06 (22.13), 20.10-93.10
PVH score; median, range, mean (SD)	1, 0-3, 1,46 (1.15)
DWMH score; median, range, mean (SD)	1, 0-3, 1.19 (0.76)

DWMH=deep white matter hyperintensities, PVH=periventricular hyperintensities, WAB-R=Western Aphasia Battery-Revised

Table 2: Correlations (Spearman's rho) between WMH scores and connectome measures of the right hemisphere (N=48).

	Short-range fibers	**Mid-range fibers**	**Long-range fibers**
	r/p-value	r/p-value	r/p-value
	Absolute number of fibers (count)		
PVH	-0.334*/0.010	-0.335*/0.010	-0.318*/0.014
DWMH	-0.262*/0.036	-0.270*/0.032	-0.293*/0.022
	Relative number of fibers (percentage)		
PVH	0.298*/0.040	-0.264/0.070	-0.296*/0.041
DWMH	0.299*/0.039	-0.140/0.340	-0.319*/0.027

DWMH=deep white matter hyperintensities, PVH=periventricular white matter hyperintensities

*=correlation is significant at the 0.05 level (1-tailed for absolute number of fibers; 2-tailed for relative number of fibers)

Table 3: Mediation analysis for the effect of PVH on WAB-AQ mediated in parallel by the number of long-range fibers and number of short-range fibers, while controlling for lesion volume. The first indirect effect of PVH on WAB-AQ mediated by the number of

long-range fibers (1st indirect effect in Figures 3 and 5) is assessed with Models 1 and 3. Model 1 determines the impact of PVH on the number of long-range fibers, and Model 3 determines the impact of the number long-range fibers on WAB-AQ. The second indirect effect of PVH on WAB-AQ mediated by the number of short-range fibers (2nd indirect effect in Figures 3 and 5) is assessed with Models 2 and 3 same as for the 1st indirect effect. The direct effect of PVH on WAB-AQ (direct effect in Figures 3 and 5) is assessed with Model 3.

Model 1
Dependent variable: number of long-range fibers in whole brain

	unstandardized coefficients B (SE)	standardized coefficients β	t	p
Model (r^2=0.24, p=0.0022)				
Constant*	17055.41 (1900.69)		8.97	<0.0001
PVH*	-2725.69 (854.38)	-0.43	-3.19	0.0026
Lesion volume	-13.39 (10.01)	-0.18	-1.34	0.1879

Model 2
Dependent variable: number of short-range fibers in whole brain

	unstandardized coefficients B (SE)	standardized coefficients β	t	p
Model (r^2=0.23, p=0.0031)				
Constant*	31422.45 (1505.18)		20.88	<0.0001
PVH*	-1593.58 (676.59)	-0.32	-2.36	0.0230
Lesion volume*	-17.97 (7.93)	-0.31	-2.27	0.0283

Model 3
Dependent variable: WAB-AQ

	unstandardized coefficients B (SE)	standardized coefficients β	t	p
Model (r^2=0.45, p<0.0001)				
Constant	130.81 (20.79)		6.29	<0.0001
PVH	-4.88 (2.46)	-0.26	-1.98	0.0540
N of long-range fibers*	0.002 (0.001)	0.77	2.99	0.0046
N of short-range fibers*	-0.003 (0.001)	-0.75	-2.93	0.0054
Lesion volume*	-0.11 (0.03)	-0.49	-3.91	0.0003

N=number, PVH=periventricular white matter hyperintensities, SE=standard error
*=variable is a significant predictor at the 0.05 level

Conclusion 7

Optimal brain health is currently considered to be the absence of overt clinical symptoms despite overwhelming evidence indicating the presence of subclinical damage long before clinical symptoms emerge.

Complex network analyses of the connectome offer powerful, non-invasive approaches for probing the macroscopic architecture of brain networks, and provide a unique methodological advantage to detecting covert brain injury not readily available to either clinical paper and pencil tests (that only detect clinically relevant cognitive deficits) or neurological imaging (that detect large or small vessel disease, stroke, AD deposition), but may not detect microinfarcts. Detecting deviations from the optimal topological structure early in life, that may result from modifiable risk factors or genetic abnormality, will lead to timely interventions that may stave off cognitive decline or prevent it completely.

This work supplements a burgeoning field of research that will undoubtedly lead to development of clinically significant diagnostic and prognostic tools by identifying relevant, quantifiable measures of sub-optimal brain function detectable in healthy individuals with CVRF, that continue to affect functional recovery in both acute and chronic stroke populations. While a lot of work remains to be done, for instance, defining the optimal topology in healthy young controls to reveal a clear dichotomy between patient and healthy populations, the disorganization of the structure of brain networks, driven by

the loss of long-range fibers maybe a viable inclusion to the symptomatology of sub-optimal brain health.

References

1. Benjamin EJ, Muntner P, Alonso A, et al. Heart Disease and Stroke Statistics-2019 Update: A Report From the American Heart Association. Circulation 2019;139:e56-e66.
2. Mensah GA, Wei GS, Sorlie PD, et al. Decline in Cardiovascular Mortality: Possible Causes and Implications. Circulation research 2017;120:366-380.
3. George MG, Tong X, Bowman BA. Prevalence of Cardiovascular Risk Factors and Strokes in Younger AdultsPrevalence of Cardiovascular Risk Factors and Strokes in Younger AdultsPrevalence of Cardiovascular Risk Factors and Strokes in Younger Adults. JAMA Neurology 2017;74:695-703.
4. Crichton GE, Elias MF, Davey A, Alkerwi A. Cardiovascular health and cognitive function: the Maine-Syracuse Longitudinal Study. PloS one 2014;9:e89317.
5. Reis JP, Loria CM, Launer LJ, et al. Cardiovascular health through young adulthood and cognitive functioning in midlife. Annals of neurology 2013;73:170-179.
6. Hajar R. Framingham Contribution to Cardiovascular Disease. Heart views : the official journal of the Gulf Heart Association 2016;17:78-81.
7. Elias MF, Sullivan LM, D'Agostino RB, et al. Framingham stroke risk profile and lowered cognitive performance. Stroke 2004;35:404-409.
8. Valdés Hernández Mdel C, Booth T, Murray C, et al. Brain white matter damage in aging and cognitive ability in youth and older age. Neurobiology of aging 2013;34:2740-2747.
9. Gorelick PB, Scuteri A, Black SE, et al. Vascular contributions to cognitive impairment and dementia: a statement for healthcare professionals from the american heart association/american stroke association. Stroke 2011;42:2672-2713.
10. Attwell D, Laughlin SB. An energy budget for signaling in the grey matter of the brain. Journal of cerebral blood flow and metabolism : official journal of the International Society of Cerebral Blood Flow and Metabolism 2001;21:1133-1145.
11. Lennie P. The cost of cortical computation. Current biology : CB 2003;13:493-497.
12. Blinder P, Tsai PS, Kaufhold JP, Knutsen PM, Suhl H, Kleinfeld D. The cortical angiome: an interconnected vascular network with noncolumnar patterns of blood flow. Nature neuroscience 2013;16:889-897.
13. Niedowicz DM, Reeves VL, Platt TL, et al. Obesity and diabetes cause cognitive dysfunction in the absence of accelerated beta-amyloid deposition in a novel murine model of mixed or vascular dementia. Acta neuropathologica communications 2014;2:64.
14. Kobayashi K, Forte TM, Taniguchi S, Ishida BY, Oka K, Chan L. The db/db mouse, a model for diabetic dyslipidemia: molecular characterization and effects of Western diet feeding. Metabolism: clinical and experimental 2000;49:22-31.
15. Okamoto K, Yamamoto K, Morita N, et al. Establishment and use of the M strain of stroke-prone spontaneously hypertensive rat. Journal of hypertension Supplement : official journal of the International Society of Hypertension 1986;4:S21-24.
16. Henning EC, Warach S, Spatz M. Hypertension-induced vascular remodeling contributes to reduced cerebral perfusion and the development of spontaneous stroke in aged SHRSP rats. J Cereb Blood Flow Metab 2010;30:827-836.
17. Smith EE, Schneider JA, Wardlaw JM, Greenberg SM. Cerebral microinfarcts: the invisible lesions. The Lancet Neurology 2012;11:272-282.

18. Summers PM, Hartmann DA, Hui ES, et al. Functional deficits induced by cortical microinfarcts. J Cereb Blood Flow Metab 2017;37:3599-3614.
19. Wang M, Ding F, Deng S, et al. Focal Solute Trapping and Global Glymphatic Pathway Impairment in a Murine Model of Multiple Microinfarcts. The Journal of neuroscience : the official journal of the Society for Neuroscience 2017;37:2870-2877.
20. Okamoto Y, Yamamoto T, Kalaria RN, et al. Cerebral hypoperfusion accelerates cerebral amyloid angiopathy and promotes cortical microinfarcts. Acta neuropathologica 2012;123:381-394.
21. Gorelick PB, Furie KL, Iadecola C, et al. Defining Optimal Brain Health in Adults: A Presidential Advisory From the American Heart Association/American Stroke Association. Stroke 2017;48:e284-e303.
22. Bullmore E, Sporns O. The economy of brain network organization. Nature reviews Neuroscience 2012;13:336-349.
23. Bullmore E, Sporns O. Complex brain networks: graph theoretical analysis of structural and functional systems. Nature reviews Neuroscience 2009;10:186-198.
24. Kaiser M. A tutorial in connectome analysis: topological and spatial features of brain networks. NeuroImage 2011;57:892-907.
25. Newman ME, Girvan M. Finding and evaluating community structure in networks. Physical review E, Statistical, nonlinear, and soft matter physics 2004;69:026113.
26. Kaiser M, Hilgetag CC. Nonoptimal component placement, but short processing paths, due to long-distance projections in neural systems. PLoS computational biology 2006;2:e95.
27. Alexander-Bloch AF, Gogtay N, Meunier D, et al. Disrupted modularity and local connectivity of brain functional networks in childhood-onset schizophrenia. Frontiers in systems neuroscience 2010;4:147.
28. Liu Y, Liang M, Zhou Y, et al. Disrupted small-world networks in schizophrenia. Brain : a journal of neurology 2008;131:945-961.
29. Feinberg I. Schizophrenia: caused by a fault in programmed synaptic elimination during adolescence? Journal of psychiatric research 1982;17:319-334.
30. Sepulcre J, Sabuncu MR, Becker A, Sperling R, Johnson KA. In vivo characterization of the early states of the amyloid-beta network. Brain : a journal of neurology 2013;136:2239-2252.
31. Nasrabady SE, Rizvi B, Goldman JE, Brickman AM. White matter changes in Alzheimer's disease: a focus on myelin and oligodendrocytes. Acta neuropathologica communications 2018;6:22.
32. Marebwa BK, Adams RJ, Magwood GS, et al. Cardiovascular Risk Factors and Brain Health: Impact on Long-Range Cortical Connections and Cognitive Performance. Journal of the American Heart Association 2018;7:e010054.
33. Lawrence AJ, Zeestraten EA, Benjamin P, et al. Longitudinal decline in structural networks predicts dementia in cerebral small vessel disease. Neurology 2018;90:e1898-e1910.
34. Marebwa BK, Fridriksson J, Yourganov G, Feenaughty L, Rorden C, Bonilha L. Chronic post-stroke aphasia severity is determined by fragmentation of residual white matter networks. Scientific reports 2017;7:8188.

35. Lambert C, Benjamin P, Zeestraten E, Lawrence AJ, Barrick TR, Markus HS. Longitudinal patterns of leukoaraiosis and brain atrophy in symptomatic small vessel disease. Brain : a journal of neurology 2016;139:1136-1151.
36. Gelber RP, Ross GW, Petrovitch H, Masaki KH, Launer LJ, White LR. Antihypertensive medication use and risk of cognitive impairment: the Honolulu-Asia Aging Study. Neurology 2013;81:888-895.
37. A Randomized Trial of Intensive versus Standard Blood-Pressure Control. New England Journal of Medicine 2015;373:2103-2116.
38. Bondy KN. Assessing cognitive function: a guide to neuropsychological testing. Rehabilitation nursing : the official journal of the Association of Rehabilitation Nurses 1994;19:24-30, 36.
39. Klasik A, Janas-Kozik M, Krupka-Matuszczyk I, Augustyniak E. [Cognitive functions, their development and modern diagnostic methods]. Przeglad lekarski 2006;63 Suppl 1:29-34.
40. Schneider EB, Sur S, Raymont V, et al. Functional recovery after moderate/severe traumatic brain injury: A role for cognitive reserve? Neurology 2014;82:1636-1642.
41. Stiles J, Reilly J, Paul B, Moses P. Cognitive development following early brain injury: evidence for neural adaptation. Trends in cognitive sciences 2005;9:136-143.
42. Nudo RJ. Recovery after brain injury: mechanisms and principles. Frontiers in Human Neuroscience 2013;7:887.
43. Long AN, Dagogo-Jack S. The Comorbidities of Diabetes and Hypertension: Mechanisms and Approach to Target Organ Protection. Journal of clinical hypertension (Greenwich, Conn) 2011;13:244-251.
44. Biessels GJ, Reijmer YD. Brain changes underlying cognitive dysfunction in diabetes: what can we learn from MRI? Diabetes 2014;63:2244-2252.
45. Leritz EC. Cardiovascular Disease Risk Factors and Cognition in the Elderly. 2011;5:407-412.
46. Caplan LR. Lacunar Infarction and Small Vessel Disease: Pathology and Pathophysiology. Journal of Stroke 2015;17:2-6.
47. Fisher CM. Lacunes: Small, deep cerebral infarcts. Neurology 2011;77:2104.
48. Hamner MA, Moller T, Ransom BR. Anaerobic function of CNS white matter declines with age. J Cereb Blood Flow Metab 2011;31:996-1002.
49. Van Essen DC, Barch DM. The human connectome in health and psychopathology. World Psychiatry 2015;14:154-157.
50. Gleichgerrcht E, Kocher M, Bonilha L. Connectomics and graph theory analyses: Novel insights into network abnormalities in epilepsy. Epilepsia 2015;56:1660-1668.
51. Contreras JA, Goñi J, Risacher SL, Sporns O, Saykin AJ. The Structural and Functional Connectome and Prediction of Risk for Cognitive Impairment in Older Adults. Current behavioral neuroscience reports 2015;2:234-245.
52. Galantucci S, Agosta F, Stankovic I, et al. Functional Connectome Organization is Altered in PD Patients with Mild Cognitive Impairment (P4.108). Neurology 2016;86.
53. Agosta F, Canu E, Basaia S, et al. Functional Connectome Architecture of Alzheimer's Disease, Mild Cognitive Impairment and Behavioral Variant of Frontotemporal Dementia: A Graph Analysis Study (P4.028). Neurology 2016;86.
54. Sporns O, Betzel RF. Modular Brain Networks. Annual review of psychology 2016;67:613-640.

55. Blair JR, Spreen O. Predicting premorbid IQ: A revision of the national adult reading test. Clinical Neuropsychologist 1989;3:129-136.
56. Bright P, Hale E, Gooch VJ, Myhill T, van der Linde I. The National Adult Reading Test: restandardisation against the Wechsler Adult Intelligence Scale-Fourth edition. Neuropsychological rehabilitation 2018;28:1019-1027.
57. Charlson ME, Pompei P, Ales KL, MacKenzie CR. A new method of classifying prognostic comorbidity in longitudinal studies: development and validation. J Chronic Dis 1987;40:373-383.
58. Stewart AL, Mills KM, King AC, Haskell WL, Gillis D, Ritter PL. CHAMPS physical activity questionnaire for older adults: outcomes for interventions. Medicine and science in sports and exercise 2001;33:1126-1141.
59. Joliot M, Jobard G, Naveau M, et al. AICHA: An atlas of intrinsic connectivity of homotopic areas. J Neurosci Methods 2015;254:46-59.
60. Behrens TE, Berg HJ, Jbabdi S, Rushworth MF, Woolrich MW. Probabilistic diffusion tractography with multiple fibre orientations: What can we gain? NeuroImage 2007;34:144-155.
61. Rubinov M, Sporns O. Complex network measures of brain connectivity: uses and interpretations. NeuroImage 2010;52:1059-1069.
62. Latora V, Marchiori M. Efficient behavior of small-world networks. Physical review letters 2001;87:198701.
63. Lo EH, Dalkara T, Moskowitz MA. Mechanisms, challenges and opportunities in stroke. Nature reviews Neuroscience 2003;4:399-415.
64. van Norden AG, de Laat KF, Gons RA, et al. Causes and consequences of cerebral small vessel disease. The RUN DMC study: a prospective cohort study. Study rationale and protocol. BMC neurology 2011;11:29.
65. van Veluw SJ, Shih AY, Smith EE, et al. Detection, risk factors, and functional consequences of cerebral microinfarcts. The Lancet Neurology;16:730-740.
66. Shi Y, Wardlaw JM. Update on cerebral small vessel disease: a dynamic whole-brain disease. Stroke and Vascular Neurology 2016;1:83-92.
67. van der Holst HM, van Uden IWM, Tuladhar AM, et al. Cerebral small vessel disease and incident parkinsonism: The RUN DMC study. Neurology 2015;85:1569-1577.
68. van Uden IW, van der Holst HM, Tuladhar AM, et al. White Matter and Hippocampal Volume Predict the Risk of Dementia in Patients with Cerebral Small Vessel Disease: The RUN DMC Study. Journal of Alzheimer's disease : JAD 2016;49:863-873.
69. van Uden IW, Tuladhar AM, de Laat KF, et al. White matter integrity and depressive symptoms in cerebral small vessel disease: The RUN DMC study. The American journal of geriatric psychiatry : official journal of the American Association for Geriatric Psychiatry 2015;23:525-535.
70. Le Bihan D, Iima M. Diffusion Magnetic Resonance Imaging: What Water Tells Us about Biological Tissues. PLoS Biology 2015;13:e1002203.
71. Croall ID, Lohner V, Moynihan B, et al. Using DTI to assess white matter microstructure in cerebral small vessel disease (SVD) in multicentre studies. Clinical Science (London, England : 1979) 2017;131:1361-1373.

72. Moonen JE, Foster-Dingley JC, van den Berg-Huijsmans AA, et al. Influence of Small Vessel Disease and Microstructural Integrity on Neurocognitive Functioning in Older Individuals: The DANTE Study Leiden. AJNR American journal of neuroradiology 2017;38:25-30.
73. Ciulli S, Citi L, Salvadori E, et al. Prediction of Impaired Performance in Trail Making Test in MCI Patients With Small Vessel Disease Using DTI Data. IEEE journal of biomedical and health informatics 2016;20:1026-1033.
74. Xie X, Shi Y, Zhang J. Structural network connectivity impairment and depressive symptoms in cerebral small vessel disease. Journal of affective disorders 2017;220:8-14.
75. Tuladhar AM, Lawrence A, Norris DG, Barrick TR, Markus HS, de Leeuw FE. Disruption of rich club organisation in cerebral small vessel disease. Human brain mapping 2017;38:1751-1766.
76. Meunier D, Lambiotte R, Fornito A, Ersche KD, Bullmore ET. Hierarchical modularity in human brain functional networks. Frontiers in neuroinformatics 2009;3:37.
77. Marebwa BK, Adams RJ, Magwood GS, et al. Fibroblast growth factor23 is associated with axonal integrity and neural network architecture in the human frontal lobes. PloS one 2018;13:e0203460.
78. Liu S, Quarles LD. How fibroblast growth factor 23 works. J Am Soc Nephrol 2007;18:1637-1647.
79. Fukumoto S. [Fibroblast growth factor (FGF) 23 works as a phosphate-regulating hormone and is involved in the pathogenesis of several disorders of phosphate metabolism]. Rinsho byori The Japanese journal of clinical pathology 2007;55:555-559.
80. Quarles LD. Role of FGF23 in vitamin D and phosphate metabolism: implications in chronic kidney disease. Experimental cell research 2012;318:1040-1048.
81. Faul C, Amaral AP, Oskouei B, et al. FGF23 induces left ventricular hypertrophy. The Journal of Clinical Investigation 2011;121:4393-4408.
82. Gutierrez OM, Januzzi JL, Isakova T, et al. Fibroblast growth factor 23 and left ventricular hypertrophy in chronic kidney disease. Circulation 2009;119:2545-2552.
83. Gutiérrez OM, Wolf M, Taylor EN. Fibroblast Growth Factor 23, Cardiovascular Disease Risk Factors, and Phosphorus Intake in the Health Professionals Follow-up Study. Clinical Journal of the American Society of Nephrology : CJASN 2011;6:2871-2878.
84. Ferrari SL, Bonjour JP, Rizzoli R. Fibroblast growth factor-23 relationship to dietary phosphate and renal phosphate handling in healthy young men. The Journal of clinical endocrinology and metabolism 2005;90:1519-1524.
85. Wright CB, Dong C, Stark M, et al. Plasma FGF23 and the risk of stroke: the Northern Manhattan Study (NOMAS). Neurology 2014;82:1700-1706.
86. Andersson JLR, Sotiropoulos SN. An integrated approach to correction for off-resonance effects and subject movement in diffusion MR imaging. Neuroimage 2016;125:1063-1078.
87. Wright CB, Shah NH, Mendez AJ, et al. Fibroblast Growth Factor 23 Is Associated With Subclinical Cerebrovascular Damage: The Northern Manhattan Study. Stroke 2016;47:923-928.

88. Benjamin EJ, Virani SS, Callaway CW, et al. Heart Disease and Stroke Statistics-2018 Update: A Report From the American Heart Association. Circulation 2018;137:e67-e492.
89. Binkofski F, Seitz RJ, Arnold S, Classen J, Benecke R, Freund HJ. Thalamic metbolism and corticospinal tract integrity determine motor recovery in stroke. Annals of neurology 1996;39:460-470.
90. Stinear CM, Barber PA, Smale PR, Coxon JP, Fleming MK, Byblow WD. Functional potential in chronic stroke patients depends on corticospinal tract integrity. Brain : a journal of neurology 2007;130:170-180.
91. den Ouden DB, Malyutina S, Basilakos A, et al. Cortical and structural-connectivity damage correlated with impaired syntactic processing in aphasia. Human brain mapping 2019.
92. Moroni F, Ammirati E, Rocca MA, Filippi M, Magnoni M, Camici PG. Cardiovascular disease and brain health: Focus on white matter hyperintensities. International journal of cardiology Heart & vasculature 2018;19:63-69.
93. Adams RJ, Ellis C, Magwood G, Kindy MS, Bonilha L, Lackland DT. Commentary: Addressing Racial Disparities in Stroke: The Wide Spectrum Investigation of Stroke Outcome Disparities on Multiple Levels (WISSDOM). Ethnicity & disease 2018;28:61-68.
94. Jones F, Partridge C, Reid F. The Stroke Self-Efficacy Questionnaire: measuring individual confidence in functional performance after stroke. Journal of clinical nursing 2008;17:244-252.
95. Duncan PW, Wallace D, Lai SM, Johnson D, Embretson S, Laster LJ. The stroke impact scale version 2.0. Evaluation of reliability, validity, and sensitivity to change. Stroke 1999;30:2131-2140.
96. Nachev P, Coulthard E, Jager HR, Kennard C, Husain M. Enantiomorphic normalization of focally lesioned brains. NeuroImage 2008;39:1215-1226.
97. Ashburner J, Friston KJ. Unified segmentation. NeuroImage 2005;26:839-851.
98. Yourganov G, Fridriksson J, Rorden C, Gleichgerrcht E, Bonilha L. Multivariate Connectome-Based Symptom Mapping in Post-Stroke Patients: Networks Supporting Language and Speech. The Journal of neuroscience : the official journal of the Society for Neuroscience 2016;36:6668-6679.
99. Andersson JL, Skare S, Ashburner J. How to correct susceptibility distortions in spin-echo echo-planar images: application to diffusion tensor imaging. Neuroimage 2003;20:870-888.
100. Hernandez M, Guerrero GD, Cecilia JM, et al. Accelerating fibre orientation estimation from diffusion weighted magnetic resonance imaging using GPUs. PloS one 2013;8:e61892.
101. Abraham HMA, Wolfson L, Moscufo N, Guttmann CRG, Kaplan RF, White WB. Cardiovascular risk factors and small vessel disease of the brain: Blood pressure, white matter lesions, and functional decline in older persons. Journal of cerebral blood flow and metabolism : official journal of the International Society of Cerebral Blood Flow and Metabolism 2016;36:132-142.
102. Prins ND, van Dijk EJ, den Heijer T, et al. Cerebral small-vessel disease and decline in information processing speed, executive function and memory. Brain : a journal of neurology 2005;128:2034-2041.

103. Zheng JJ, Lord SR, Close JC, et al. Brain white matter hyperintensities, executive dysfunction, instability, and falls in older people: a prospective cohort study. The journals of gerontology Series A, Biological sciences and medical sciences 2012;67:1085-1091.
104. Gouw AA, Seewann A, van der Flier WM, et al. Heterogeneity of small vessel disease: a systematic review of MRI and histopathology correlations. Journal of neurology, neurosurgery, and psychiatry 2011;82:126-135.
105. Cloonan L, Fitzpatrick KM, Kanakis AS, Furie KL, Rosand J, Rost NS. Metabolic determinants of white matter hyperintensity burden in patients with ischemic stroke. Atherosclerosis 2015;240:149-153.
106. Lloyd-Jones D, Adams RJ, Brown TM, et al. Executive summary: heart disease and stroke statistics--2010 update: a report from the American Heart Association. Circulation 2010;121:948-954.
107. Wade DT, Hewer RL, David RM, Enderby PM. Aphasia after stroke: natural history and associated deficits. Journal of neurology, neurosurgery, and psychiatry 1986;49:11-16.
108. Bonilha L, Rorden C, Fridriksson J. Assessing the clinical effect of residual cortical disconnection after ischemic strokes. Stroke 2014;45:988-993.
109. Catani M, ffytche DH. The rises and falls of disconnection syndromes. Brain : a journal of neurology 2005;128:2224-2239.
110. Catani M, Mesulam M. What is a disconnection syndrome? Cortex 2008;44:911-913.
111. Epelbaum S, Pinel P, Gaillard R, et al. Pure alexia as a disconnection syndrome: new diffusion imaging evidence for an old concept. Cortex; a journal devoted to the study of the nervous system and behavior 2008;44:962-974.
112. Basilakos A, Fillmore PT, Rorden C, Guo D, Bonilha L, Fridriksson J. Regional white matter damage predicts speech fluency in chronic post-stroke aphasia. Frontiers in human neuroscience 2014;8:845.
113. Bonilha L, Fridriksson J. Subcortical damage and white matter disconnection associated with non-fluent speech. Brain : a journal of neurology 2009;132:e108.
114. Bonilha L, Gleichgerrcht E, Nesland T, Rorden C, Fridriksson J. Success of Anomia Treatment in Aphasia Is Associated With Preserved Architecture of Global and Left Temporal Lobe Structural Networks. Neurorehabil Neural Repair 2016;30:266-279.
115. Bonilha L, Gleichgerrcht E, Fridriksson J, et al. Reproducibility of the Structural Brain Connectome Derived from Diffusion Tensor Imaging. PloS one 2015;10:e0135247.
116. Kertesz A. The Western Aphasia Battery - Revised. New York: Grune & Stratton, 2007.
117. Faria AV, Joel SE, Zhang Y, et al. Atlas-based analysis of resting-state functional connectivity: evaluation for reproducibility and multi-modal anatomy-function correlation studies. NeuroImage 2012;61:613-621.
118. Hagmann P, Kurant M, Gigandet X, et al. Mapping human whole-brain structural networks with diffusion MRI. PloS one 2007;2:e597.
119. Bonilha L, Nesland T, Martz GU, et al. Medial temporal lobe epilepsy is associated with neuronal fibre loss and paradoxical increase in structural connectivity of limbic structures. Journal of neurology, neurosurgery, and psychiatry 2012;83:903-909.
120. Fedorenko E, Thompson-Schill SL. Reworking the language network. Trends in cognitive sciences 2014;18:120-126.

121. van den Heuvel MP, Sporns O. Rich-club organization of the human connectome. The Journal of neuroscience : the official journal of the Society for Neuroscience 2011;31:15775-15786.
122. Gleichgerrcht E, Kocher M, Nesland T, Rorden C, Fridriksson J, Bonilha L. Preservation of structural brain network hubs is associated with less severe post-stroke aphasia. Restor Neurol Neurosci 2015;34:19-28.
123. Barrett AM, Hamilton RH. Drawing on the right brain for aphasia recovery. Neurology 2016;86:1566-1567.
124. King KS, Peshock RM, Rossetti HC, et al. Effect of normal aging versus hypertension, abnormal body mass index, and diabetes mellitus on white matter hyperintensity volume. Stroke 2014;45:255-257.
125. de Leeuw FE, de Groot JC, Achten E, et al. Prevalence of cerebral white matter lesions in elderly people: a population based magnetic resonance imaging study. The Rotterdam Scan Study. Journal of neurology, neurosurgery, and psychiatry 2001;70:9-14.
126. Grueter BE, Schulz UG. Age-related cerebral white matter disease (leukoaraiosis): a review. Postgraduate medical journal 2012;88:79-87.
127. Kim GM, Park KY, Avery R, et al. Extensive leukoaraiosis is associated with high early risk of recurrence after ischemic stroke. Stroke 2014;45:479-485.
128. Wen W, Sachdev PS. Extent and distribution of white matter hyperintensities in stroke patients: the Sydney Stroke Study. Stroke 2004;35:2813-2819.
129. Prins ND, van Dijk EJ, den Heijer T, et al. Cerebral white matter lesions and the risk of dementia. Archives of neurology 2004;61:1531-1534.
130. Arsava EM, Bayrlee A, Vangel M, et al. Severity of leukoaraiosis determines clinical phenotype after brain infarction. Neurology 2011;77:55.
131. Henon H, Vroylandt P, Durieu I, Pasquier F, Leys D. Leukoaraiosis more than dementia is a predictor of stroke recurrence. Stroke 2003;34:2935-2940.
132. ten Dam VH, van den Heuvel DM, de Craen AJ, et al. Decline in total cerebral blood flow is linked with increase in periventricular but not deep white matter hyperintensities. Radiology 2007;243:198-203.
133. Bisschops RH, van der Graaf Y, Mali WP, van der Grond J. High total cerebral blood flow is associated with a decrease of white matter lesions. Journal of neurology 2004;251:1481-1485.
134. Liao D, Cooper L, Cai J, et al. Presence and severity of cerebral white matter lesions and hypertension, its treatment, and its control. The ARIC Study. Atherosclerosis Risk in Communities Study. Stroke 1996;27:2262-2270.
135. De Groot JC, De Leeuw FE, Oudkerk M, et al. Periventricular cerebral white matter lesions predict rate of cognitive decline. Annals of neurology 2002;52:335-341.
136. Liou LM, Chen CF, Guo YC, et al. Cerebral white matter hyperintensities predict functional stroke outcome. Cerebrovascular diseases (Basel, Switzerland) 2010;29:22-27.
137. Wright A, Tippett D, Saxena S, et al. Leukoaraiosis is independently associated with naming outcome in poststroke aphasia. Neurology 2018;91:e526.
138. Moon HI, Nam JS, Leem MJ, Kim KH. Periventricular White Matter Lesions as a Prognostic Factor of Swallowing Function in Older Patients with Mild Stroke. Dysphagia 2017.

139. Kang HJ, Stewart R, Park MS, et al. White matter hyperintensities and functional outcomes at 2 weeks and 1 year after stroke. Cerebrovascular diseases (Basel, Switzerland) 2013;35:138-145.
140. Arsava EM, Rahman R, Rosand J, et al. Severity of leukoaraiosis correlates with clinical outcome after ischemic stroke. Neurology 2009;72:1403.
141. Sporns O. Contributions and challenges for network models in cognitive neuroscience. Nature Neuroscience 2014;17:652.
142. Buzsaki G. Rhythms of the Brain: Oxford University Press, 2006.
143. Kertesz A. The Western Aphasia Battery - Revised. New York: Grune & Stratton, 2007.
144. Fazekas F, Chawluk JB, Alavi A, Hurtig HI, Zimmerman RA. MR signal abnormalities at 1.5 T in Alzheimer's dementia and normal aging. AJR American journal of roentgenology 1987;149:351-356.
145. Fridriksson J, den Ouden D-B, Hillis AE, et al. Anatomy of aphasia revisited. Brain : a journal of neurology 2018.
146. Kertesz A. Western Aphasia Battery-Revised. San Antionio, TX: Pearson, 2007.
147. Cohen J. Statistical power analysis for the behavioral sciences 2nd ed. ed. Hillsdale, NJ: Lawrence Erlbaum, 1988.
148. Hayes AF. Introduction to mediation, moderation, and conditional process analysis: A regression-based perspective., 2nd ed. New York, NY: The Guilford Press, 2018.
149. Kane L, Ashbaugh AR. Simple and parallel mediation: A tutorial exploring anxiety sensitivity, sensation seeking, and gender. The Quantitative Methods for Psychology 2017;13:148-165.
150. Keith TZ. Multiple regression and beyond. Upper Saddle River, NJ: Pearson Education, 2006.
151. Pantoni L, Garcia JH. Pathogenesis of leukoaraiosis: a review. Stroke 1997;28:652-659.
152. Bonilha L, Gleichgerrcht E, Nesland T, Rorden C, Fridriksson J. Success of Anomia Treatment in Aphasia Is Associated With Preserved Architecture of Global and Left Temporal Lobe Structural Networks. Neurorehabilitation and neural repair 2015.
153. Marebwa BK, Fridriksson J, Yourganov G, Feenaughty L, Rorden C, Bonilha L. Chronic post-stroke aphasia severity is determined by fragmentation of residual white matter networks. Scientific reports 2017;7:8188.
154. Taylor AB, MacKinnon DP, Tein JY. Tests of the three-path mediated effect. Organizational Research Methods 2008;11:241-269.